CHLOROPLAST DIVISION PROTEIN ARC3: EFFECTS ON FTSZ2 ASSEMBLY AND GTPASE ACTIVITY

A Dissertation

by

RAHAMTHULLA S. SHAIK

Submitted to the Office of Graduate and Professional Studies of
Texas A&M University
in partial fulfillment of the requirements for the degree of

DOCTOR OF PHILOSOPHY

Chair of Committee,	Andreas Holzenburg
Committee Members,	Karl Aufderheide
	James Erickson
	Junjie Zhang
Head of Department,	Thomas McKnight

December 2017

Major Subject: Biology

ABSTRACT

Chloroplasts evolved from cyanobacterial endosymbiotic ancestors and their division is a complex process initiated by assembly of cytoskeletal FtsZ proteins into a ring structure at the division site (Z-ring). The cyanobacterial Z-ring positioning system (MinCDE proteins) is also conserved in chloroplasts except that MinC was lost and replaced by the eukaryotic ARC3. Both MinC and ARC3 act as negative regulators of FtsZ assembly, but ARC3 bears little sequence similarity with MinC. Here, light scattering assays, co-sedimentation, light microscopy, GTPase assay and transmission electron microscopy in conjunction with single particle analysis have been used to elucidate the structure of ARC3 and its effect on its main target in chloroplast division: FtsZ2. Analysis of FtsZ2 *in vitro* assembly reactions in the presence and absence of GMPCPP showed that ARC3 promotes FtsZ2 debundling and disassembly of existing filaments in a concentration-dependent manner and requires GTP hydrolysis. 3D reconstruction of ARC3 revealed an almost circular molecule in which the FtsZ-binding N-terminus and the C-terminal PARC6-binding MORN domain are in close proximity and suggests a model for PARC6-enabled binding of ARC3 to FtsZ2. The latter is corroborated by *in vivo* data.

DEDICATION

To my parents, Abdulla Sharif and Mahaboob Bi Shaik for their endless love, support and encouragement. To my wife Jareena Begum Shaik, my son Irfan Sharif Shaik and my little daughter Hasifa Begum Shaik for their support, encouragement and patience. To my sister Rajiya Begum and brother Jamal Sharif Shaik for their support. To all those family members who have supported me and made this dissertation possible.

ACKNOWLEDGEMENTS

I would like to thank my advisor, Dr. Andreas Holzenburg for the opportunity to perform research in his lab, for his guidance, support, patience and encouragement throughout the duration of this research.

I would like to thank Dr. Stanislav Vitha for his advice, patience, technical guidance and support over the entire duration of this research.

I thank my committee members, Dr. Karl Aufderheide, Dr. James Erickson and Dr. Junjie Zhang for their insightful suggestions and helpful discussions for successful completion of this research.

Thanks to my colleagues Min Woo Sung, Jeremy Wood and Jeng-Yih for thoughtful discussions on my research project. Thanks also goes to the staff of Microscopy and Imaging Center for their technical assistance and the Office of the Vice President for Research for providing excellent research resources. I wish to extend my thanks to my friends and the staff of department of Biology for making my time at Texas A&M University a valuable and rewarding experience.

CONTRIBUTORS AND FUNDING SOURCES

Contributors

This work was supervised by a dissertation committee consisting of Dr. Andreas Holzenburg, Dr. Karl Aufderheide and Dr. James Erickson of the Department of Biology and Dr. Junjie Zhang of the Department of Biochemistry and Biophysics.

The data analysis for Figure 26 of Chapter 3 was performed in collaboration with Min Woo Sung of the Department of Biology at Texas A&M University. The data for Figure 28 of Chapter 3 was generated in collaboration with Dr. Stanislav Vitha of the Microscopy and Imaging Center at Texas A&M University.

All other work conducted for the dissertation was completed by the student independently.

Funding Sources

The support of the Office of the Vice President for Research, Division of Research at Texas A&M University, is acknowledged.

NOMENCLATURE

ARC3	Accumulation and replication of chloroplast 3
ARC5	Accumulation and replication of chloroplast 5
ARC6	Accumulation and replication of chloroplast 6
arc	Accumulation and replication of chloroplast mutants
At	*Arabidopsis thaliana*
C-terminus	Carboxyl terminus of a protein
EM	Electron microscopy
FRAP	Fluorescence recovery after photobleaching
FSC	Fourier shell correlation
FtsZ	Filamentation temperature sensitive Z protein
FtsZ1	Filamentation temperature sensitive Z1 protein
FtsZ2	Filamentation temperature sensitive Z2 protein
GDP	Guanosine diphosphate
GTP	Guanosine triphosphate
GMPCPP	Guanosine -5'-[(α, β)-methyleno] triphosphate
MCD1	MULTIPLE CHLOROPLAST DIVISION SITE 1
mCFP	Monomeric cyan fluorescent protein
mYFP	Monomeric yellow fluorescent protein
mOrange2	Monomeric orange fluorescent protein
MEMK6.5	Protein assembly buffer

MES	2-(*N*-morpholino) ethanesulfonic acid
µm	Micrometer
nm	Nanometer
N-terminus	Amino terminus of a protein
PAGE	Polyacrylamide gel electrophoresis
PARC6	Paralog of ARC6
PDV1	PLASTID DIVISION 1
PDV2	PLASTID DIVISION 2
SDS	Sodium dodecyl sulfate
SEM	Scanning electron micrograph
$t_{1/2}$	Half time to fluorescence recovery
TAIR	The *Arabidopsis* Information Resource
TEM	Transmission electron microscope
UA	Uranyl acetate
WT	Wild-type
YPD	Yeast extract peptone dextrose

TABLE OF CONTENTS

Page

LIST OF FIGURES

LIST OF TABLES

CHAPTER I

INTRODUCTION

Chloroplast Division

All plastids including chloroplasts originated as a result of the endosymbiotic relationship between the ancient photosynthetic cyanobacteria and a non-photosynthetic eukaryotic host. Chloroplasts are known for their role in photosynthesis but other plastids such as chromoplasts and amyloplasts also perform important functions such as storage of pigments and starch, respectively [1-3]. Due to essential functions of plastids, it is necessary that their numbers are maintained and regulated tightly throughout the growth and development. Chloroplast continuity during cell division and reproduction is maintained via the binary fission of the preexisting organelles. The division involves the formation of septum at mid-point of the chloroplast, which progressively tightens and eventually results in the formation of two daughter organelles [4]. Chloroplast division is a complex process requiring the coordination of both temporal and spatial events. The division machinery includes the prokaryotic components located within the chloroplast stroma as well as the eukaryotic components located in the cytosol. Improper localization or loss of synchronization among the division components results in abnormal chloroplast division. Isolation of the ARC (**A**ccumulation and **R**eplication of **C**hloroplasts) loci from *Arabidopsis* mutant collection has led to the identification several key proteins involved in chloroplast division [5]. The chloroplast division proteins are nuclear encoded and

imported into stroma by N-terminal transit peptide, which is cleaved off after import releasing the mature protein into stroma.

In cells that undergo division, chloroplasts must replicate and be partitioned into daughter cells. Additional rounds of chloroplast division in leaf cells increase chloroplast numbers to provide maximal photosynthetic performance. Tightly controlled plastid division thus plays a crucial role for maintenance of plant life and response to environmental and developmental signals. Due to their endosymbiotic origin, the division machineries of chloroplasts and all plastids share some core similarities with the bacterial division apparatus. Both divide by binary fission driven by a ring-shaped division machinery, whose assembly is initiated by polymerization of a tubulin-like GTPase, FtsZ, into a ring (Z-ring) [6, 7]. In contrast to bacteria, chloroplasts possess a second ring-shaped division machinery located on the outer, cytosolic side of the chloroplast envelope (Figure 1) [8]. Both the inner and outer rings work together to constrict the organelle and produce two new daughter chloroplasts. The focus of the current study is on the inner, stroma-localized Z-ring in conjunction with the critically involved accessory proteins that control FtsZ assembly and Z-ring positioning [9].

Bacterial and Chloroplast Division Proteins

The formation of the stromal Z-ring at the division site is the primary event in division. The Z-ring (Figure. 1) is composed of the FtsZ (**F**ilamentous **t**emperature **s**ensitive **Z**) proteins, the most conserved key components of both bacterial and plastid division machineries [2-5]. FtsZ proteins are tubulin-like self-activating GTPases that can polymerize to form Z-ring. FtsZ protein is composed of distinct N-terminal and C-terminal

domains and a central core helix, H7 (Figure 2). Purified bacterial FtsZ monomers have been shown to combine in the presence of GTP to form single stranded protofilaments

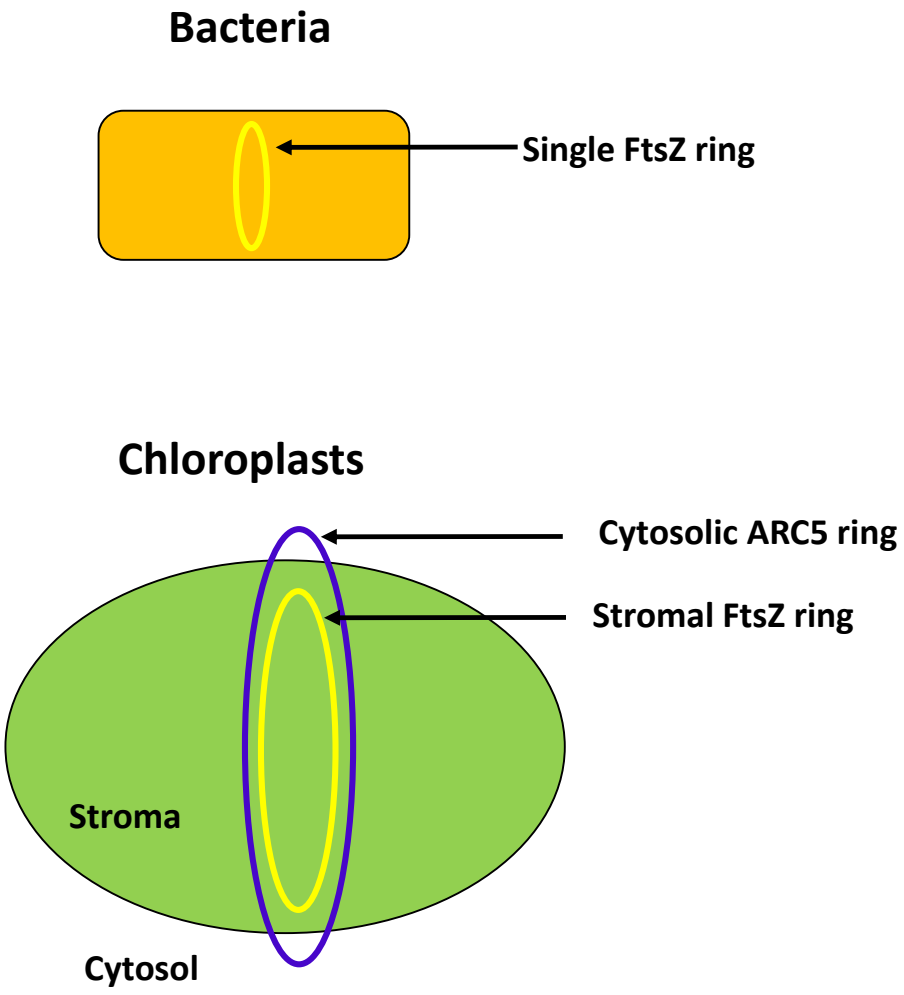

Figure 1. **Ring-shaped division machineries in bacteria and chloroplasts.** Most bacteria contain a single ring-shaped division machinery, whose assembly is initiated by polymerization of a tubulin-like GTPase, FtsZ, into a ring (Z-ring) at mid-cell. Plastids including chloroplasts have two ring-shaped division machineries, one on the outer, cytosolic side of the double envelope membrane, and one on the inner, stromal side , that are assembled in a coordinated manner.

(called polymerization or assembly) ~5nm wide (Figure 3), which may further associate to form filament bundles (bundling), spiral structures and sheets under various in vitro experimental conditions including the presence of Ca^{+2}, molecular crowding agents and other cell division proteins such as ZipA or ZapA that cross link FtsZ filaments [10]. The polymerization of FtsZ requires a minimum concentration of protein, termed as critical

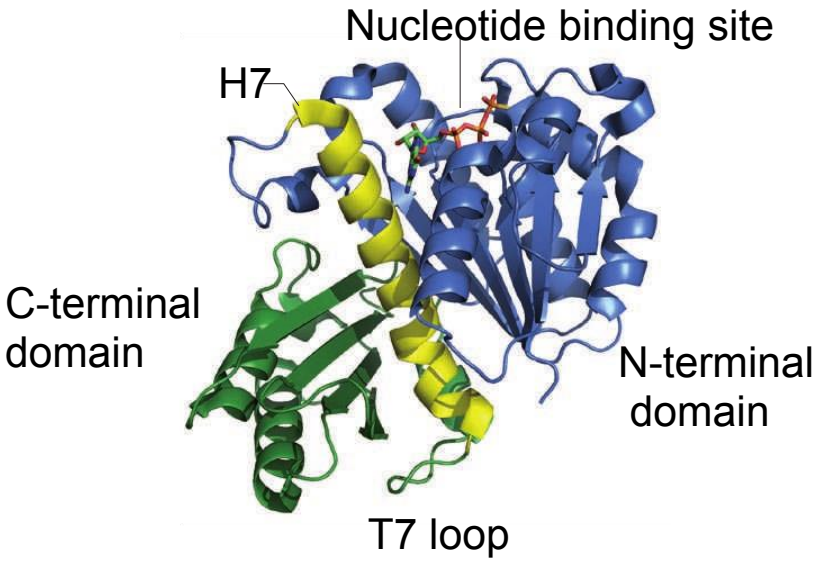

Figure 2. **The crystal structure of *B. subtilis* FtsZ monomer bound to GTP- γS.** FtsZ is composed of two independently folding domains and a central core helix, H7. The amino-terminal domain contains the tubulin signature motif, GGGTGTG, and forms the nucleotide-binding site. At the base of the carboxy-terminal domain, followingH7, is the catalytic T7or synergy loop. The extreme C-terminal tail, which forms the binding site for several division proteins, is not visible in the crystal structure [11]. Reprinted with permission from Nature Publishing Group.

concentration. FtsZ monomers continue to assemble to form polymers above this critical concentration until monomer concentration in the solution falls below the critical concentration. While single protofilaments are assembled at lower FtsZ concentrations, filament bundles are favored (Figure 4) at higher concentrations of FtsZ [12].

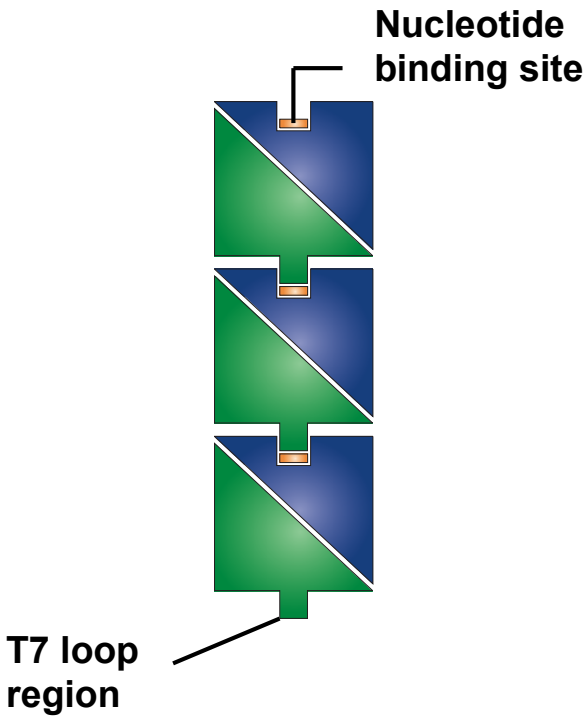

Figure 3. **FtsZ assembles in a GTP dependent manner.** FtsZ has a higher affinity to GTP than GDP. FtsZ polymerizes by the head-to-tail association of individual subunits, shown in blue and green, to form a single-stranded protofilament with a longitudinal subunit repeat that is similar to that of tubulin. Insertion of the T7 loop into the nucleotide-binding site (orange) of the subunit below places two highly conserved aspartate residues in the vicinity of the FtsZ γ-phosphate [11]. Reprinted with permission from Nature Publishing Group.

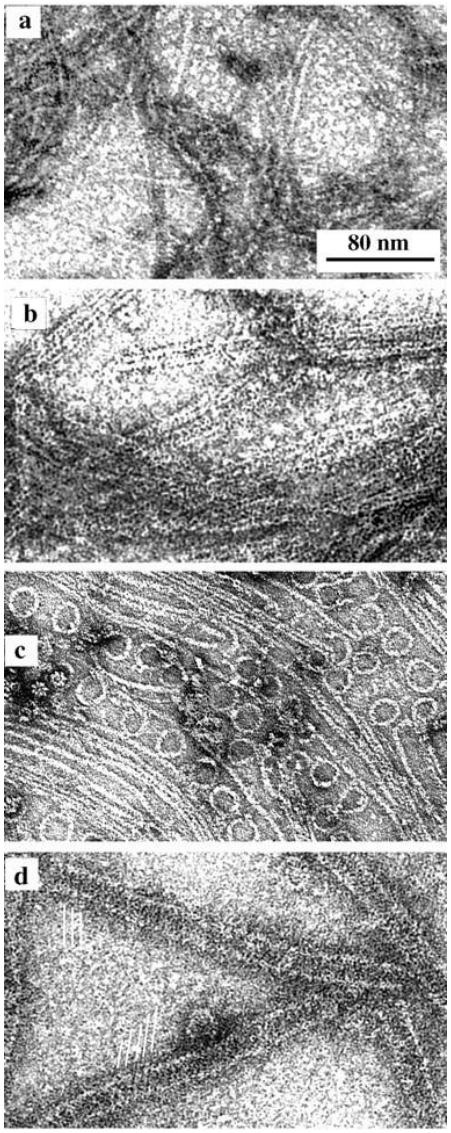

Figure 4. The four types of polymers formed by FtsZ in MEMK6.5. **(A)** Straight protofilaments formed with GTP but without DEAE-dextran. **(B)** Sheets of straight protofilaments assembled from FtsZ plus DEAE-dextran. **(C)** Minirings assembled with GDP and adsorbed onto a cationic lipid monolayer. **(D)** FtsZ tubes assembled with GDP and DEAE-dextran. The parallel white lines indicate the helical protofilaments in these tubes [13]. Reprinted with permission from American Society for Microbiology.

The interaction of two FtsZ monomers during polymerization leads to the formation of an active site for GTP hydrolysis, thus coupling the requirement of polymerization for GTP hydrolysis (also called GTPase activity). The GTP hydrolysis makes FtsZ filaments to adopt a curved conformation [13] leading to destabilization, detachment of FtsZ-GDP subunits, termed as fragmentation (Figure 5). The fragmentation of protofilament is immediately followed by exchange of subunits (GDP bound subunits within the protofilament are replaced with GTP bound subunits in the cytoplasm or in solution) leading to re- association of GTP bound subunit to protofilament, termed as annealing. The length of protofilament is determined by the rates of polymerization and of GTP hydrolysis [10, 14, 15]. The process of fragmentation, nucleotide exchange and recycling of subunits into existing protofilaments occurs very rapidly (dynamic) and described as "turnover". Continuous fragmentation and annealing of filaments leads to dynamic remodeling of the Z-ring in vivo, which is responsible for generation of the constriction force [16]. The rates of Z-ring turnover in vivo and of protofilaments turnover in vitro have been shown to correlate with FtsZ GTPase activity [17, 18].

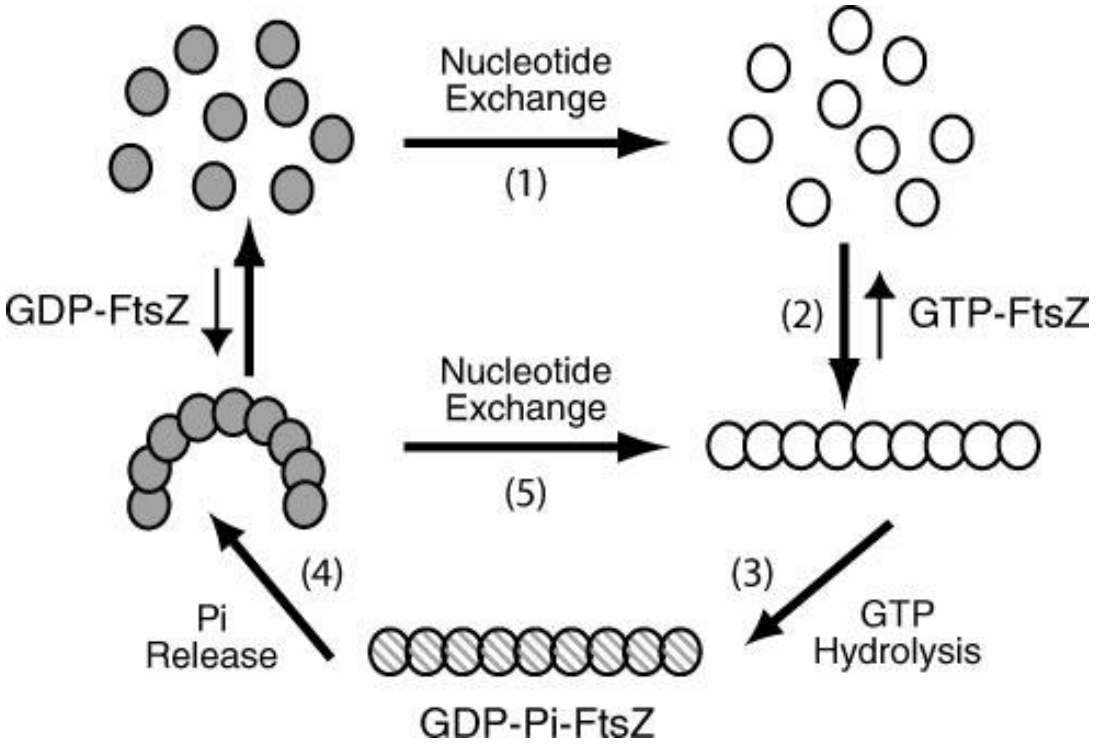

Figure 5. **Model for FtsZ's GTP hydrolysis cycle.** FtsZ's hydrolysis cycle is connected to polymer assembly and disassembly. **1**: Monomers rapidly exchange nucleotide with solution. In vivo, more GTP than GDP exists in the cytoplasm. **2**: When bound to GTP, FtsZ assembly is enhanced. **3**: Once assembled, FtsZ can hydrolyze the GTP**. 4**: Phosphate release follows. GDP-containing polymers are more likely to be curved or to disassemble than GTP-containing polymers. **5:** Nucleotide exchange might occur without complete disassembly of the polymer [19]. Reprinted with permission from Annual Reviews.

	Bacteria	Plants	Function
Medial ring	FtsZ	FtsZ1 and FtsZ2	Mark division site, constriction
Min system	**MinC**, D , E or DivIVA	**ARC3**, MinD, MinE, PARC6 and MCD1	Division site placement
Tethering	ZipA, FtsA and ZipN /Ftn2	ARC6, PARC6	Membrane anchoring
Inner/Outer rings	None	PD rings, PDV1, PDV2 and ARC5 (DRP5B)	Constriction and separation

Table 1. Key proteins of bacterial and Chloroplast division and their function. MinC in bacteria is replaced by ARC3 in chloroplasts (highlighted in bold).

In contrast to bacteria, *Arabidopsis* and other plants possess two functionally distinct families of FtsZ proteins (Figure 6 and Table 1) termed as FtsZ1 and FtsZ2 [3, 20, 21]. Both FtsZ1 and FtsZ2 can bind GTP and polymerize into protofilaments and bundles in a GTP dependent pathway [3, 22]. In *Arabidopsis*, FtsZ1 and FtsZ2 assemble into heteropolymers at the division site (Figure 8). The direct interaction between ARC6 and

FtsZ2 stabilizes and tethers these heteropolymers to the inner envelope membrane to form a Z-ring. ARC6 is a chloroplast inner envelope membrane protein and a homologue of cyanobacterial Ftn2/ZipN [23-25]. Following the formation of the stromal Z-ring, two

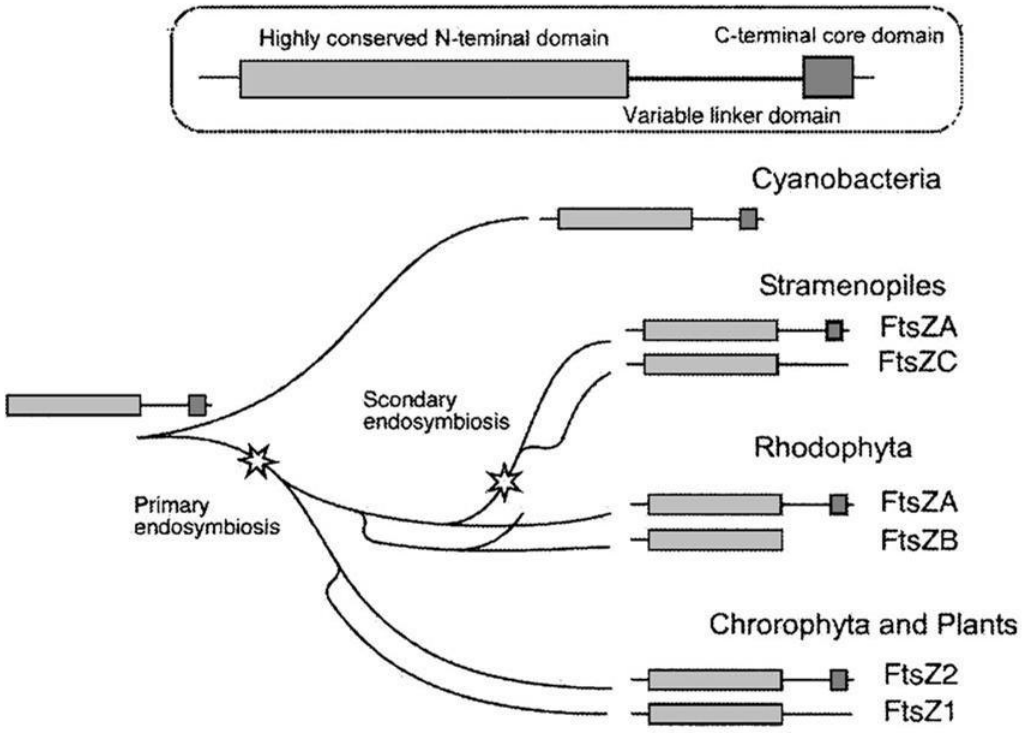

Figure 6. Origin and evolution of the plastid FtsZ family [21]. Reprinted with permission from Springer-Verlag New York Inc.

electron dense-rings including an inner plastid dividing (PD ring) on the stromal surface of the inner envelope membrane and outer PD ring on the cytosolic surface of the outer

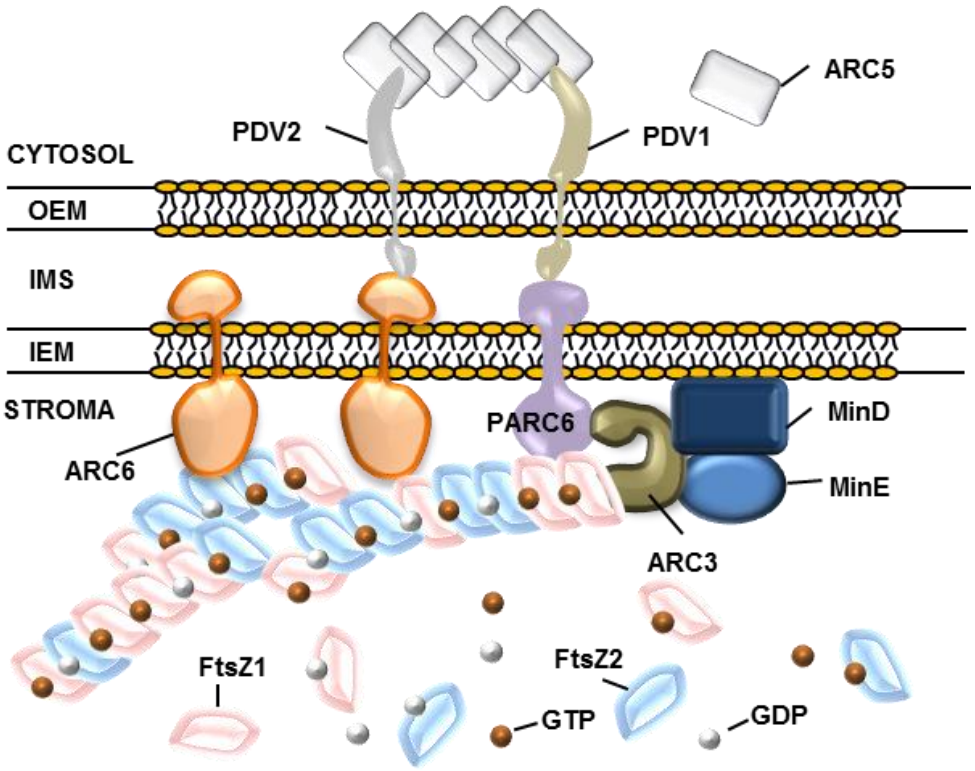

Figure 7. A model of chloroplast division machinery. FtsZ1 and FtsZ2 co-assemble into filaments that form the Z-ring. FtsZ assembly is promoted by a membrane-anchored ARC6. The negative control system (ARC3, PARC6, MinD, MinE) prevents Z-ring assembly at improper sites and remodels the Z-ring. IEM, OEM: inner and outer envelope membranes, respectively; IMS: Intermembrane space. Some components were omitted for clarity.

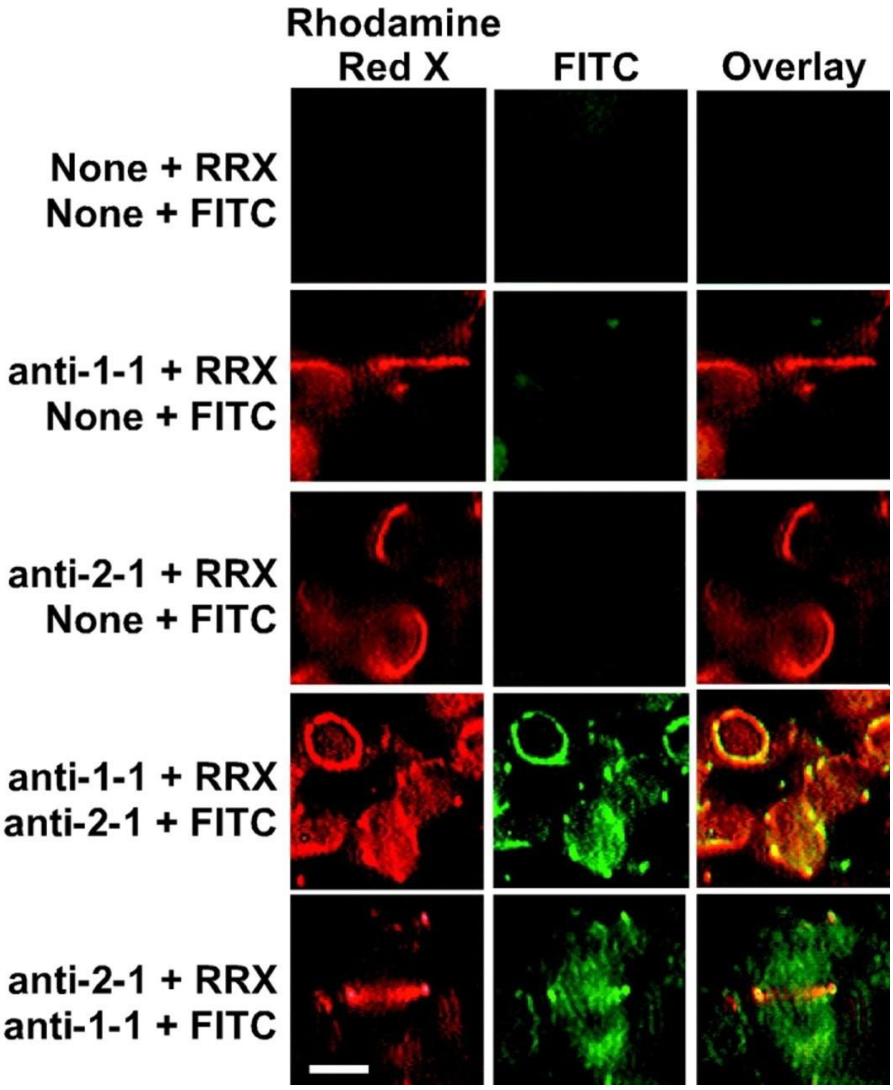

Figure 8. Co-localization of *At*FtsZ1-1 and *At*FtsZ2-1 rings. Leaf sections from wild-type Arabidopsis plants were subjected to sequential, double immunofluorescence labeling of *At*FtsZ1-1 and *At*FtsZ2-1. The order of antibody application is indicated on the left. Tissue sections were incubated first with no antibodies (None), anti–*At*FtsZ1-1 antibodies (anti–1-1), or anti–*At*FtsZ2-1 antibodies (anti–2-1), followed by monovalent anti–rabbit antibody conjugated to Rhodamine red– X (RRX). Sections were then treated with no, anti–*At*FtsZ1-1, or anti–*At*FtsZ2-1 antibody, followed by anti–rabbit FITC conjugate. The labeled sections were viewed using FITC (green) and Texas red (red) filter sets. The yellow color in the overlay of the red and green signals indicates colocalization of *At*FtsZ1-1 and *At*FtsZ2-1. Bar, 2 μm [26]. Reprinted with permission from Rockefeller University Press.

envelope membrane are assembled [27]. The outer PD ring is made up of a bundle of ~10 nm-filaments composed of a glycogenin-like protein, PDR1. The inner PD ring is ~5 nm thick but the composition is currently unknown. The cyanobacterial-derived FtsZ ring forms a complex with host-derived PD rings during the division. Subsequent to formation of PD rings, another cytosolic ring, the ARC5 (DRP5B) ring appears external to the outer PD ring. ARC5 is a GTPase and is a member of eukaryotic dynamin family of membrane-fission proteins [1, 28, 29]. The absence of PD rings and the ARC5 ring in bacteria indicate that these rings are eukaryotic in origin. While the Z-ring and PD rings play role in early constriction [30], the ARC5 ring helps in late constriction and final separation of daughter chloroplasts. Thus, the FtsZ ring together with PD rings and ARC5 ring brings about the constriction of the chloroplast (Figure 7).

Bacterial and Chloroplast Min System

The precise placement of Z-ring in bacteria or chloroplasts is essential to achieve symmetric division and produce daughter cells or organelles of equal size. The selection of division site at the mid cell in bacteria is regulated by a macromolecular complex called "Min system" (*Minicell* system). Min system in bacteria includes MinC, MinD, MinE or DivIVA proteins, although many species of bacteria lack Min system and placement of FtsZ ring is regulated by other mechanisms [31] . MinC, in bacteria has been shown to play a key role to restrict the FtsZ ring to mid cell by inhibiting the FtsZ polymerization at improper sites through its direct interaction with FtsZ (Figure 9) and by working in concert with MinD, MinE or DivIVA [32-36]. In chloroplasts, MinD and MinE are conserved, but MinC and DivIVA were lost and novel eukaryotic components ARC3,

PARC6 and MCD1 have been acquired during evolution. Thus the current "Chloroplast Min system" consists of ARC3, MinD, MinE, PARC6 (also called CDP1) and MCD1 (Figure 10) [37, 38]. Plant derived ARC3 has been suggested to be a functional replacement for bacterial MinC based on the findings that (i) Overexpression of ARC3 inhibits chloroplast division resulting in drastically enlarged chloroplasts [39] (ii) Lack of ARC3 in arc3 mutants led to multiple constrictions in the chloroplasts and misplaced Z-rings [39, 40] [41] ARC3 directly interacts with FtsZ1, FtsZ2, MinD, MinE and PARC6 [38, 39, 42-44] and (iv) ARC3 inhibits FtsZ1 and FtsZ2 filament formation *in vivo* in the heterologous *S. pombe* expression system [44, 45]. However, the mechanism by which ARC3 regulates FtsZ polymerization is not clear. A recent study in *Arabidopsis* from our laboratory showed that the loss of ARC3 in arc3 mutant plants resulted in dramatic decrease in FtsZ1 turnover suggesting that ARC3 destabilizes the already assembled FtsZ filaments instead of directly inhibiting FtsZ polymerization [46]. Although it has been shown that ARC3 can interact with other known proteins of the Min system including MinD, MinE and PARC6, the effect of these interactions on FtsZ assembly/disassembly or FtsZ GTPase activity (turnover) is currently unknown. Although ARC3 has been suggested to be a functional analog of MinC, it bears very little sequence similarity with MinC [39, 47] and no structural data is available for ARC3 to date. The lack of structural and functional details impairs our understanding of the role of ARC3 in chloroplast division.

The objective of the current study is to understand the molecular mechanisms of ARC3-mediated regulation of chloroplast division. To make progress in this direction, this

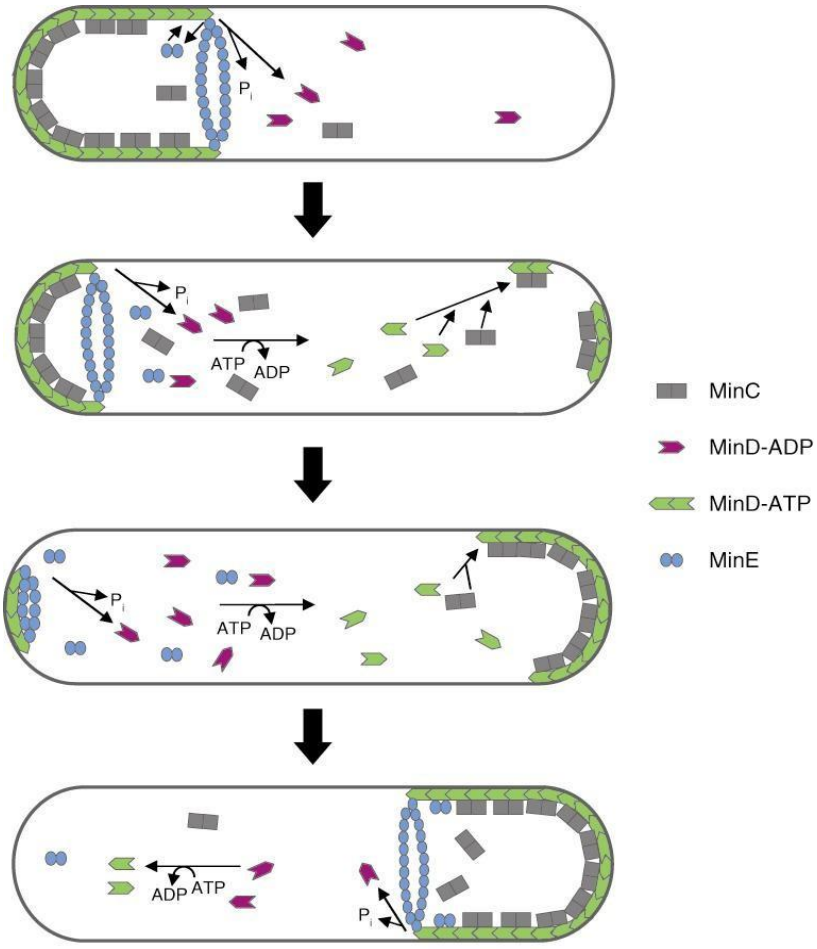

Figure 9. The Bacterial Min system: Min proteins in *Escherichia coli* oscillate to assist in FtsZ-ring positioning. MinD-ATP binds to the membrane and recruits MinC. MinE displaces MinC and stimulates MinD ATPase, causing release of the proteins from the membrane. Whereas released MinE can immediately rebind to MinD on the membrane, the released MinD must undergo nucleotide exchange to regenerate MinD-ATP. In the model by Huang et al., the concentration of MinD-ATP in the vicinity of the old pole is lowered because it binds cooperatively to the membrane already containing bound MinD. In contrast, the MinD-ATP concentration increases at the other pole, which lacks bound MinD. As the concentration rises, it eventually binds, forming a new polar zone. As MinE is released from the old pole, it binds to the ends of the MinD polar zone [33]. Reprinted with permission from Annual Reviews.

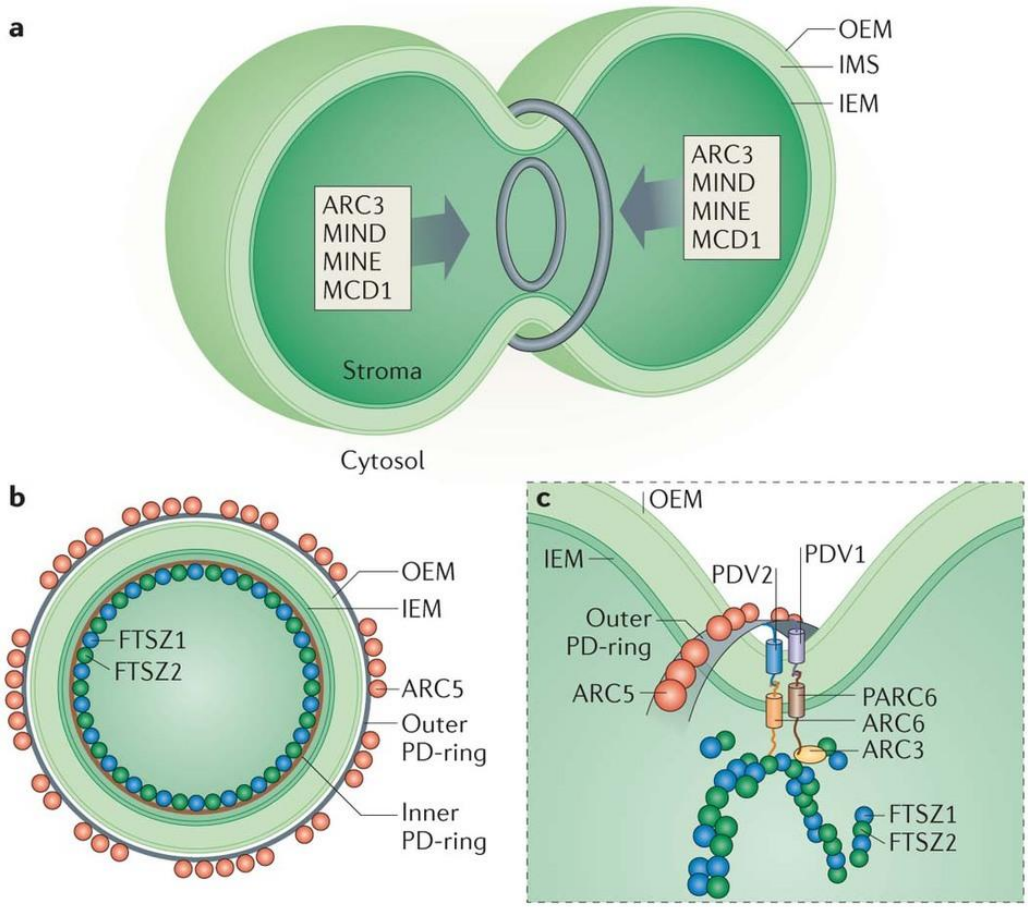

Figure 10. The Chloroplast Min system: During the chloroplast division, **(a)**. the correct positioning of the division machinery at the constriction zone is mediated by the MIN (MINICELL) system (grey arrows), which acts to control Z-ring formation. **(b)**. Multiple rings surround the organelle at the division site to enable constriction. On the stromal side, the Z-ring (comprising functionally distinct FTSZ1 and FTSZ2 homologues) and the inner PD-ring (of uncertain composition) are present. On the cytosolic side, an outer PD-ring that is composed of polyglucan filaments and a discontinuous ring of dynamin-related ARC5 (ACCUMULATION AND REPLICATION OF CHLOROPLASTS 5) operate. **(c)** Positional information from the stromal Z-ring is conveyed to the cytosolic components through ARC6 and PARC6 in the inner membrane and PDV1 (PLASTIC DIVISION 1) and PDV2 in the outer membrane through specific interactions in the intermembrane space [48]. Correctly positioned PDV proteins enable the recruitment of ARC5 at the constriction zone. Z-ring formation is dynamically controlled by the action of PARC6 and ARC3. IEM, inner envelope membrane; MCD1, MULTIPLE CHLOROPLAST DIVISION SITE 1; OEM, outer envelope membrane [2]. Reprinted with permission from Nature Publishing Group.

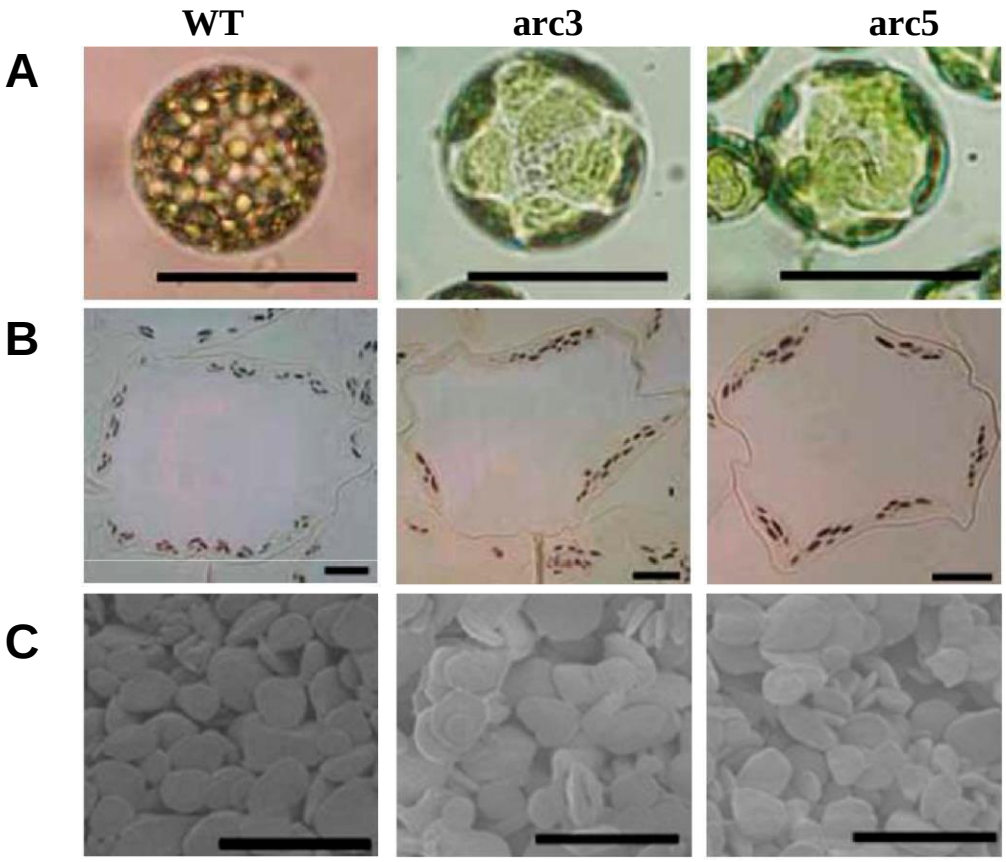

Figure 11. Phenotypes of the *arc* mutants and their wild-types. A, Protoplasts were isolated from four-week-old plants. Leaf tissue was sliced with razor and incubated in 400 mM sorbitol, 20 mM MES-KOH (pH 5.2), 0.5 mM $CaCl_2$ for 30 min with illumination, then for a further 3 h following addition of 1% (w/v) Cellulase R-10 and 0.25% (w/v) Macerozyme R-10 (both desalted; Yakult, Tokyo, Japan). Protoplasts were released by gentle agitation with a glass rod. Bar represents 50 μm. B, Light micrographs of 1-μm thick sections of mesophyll cells stained with iodine solution. Bar represents 10 μm. (C) Scanning electron micrographs of isolated starch granules. Bar represents 5 μm. [49]. Reprinted with permission from American Society of Plant Biologists.

study aims to (i) Decipher the mechanism of ARC3-mediated remodeling of FtsZ filaments *in vitro* (ii) Characterize structural features of ARC3 in order to understand the structure-function relationships.

The results from the current study provided important insights into how the FtsZ polymerization dynamics are regulated by ARC3 and thus revealed clues about the mechanism of division site selection during chloroplast division. Elucidation of the mechanism of plastid division is important not only from the evolutionary and cell biological perspective, but also has important commercial implications. For example, the stromal FtsZ protein levels have been shown to affect the size of amyloplasts (starch storing plastids) in potato. An important property that determines the suitability of starch for specific commercial applications is the granule size (Figure 11) which is in turn controlled by the size of amyloplasts [49, 50]. Modulation of the starch granule size has also been shown to be useful in economically important crops such as potato, corn and rice. Improvement in starch granule size led to estimated gross value gains of $280 million per year domestically [51]. Understanding the mechanism of chloroplast division could also contribute to our increased attention towards the use of chloroplasts as bioreactors for production of many recombinant proteins intended for therapeutic applications both in humans and animals [52].

CHAPTER II

EFFECTS OF ARC3 ON FTSZ ASSEMBLY AND GTPase ACTIVITY

Introduction

Chloroplasts evolved from cyanobacterial endosymbiotic ancestors and their division is a complex process involving co-assembly of tubulin-like cytoskeletal proteins FtsZ1 and FtsZ2 and formation of a ring structure at the division site, the Z-ring. The division machinery includes the components of prokaryotic ancestry located within the chloroplast stroma as well as the components of eukaryotic origin located in the cytosol. Improper localization or loss of synchronization among the division components results in abnormal chloroplast division. The chloroplast division proteins are nuclear encoded and imported into stroma by N-terminal transit peptide, which is cleaved off after import releasing the mature protein into stroma. The formation of the stromal Z-ring at the division site is the primary event in division. The Z-ring is composed of the FtsZ (**F**ilamentous **t**emperature **s**ensitive **Z**) proteins, the most conserved key components of both bacterial and plastid division machineries [1, 53]. Both FtsZ1 and FtsZ2 can bind GTP and polymerize into protofilaments and bundles in a GTP dependent manner [22, 54]. In *Arabidopsis,* FtsZ1 and FtsZ2 assemble into heteropolymers at the division site (Figure 12) [22, 26].

The precise placement of Z-ring in bacteria or chloroplasts is essential to achieve symmetric division and produce daughter cells or organelles of equal size. The selection of division site at the mid cell in bacteria is regulated by a macromolecular complex called

"Min system" (*Minicell* system). The MinC protein has been shown to play a key role to restrict the FtsZ ring to mid cell by inhibiting the FtsZ polymerization at improper sites through its direct interaction with FtsZ and by working in concert with MinD, MinE or DivIVA [32-36]. In chloroplasts, MinD and MinE (Figure 13) are conserved, but MinC and DivIVA were lost and novel eukaryotic components have been acquired during evolution.

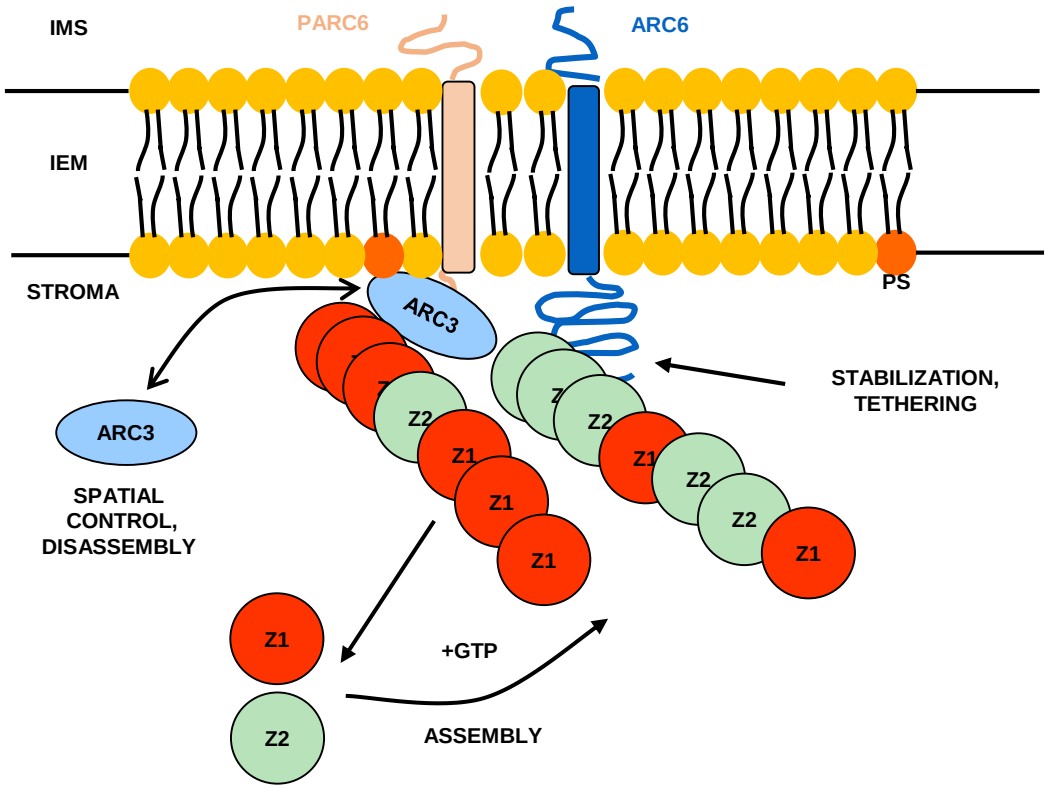

Figure 12. The inner (stromal) chloroplast division ring: The most important components and their hypothetical arrangement are shown. FtsZ1/FtsZ2 heteropolymers at the division site are stabilized and anchored to inner envelope membrane via ARC6-FtsZ2 interaction. ARC3 and PARC6 interact to remodel or destabilize the filaments. FtsZ assembly is promoted by GTP binding. Hydrolysis of GTP causes conformational changes in FtsZ and is thought to promote filament curvature.

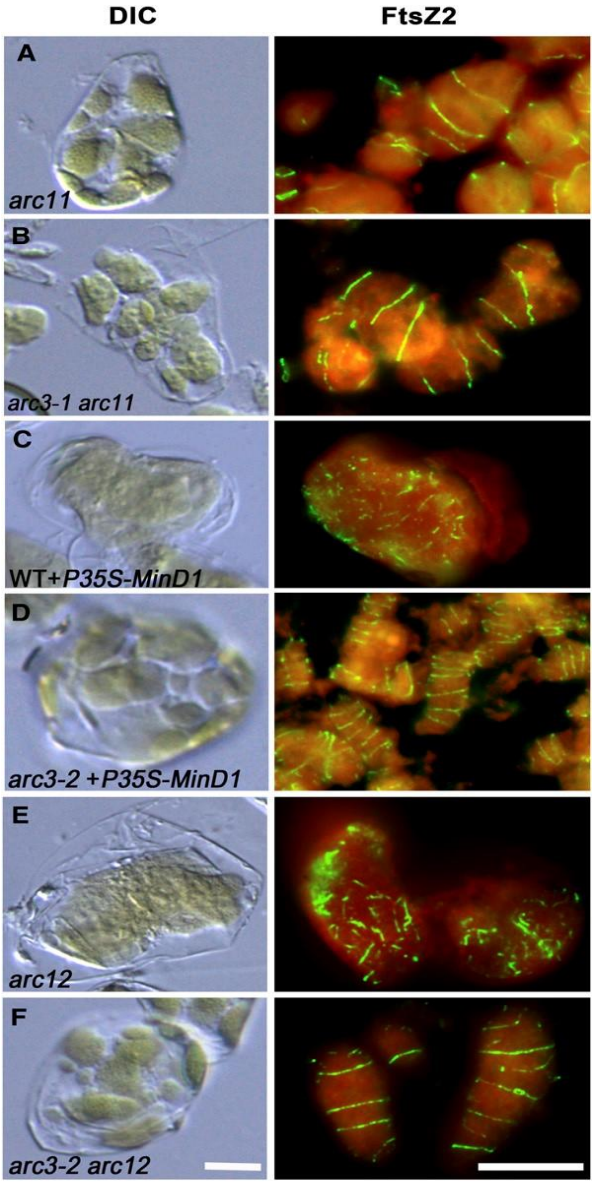

Figure 13. ARC3 Is Required for MinD1- and MinE1-Mediated Z-Ring Positioning. **(A)** to **(F)** Chloroplast phenotypes imaged by DIC and FtsZ immnunolocalization in the indicated genotypes. Anti-FtsZ2-1 antibody was used for FtsZ localization. WT, the wild type. Bars = 10 mm [44]. Reprinted with permission from American Society of Plant Physiologists.

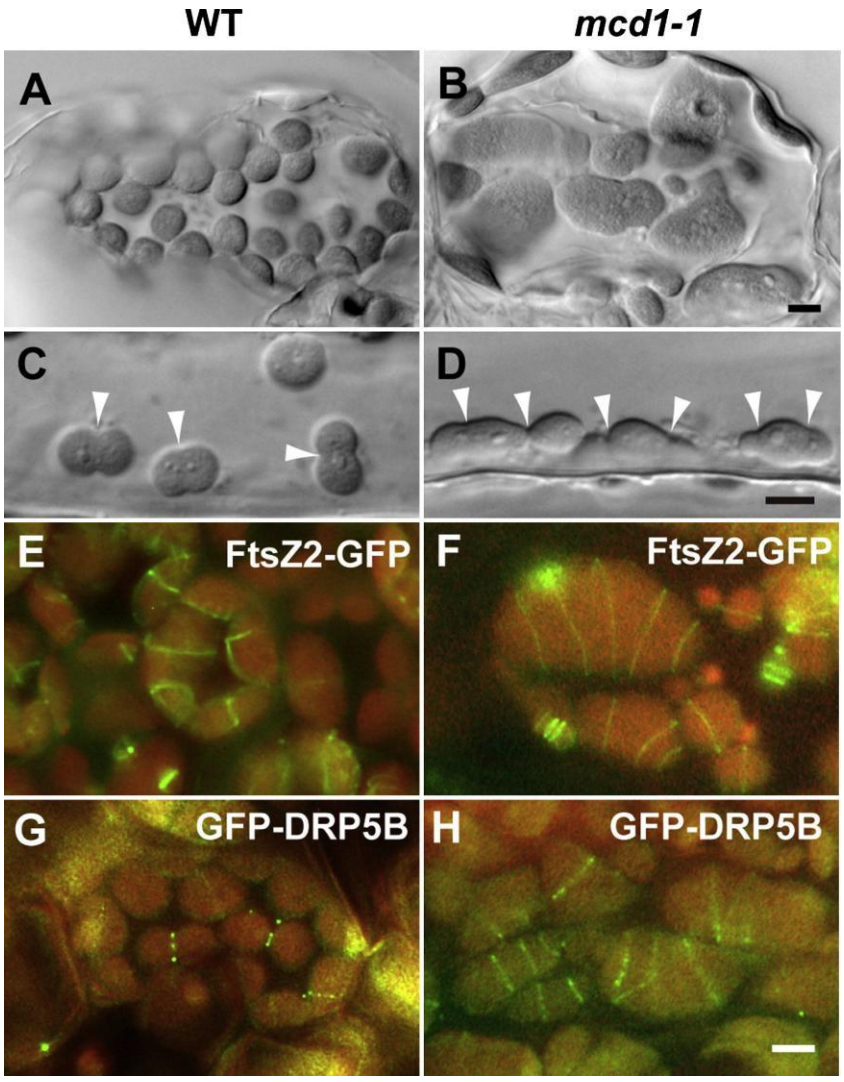

Figure 14. Multiple chloroplast division in *mcd1* mutants. (A–D) Chloroplasts were observed by Nomarski optics in leaf mesophyll cells (A, B) and in petiole cells (C, D). Wild-type (A, C) and *mcd1-1* mutant (B, D) are shown. Arrows indicate the constriction sites of dividing chloroplasts. **(E–H)** Localization of FtsZ2-GFP (E, F) and GFP-DRP5B (G, H) in wild-type (E, G) and *mcd1-1* mutant (F, H). The fluorescence of GFP is green and the auto fluorescence of chlorophyll is red. Each set of images (A and B, C and D, and E–H) are shown at the same magnification. Scale bars correspond to 5 μm [43]. Reprinted with permission from Cell Press.

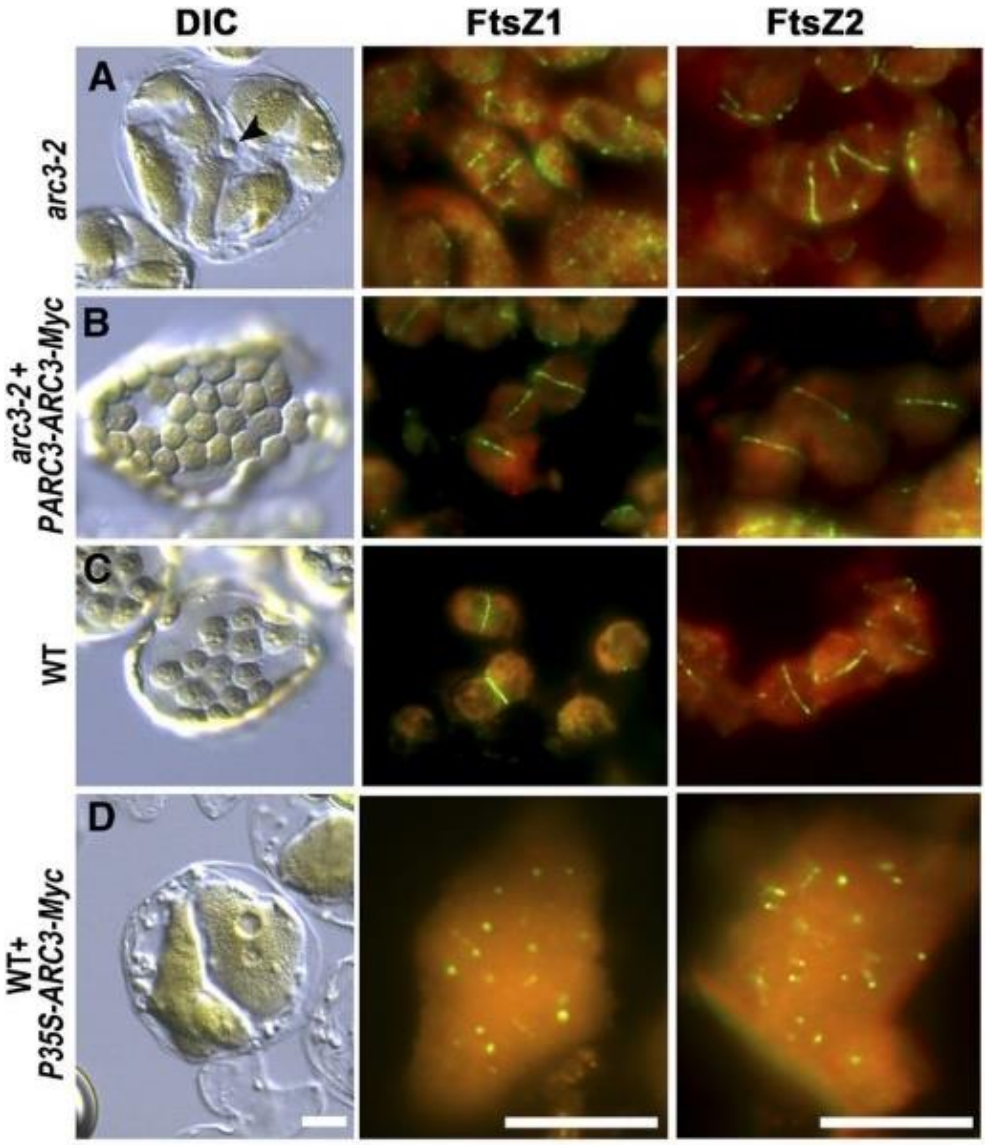

Figure 15. Overexpression of ARC3 Inhibits Z-Ring Assembly in *Arabidopsis*. (A) to **(D)** Chloroplast phenotypes imaged with differential interference contrast (DIC) optics and immunofluorescence localization of FtsZ in mesophyll cells of the indicated genotypes. *arc3-2 + PARC3-ARC3-Myc*, *arc3-2* mutants complemented with *PARC3-ARC3-Myc*; wild type + *P35S-ARC3-Myc*, wild-type (WT) plants expressing *P35S-ARC3-Myc*. FtsZ1 and FtsZ2 were immunolabeled with antibodies specific for FtsZ1 and FtsZ2-1, respectively. Green, Alexa Fluor 488–labeled FtsZ1 or FtsZ2-1; red, chlorophyll autofluorescence. Bars = 10 μm [44]. Reprinted with permission from American Society of Plant Physiologists.

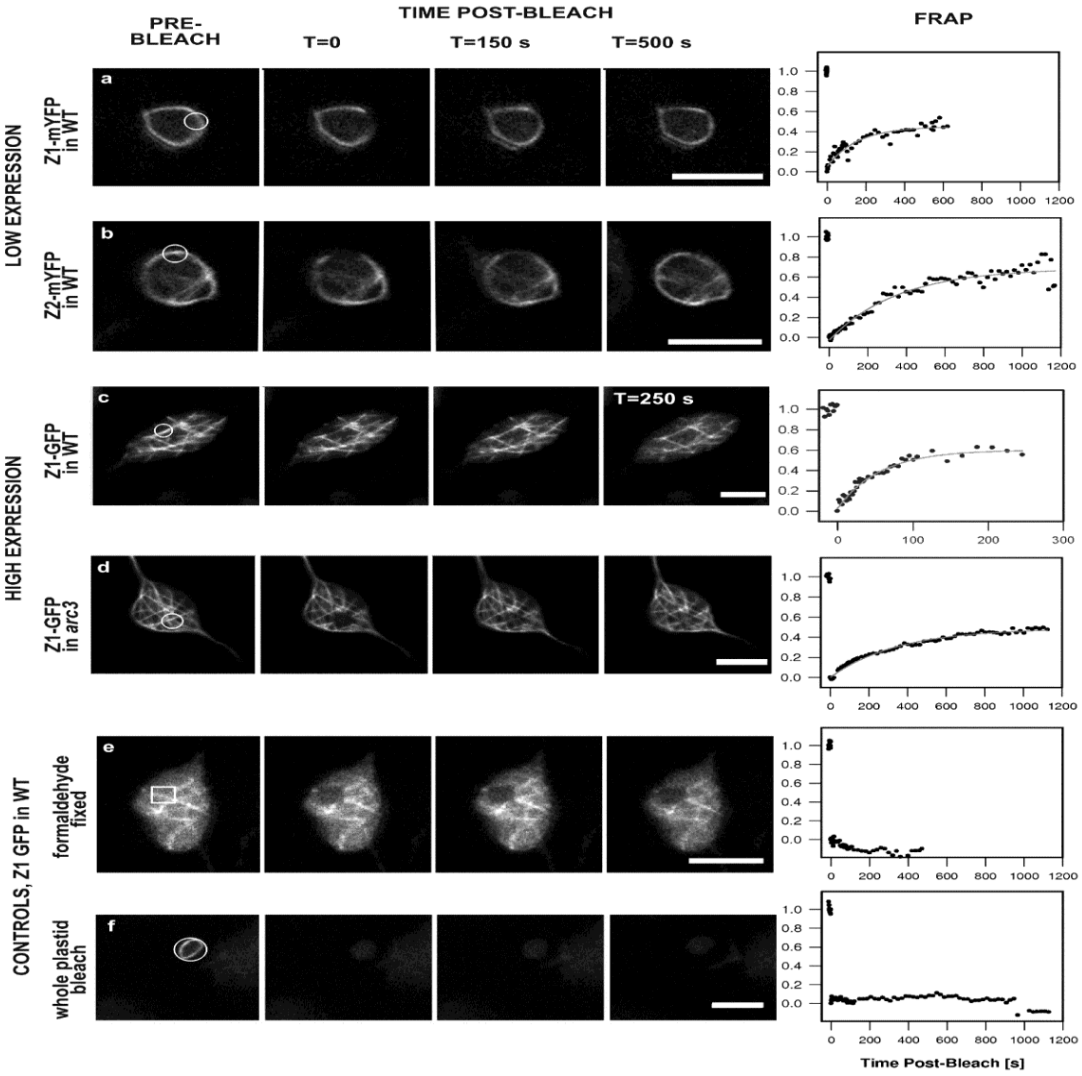

Figure 16. FRAP analysis of FtsZ1 and FtsZ2 filament turnover in chloroplasts. Prebleach and selected postbleach frames from the time-lapse sequence are shown. The circled or boxed area at T = 0 indicates the bleached region. The rightmost column shows representative recovery curves from FRAP experiments, the vertical axis denotes the corrected, normalized fluorescence Fb, corr, norm. Vertical lines in FRAP plots indicate the t1/2 of recovery. a, b: FRAP of FtsZ1-YFP (a) and FtsZ2-YFP (b) expressed in wild-type (WT) background at WT-like levels. c, d: FRAP of FtsZ1-GFP overexpressed in WT (c) or arc3 mutant background. Please note the different time scale in the FRAP curve in (c). e, f: controls. FRAP of small region of interest in formaldehyde-fixed leaf tissue (e) and whole-plastid photobleaching in live tissue (f). The dip in fluorescence intensity at 1,000 s postbleach in (f) is because of a focus shift. Scale bar is 5 μm [46]. Reprinted with permission from Microscopy Society of America.

Thus the current "Chloroplast Min system" consists of ARC3, MinD, MinE, PARC6 (also called CDP1 or ARC6H) MCD1 [37, 38] and also MSL1 and MSL2 [55]. MCD1 mutants show the multiple Z-ring phenotype (Figure 14) similar to ARC3 mutants (Figure 15). The plant derived ARC3 has been suggested to be a functional replacement for bacterial MinC based on the findings that (i) Overexpression of ARC3 disrupts the Z-ring and inhibits chloroplast division resulting in drastically enlarged chloroplasts [39, 44] (ii) Lack of ARC3 in *arc3* mutants led to multiple constrictions in the chloroplasts and misplaced Z- rings [39, 44] (ii) ARC3 directly interacts with FtsZ1, FtsZ2, MinD, MinE and PARC6 [38, 39, 42-44] and (iv) ARC3 inhibits FtsZ1 and FtsZ2 filament formation *in vivo* in the heterologous *S. pombe* expression system [44, 45]. However, the mechanism by which ARC3 regulates FtsZ polymerization is not clear. A recent study in *Arabidopsis* from our laboratory showed that the loss of ARC3 in *arc3* mutant plants resulted in dramatic decrease in FtsZ1 turnover (Figure 16) suggesting that ARC3 destabilizes the already assembled FtsZ filaments instead of directly inhibiting FtsZ polymerization [46]. For comparison, the FtsZ GTPase activity and turnover in plants versus bacteria are listed in Table 2.

Organism	Turnover of FtsZ, $t_{1/2}$ (s)	GTPase activity (mol GTP mol protein/min)
A. thaliana FtsZ1 (in planta)	100	1-3
A. thaliana, FtsZ1 (in yeast)	30	
A. thaliana, FtsZ2 (in planta)	300	0.5-1.0
A. thaliana, FtsZ2 (in yeast)	90	
Escherichia coli, FtsZ	10	5-15
E. coli, FtsZQ47K mutant	300	0.5
Bacillus subtilis	8	0.5
Mycobacterium tuberculosis	25-63	0.47

Table 2. FtsZ turnover and GTPase activity in Plants and Bacteria. Table adapted from [46].

Results

Expression and purification of recombinant mARC3, tARC3 and FtsZ2 proteins.

ARC3 consist of three domains, the N-terminal domain with prokaryotic FtsZ-like sequence, a middle domain with no recognizable motifs, and the C-terminal domain with partial similarity to PIP5K bearing several MORN motifs [39, 47]. The MORN domain interacts with a chloroplast division protein PARC6 [42] but prevents interaction of ARC3 with FtsZ1, FtsZ2, MinD and MinE proteins [39, 44]. Hence, both the full length ARC3 harboring the MORN domain (mARC3; residues 41-741) and the biochemically active truncated ARC3 lacking the MORN domain (tARC3; residues 41-598) were designed to understand how the MORN domain inhibits the interaction of ARC3 with FtsZ proteins and to dissect the mechanism of ARC3-mediated inhibition of FtsZ2 assembly. Since ARC3 has been shown to mainly exert its negative effect on FtsZ assembly through its interaction with FtsZ2 [44], a construct encoding a full length mature form of FtsZ2 was designed.

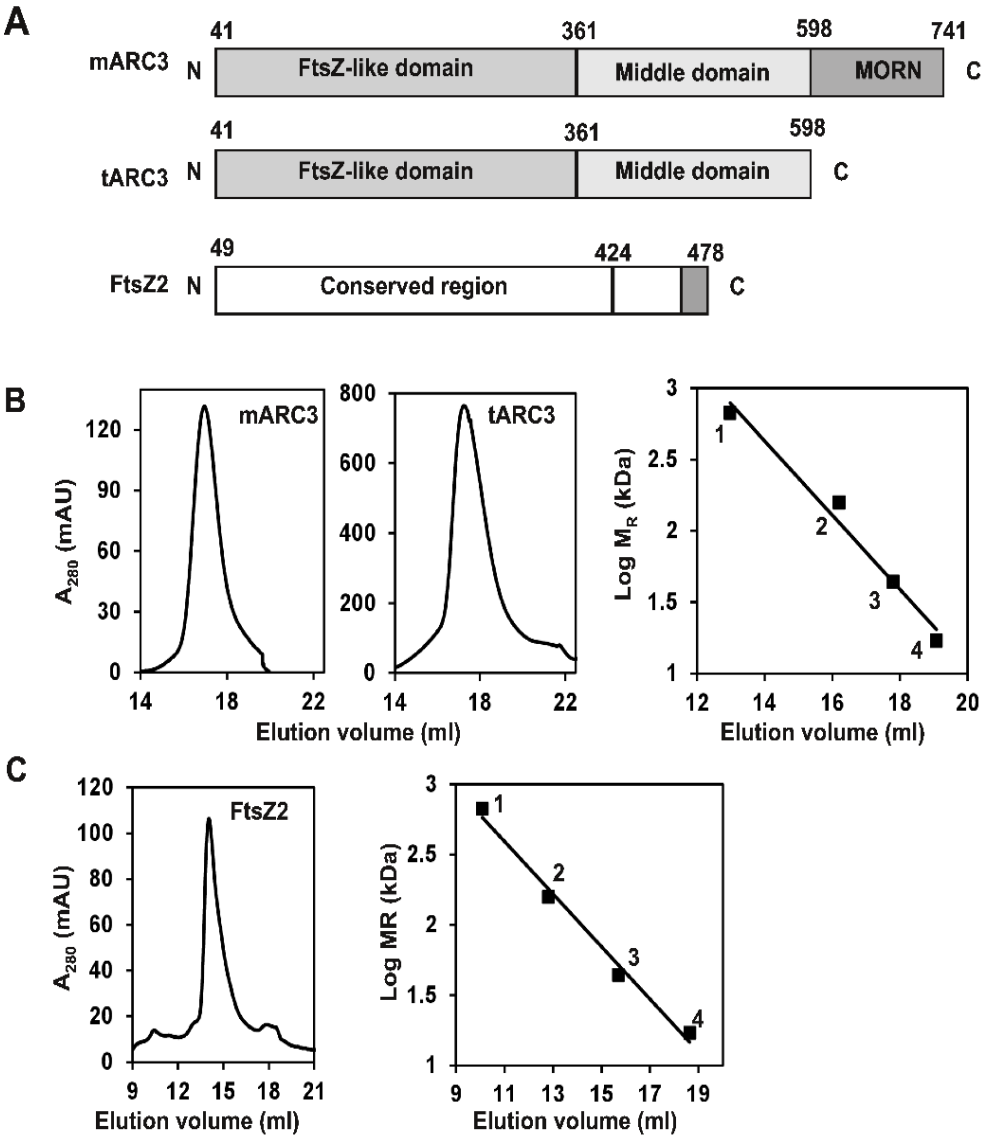

Figure 17. Construct design and purification of recombinant proteins. (A) All constructs were designed without the N-terminal chloroplast transit peptide: A full length, mature form of ARC3 (mARC3), a truncated form of ARC3 (tARC3) lacking the MORN domain, and the mature full-length form of FtsZ2. **(B)** Gel filtration chromatogram (GPC) profiles of mARC3 and tARC3 purified on Superose 6 column. Right panel shows the calibration plot. Standards and their relative molecular mass (M_R): 1, thyroglobulin (670 kDa); 2, bovine γ-globulin (158 kDa); 3, chicken ovalbumin (44 kDa), 4: equine myoglobin (17 kDa). **(C)** GPC elution profile of FtsZ2 purified on SEC650 column. Right panel: elution volume calibration, using the same standards as in (B).

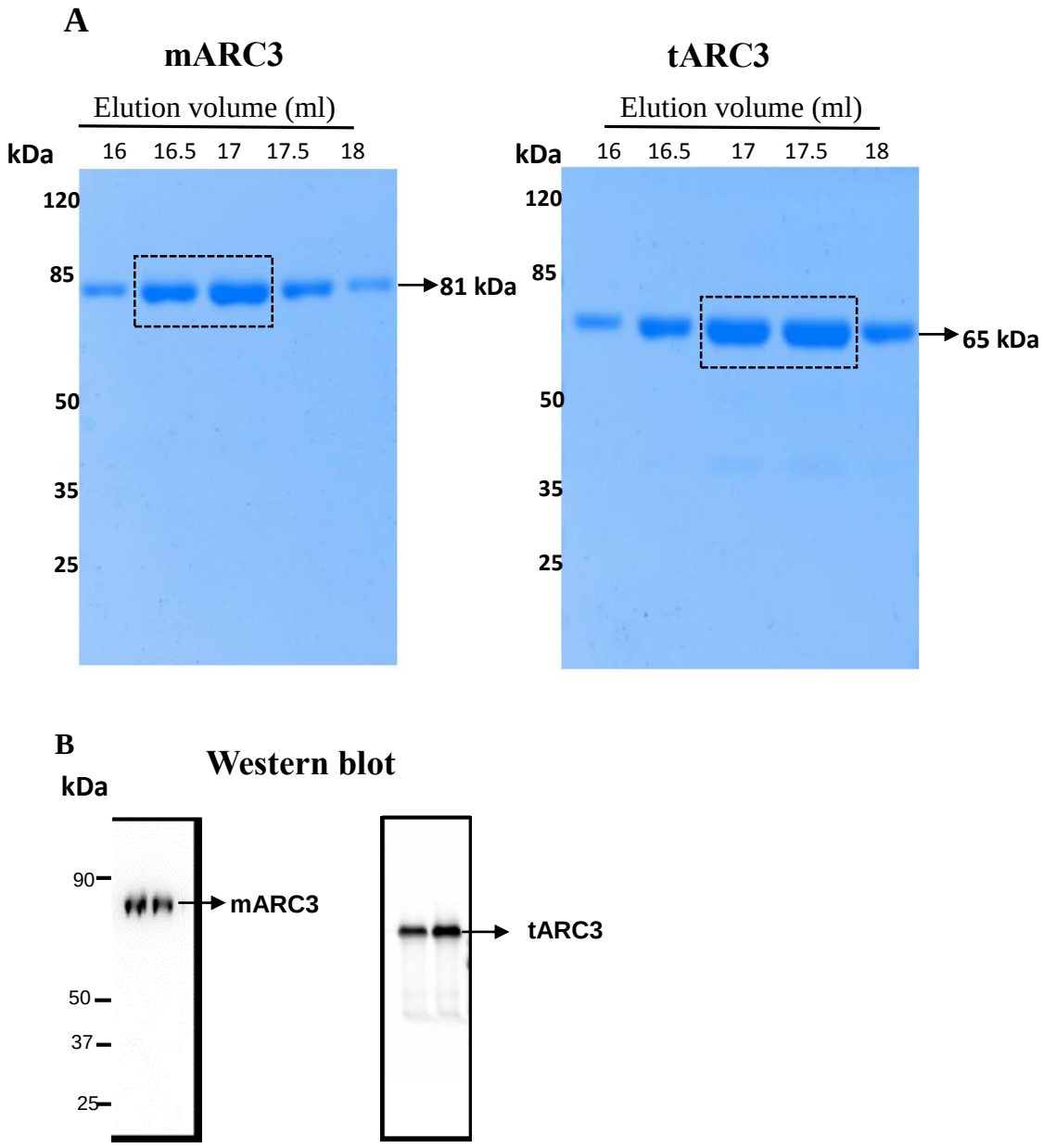

Figure 18. Analysis of purified mARC3 and tARC3 protein fractions. (A) SDS-PAGE and Coomassie Blue staining and **(B)** Western blot analysis of the fractions outlined by box in (A).

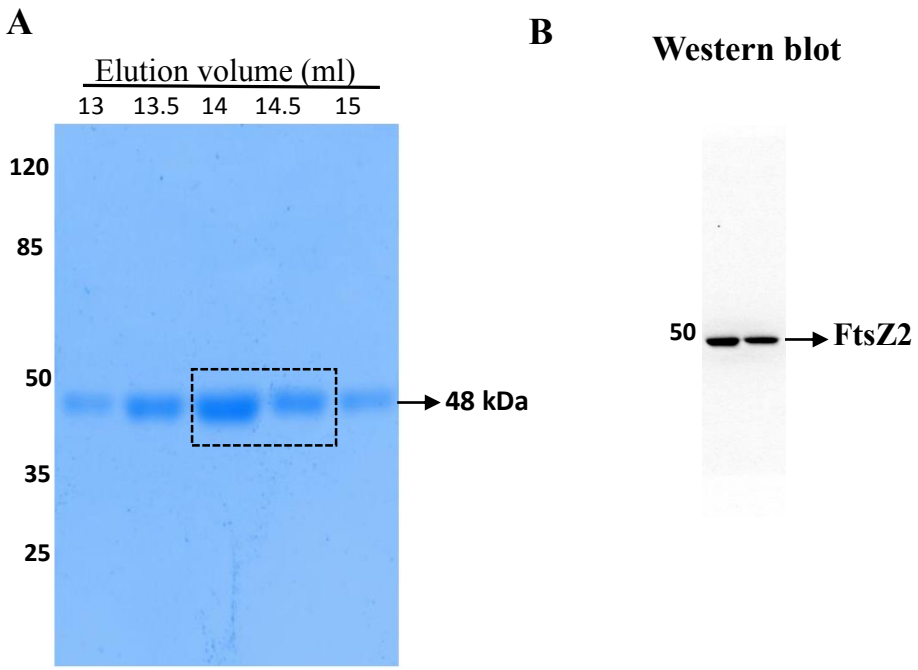

Figure 19. Analysis of purified FtsZ2 protein fractions. (A) SDS-PAGE and Coomassie Blue staining of peak fractions from FtsZ2 GPC. **(B)** Western blot analysis of the fractions outlined by box in (A).

All of the constructs were designed without the N-terminal chloroplast transit peptide that is cleaved upon import into the chloroplast (Figure 17A). Gel Permeation Chromatography of mARC3 and tARC3 revealed a single peak with relative molecular mass corresponding to a monomer (Figure 17B), while FtsZ2 eluted as a single peak corresponding to a dimer (Figure 17C) consistent with a previous report [56]. Peak fractions from each of the above purifications were used to verify the purity of the recombinant proteins by SDS-PAGE and Coomassie Blue staining (Figure 18 and 19). The identity of the recombinant proteins was confirmed by Western blots with anti-cmyc or anti-histidine antibodies (Figure 18 and 19).

ARC3 and FtsZ2 assembly

Transmission electron microscopy, light scattering, FtsZ GTPase activity, and FtsZ polymer sedimentation assays were employed to understand the ARC3-mediated modulation of FtsZ2 assembly/disassembly. These assays employed the active, truncated form of ARC3 (tARC3) without the MORN domain.

Light scattering provides a useful measure of FtsZ2 polymerization and filament bundling as the light scattering signal is directly proportional to the extent of polymerization. Increased levels of light scattering indicate extensive polymerization, no change in light scattering a steady state, and a decrease in light scattering means depolymerization and debundling [57]. In assembly reactions with FtsZ2 and tARC3, the slope and maximum level of light scattering was inversely proportional to tARC3 concentration (Figure 20A) indicating that tARC3 inhibition of FtsZ2 assembly is concentration-dependent. These results are consistent with a previous report by Zhang at al., [44]. In sedimentation assays of the same reaction mixtures, the amount of FtsZ2 in the pellet was proportionally reduced with increased concentration of tARC3 (Figure 20B, C), again indicating that tARC3 inhibits FtsZ2 polymerization in a quantitative manner. In control reactions with the inactive, full length mARC3 the amount of FtsZ2 in the pellet did not change with increasing concentrations of mARC3 (Figure 20D). The mARC3 remained in the supernatant indicating that mARC3 is unable to interact with FtsZ2, consistent with previous reports [39, 44].

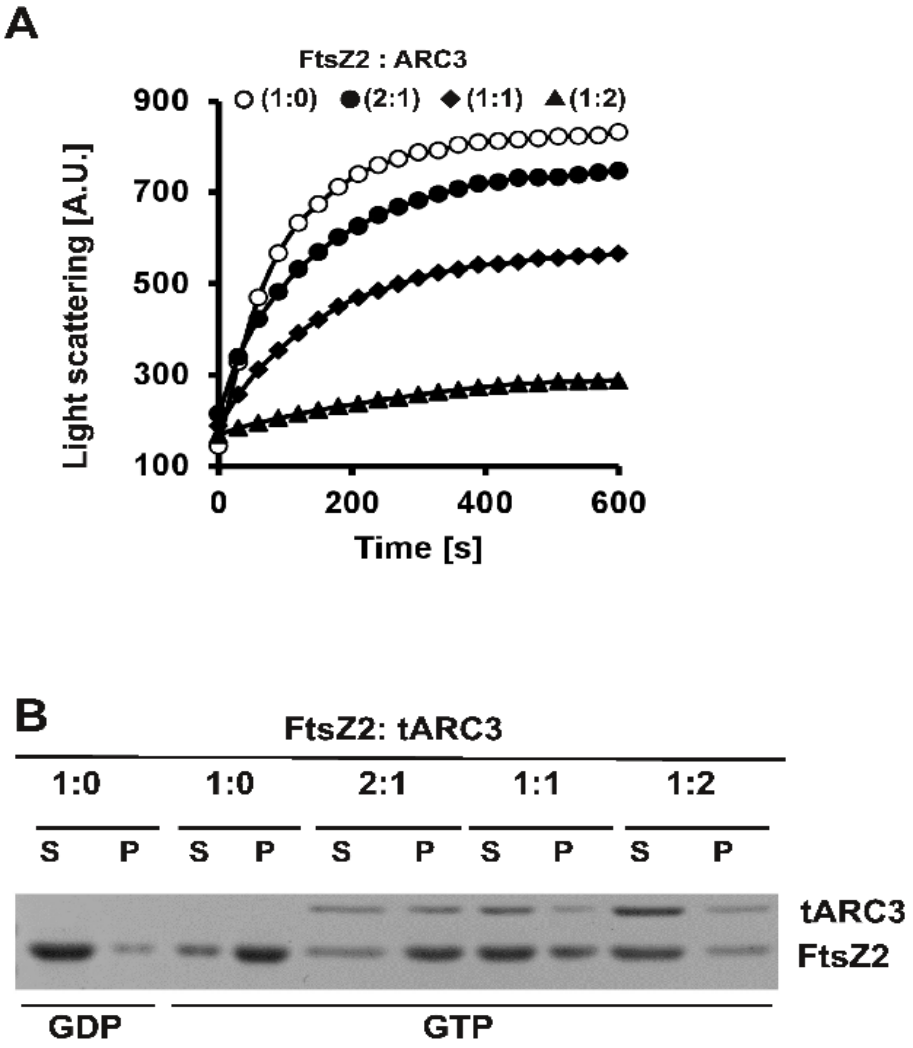

Figure 20. Concentration-dependent ARC3-mediated inhibition of FtsZ2 assembly. **(A)** Light scattering assay. FtsZ2 (4 µM) was polymerized with increasing concentrations of tARC3 (0-8 µM. Assembly was triggered with addition of 1mM GTP. **(B)** FtsZ2 Sedimentation assay. The amount of tARC3 and FtsZ2 in the pellet (P) and supernatant (S) fractions was analyzed by SDS-PAGE and Coomassie Brilliant Blue staining. The nucleotide used in the assembly reactions is indicated below the gel lanes. **(C)** Quantification of pelleted FtsZ2 from assembly reactions with increasing amount of tARC3, from a gel shown in (B). The amount of FtsZ2 alone pelleted was set at 100%. Error bars represent ± SD (n=3). **(D)** Sedimentation assay from a control experiment, using the inactive mARC3 protein.

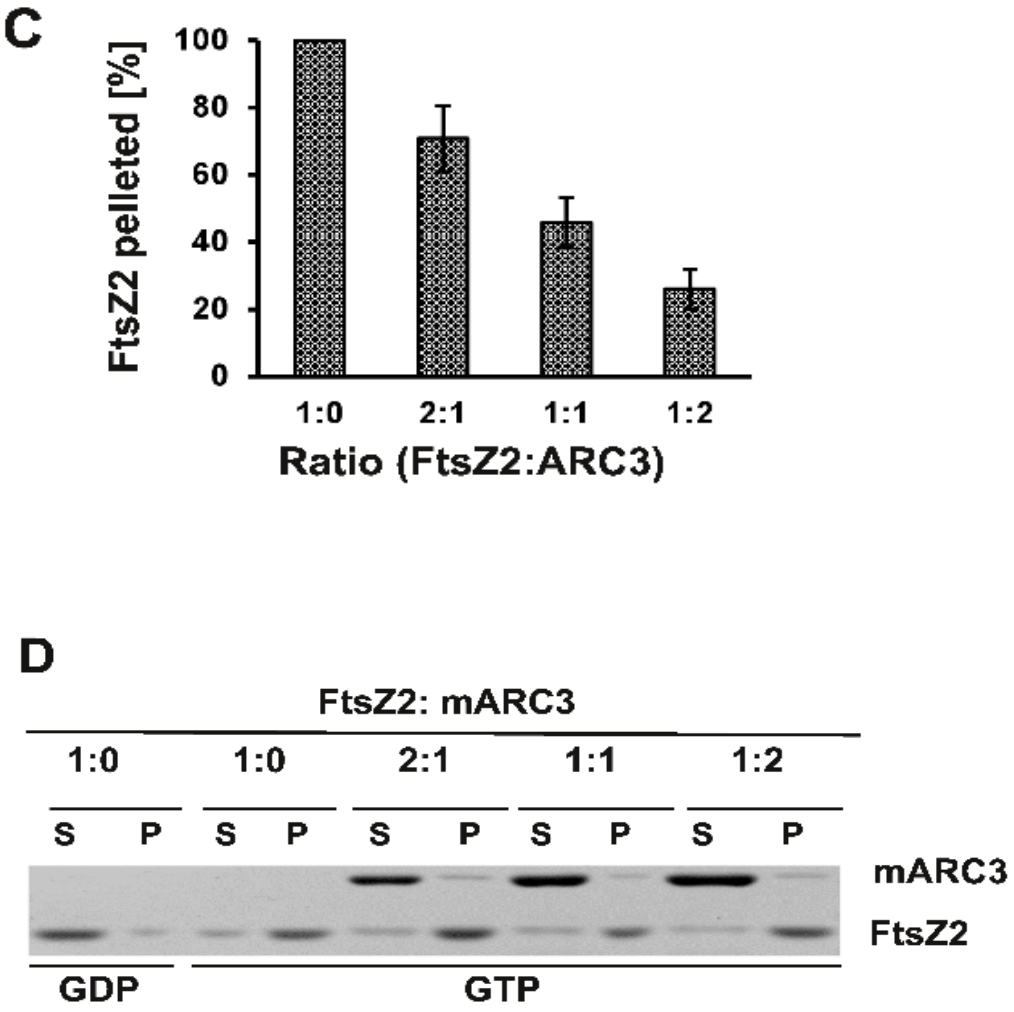

Figure 20 Continued.

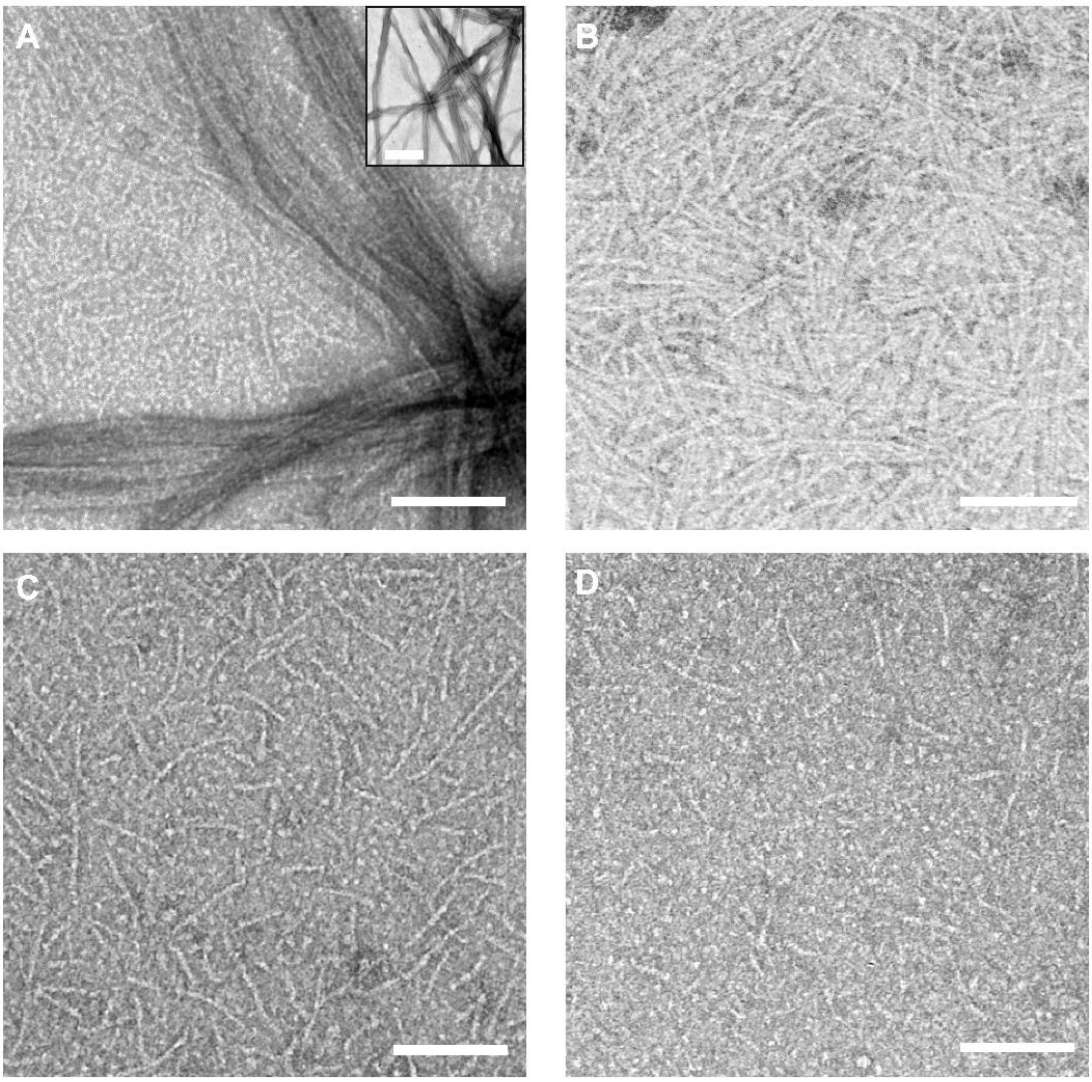

Figure 21. Effect of ARC3 on FtsZ2 filament bundling. Representative electron micrographs of 4 µM FtsZ2 polymerized **(A)** in the absence or presence of 2 µM **(B)** 4 µM **(C)** or 8 µM **(D)** tARC3. The inset in (A) shows a lower-magnification view of FtsZ2 filament bundles. Scale bars represent 100 nm.

ARC3 promotes FtsZ2 filament debundling

Although ARC3 bears very little sequence similarity with MinC [47], it has been suggested to be a functional replacement for bacterial MinC based on its localization pattern similar to MinC [39], the fact that ARC3-deficient mutants show multiple constrictions in the chloroplasts and misplaced Z-rings [39, 44] and that ARC3 inhibits FtsZ1 and FtsZ2 filament formation *in vivo* in the heterologous *S. pombe* expression system [44, 45]. To explore this possibility, we studied the FtsZ2 assembly in the absence/presence of tARC3 by transmission electron microscopy [58].

TEM of negatively stained assembly reactions at end-point (10 min) revealed large FtsZ2 filament bundles with FtsZ2 alone (Figure 21A). The presence of tARC3 in assembly reactions eliminated the large bundles and resulted in shorter, thin filament bundles suggesting that ARC3 affects longitudinal interactions and also interferes with lateral associations between FtsZ filaments. The severity of the effect correlated with increased tARC3 concentrations (Figures 21B-D).

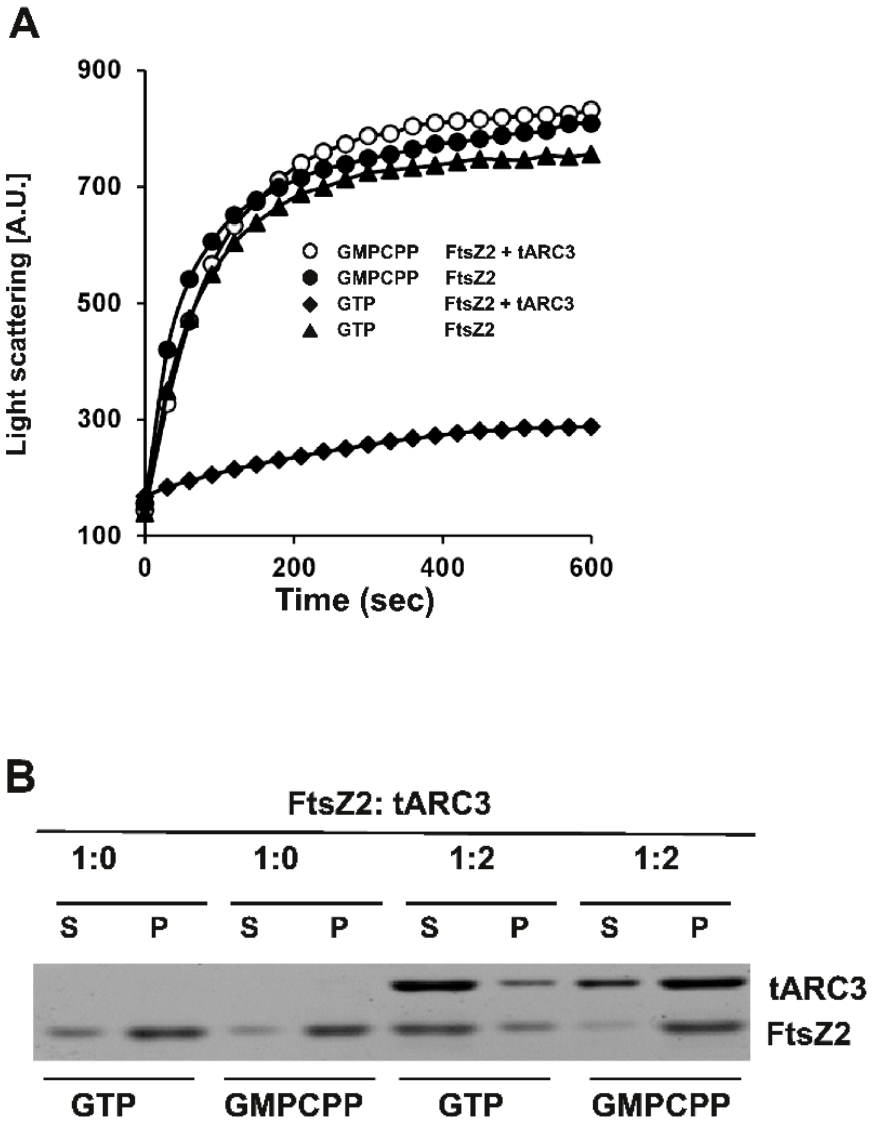

Figure 22. Effect of nucleotides on ARC3-mediated inhibition of FtsZ2 assembly. (A) Light scattering assay of FtsZ2 assembly in the absence/presence of tARC3. Assembly was triggered with GTP or GMPCPP. **(B)** Sedimentation assay showing the effect of tARC3 on FtsZ2 polymers in the presence of GMPCPP. The pellet (P) and supernatant (S) fractions were analyzed by SDS-PAGE and Coomassie Brilliant Blue staining. **(C)** FtsZ2 was polymerized with GTP or GMPCPP for 5 minutes, then tARC3 or assembly buffer was added and light scattering monitored for additional 5 min. **(D)** Representative electron micrograph of FtsZ2 polymerized with GTP for 5 min, before the addition of tARC3. **(E)** 5 min after tARC3 was added. Scale bars represent 100 nm.

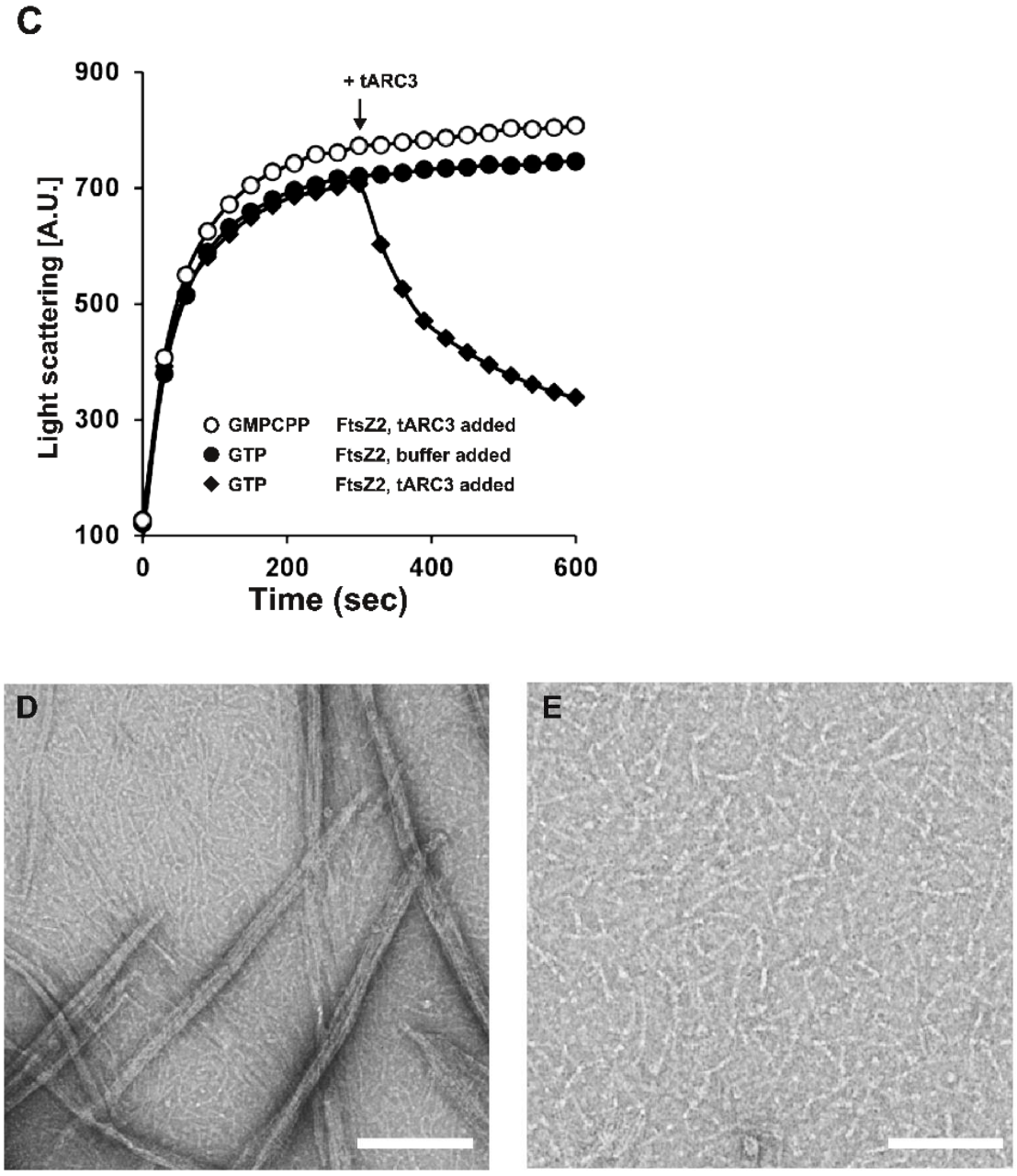

Figure 22 Continued.

Importance of GTP hydrolysis for ARC3 effect on FtsZ2 filaments

The interaction of two FtsZ molecules during polymerization leads to the formation of an active site for GTP hydrolysis, thus polymerization is a prerequisite for GTP hydrolysis [59, 60]. After hydrolysis of GTP to GDP, the GDP-bound FtsZ molecules rapidly dissociate from the filament and are replaced by a new GTP-bound FtsZ molecule. This rapid turnover is a characteristic feature of FtsZ filaments in both bacteria and plant chloroplasts [45, 46, 61]. Negative regulators of bacterial FtsZ assembly including SulA and MinC require FtsZ GTP hydrolysis in order to exert their inhibitory effect on FtsZ assembly, although SulA and MinC act by very different mechanisms [32, 62]. SulA directly inhibits FtsZ polymerization whereas MinC act by debundling the existing filaments [32, 63]. The nucleotide occlusion factor SlmA also requires FtsZ GTPase activity to antagonize FtsZ assembly [64]. Since debundling of FtsZ2 filaments by ARC3 seemed similar to the effect of MinC, it was tested whether GTP hydrolysis and subunit turnover are required for ARC3 mediated inhibition of FtsZ2 assembly. Therefore, GTP in assembly reactions was replaced with GMPCPP, a slowly-hydrolysable analog of GTP [32]. Filaments assembled with GMPCPP essentially contain only GTP and no GDP and are thus rendered more stable, with negligible disassembly or FtsZ2 turnover. In the absence of tARC3, FtsZ2 assembled at the same rate in reactions with either GTP or GMPCPP. When tARC3 was present, FtsZ2 assembly was reduced in reactions with GTP, but not in GMPCPP-containing reactions (Figure 22A). These results were confirmed by sedimentation analysis, where GMPCPP-containing reactions were

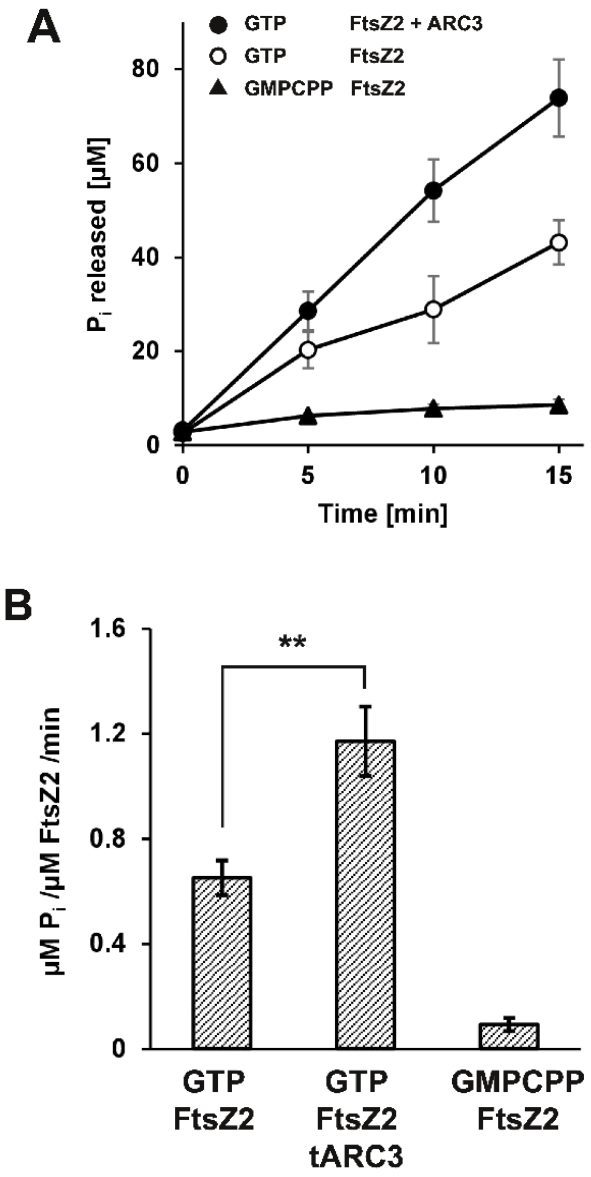

Figure 23. Effect of ARC3 on FtsZ2 GTPase activity. FtsZ2 was polymerized in the presence or absence of tARC3 with GTP or GMPCPP. GMPCPP served as control. Reaction were incubated at room temperature for 5, 10 or 15 min. **(A)** The amount of inorganic phosphate (Pi) released over time. Error bars represent ± SD (n=3). **(B)** The rate of GTP hydrolysis measured as µM P_i released per µM FtsZ2 per min. Error bars represent ± SD (n=3); ** indicates a significant difference ($p < 0.01$, Student's t-test).

insensitive to tARC3 (Figure 22B). This suggests that tARC3 does not simply inhibit FtsZ polymerization but acts upon FtsZ dynamics (turnover). In a complementary experiment, addition of tARC3 to pre-assembled FtsZ2 caused rapid disassembly in reactions with GTP, while no effect was seen in GMPCPP-containing reactions (Figure 22C). Together with the TEM analysis of samples before and after addition of tARC3 (Figure 22D, E), these results confirmed that tARC3 acts as a disassembly factor that accelerates fragmentation and depolymerization of existing FtsZ2 filaments.

ARC3 enhances GTPase activity of FtsZ2

Negative regulators of bacterial FtsZ assembly have varied effects on its GTPase activity. For example, EzrA and MipZ enhance FtsZ GTPase activity [65, 66]. SulA and MciZ inhibit FtsZ GTPase activity [63, 67]. MinC and SlmA do not affect FtsZ GTPase activity at all [68, 69].

Here, the presence of ARC3 in FtsZ2 reactions lead to increased levels of free phosphate release over time compared to FtsZ2 alone reactions (Figure 23A). GTPase activity of FtsZ2 alone (0.68 μM Pi/μM FtsZ2/min) was comparable to previous report [22], while the GTPase activity in the presence of ARC3 (1.14 μM P_i/μM FtsZ2/min) was significantly higher ($p<0.01$) (Figure 23B). In replicate experiments (n=3), FtsZ2 GTPase activity increased by 1.6-1.9 fold in the presence of tARC3. Control reactions with the stable GTP analogue GMPCPP had minimal levels of phosphate released over the same duration. Since GDP-bound FtsZ molecules in the assembled filament have higher unbinding (dissociation) rates than the GTP-bound subunits, increased GTPase activities correlate with higher turnover of FtsZ filaments and vice versa [17, 18]. A study *in planta*

A

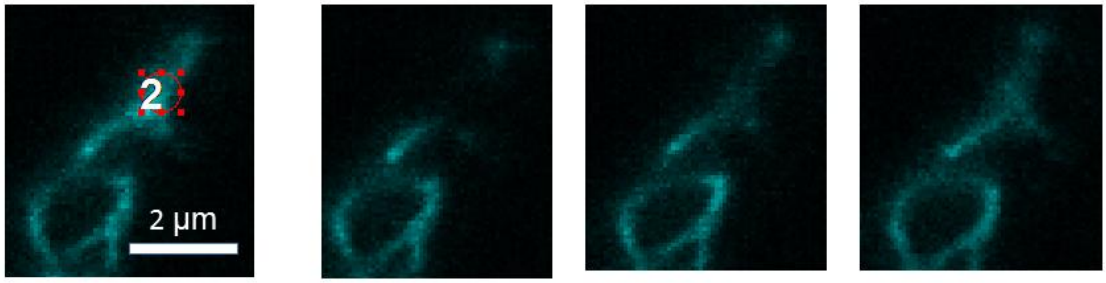

Pre-bleach | Post-Bleach; T=1.6s | Post-Bleach; T= 61s | Post-Bleach; T= 121s

B

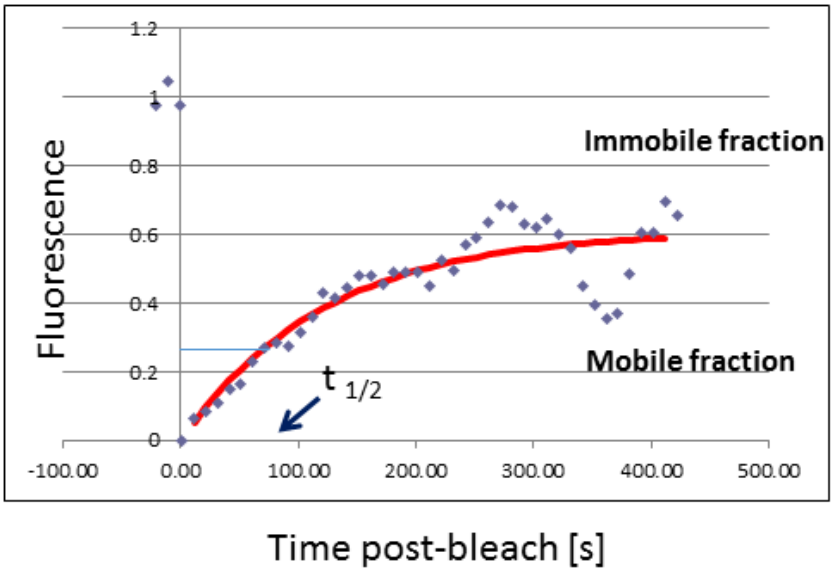

Figure 24. Effect of ARC3 on FtsZ2 turnover. FtsZ2 turnover was measured with FRAP. **(A)** Prebleach and post bleach images. The dotted region indicates the region of interest (ROI) before bleaching. The recovery of fluorescence in the photobleached section of the filament was recorded in a time-lapse sequence. **(B)** Fluorescence recovery curve in bleached ROI, after background subtraction, correction for fading and normalization.

confirmed that ARC3 increases FtsZ turnover [46].

Effect of ARC3 on FtsZ2 turnover in Schizosaccharomyces pombe

FtsZ2-mCFP and tARC3-mYFP were expressed in *Schizosaccharomyces pombe* (*S. pombe*) *S. pombe* and the FtsZ2 turnover was measured by FRAP analysis as described before [44, 46]. The half time to fluorescence recovery ($t_{1/2}$) of FtsZ2-mCFP in the absence and presence of tARC3-mYFP was 176 s ± 131 (n=10) and 139 s ± 67 (n=7), respectively. The corresponding percentage recovery of fluorescence in the absence and presence of ARC3 was 34 ± 26 and 57 ± 13, respectively (Figure 24 A, B).

Discussion

ARC3 effect is concentration-dependent

In the current study the mechanism of the ARC3-mediated effect on FtsZ2 assembly and the structural/functional significance of the MORN domain were investigated. The finding that the tARC3 effect is concentration-dependent (Figure 20A) and that tARC3 turn pre-assembled FtsZ2 bundles into thinner and shorter assemblies (Figure 21) suggested that tARC3 prevents longitudinal and lateral contacts between FtsZ subunits. similar to bacterial MinC [32]. Co-sedimentation assays confirmed the quantitative relationship between tARC3 concentration and FtsZ assembly (Figure 20B). In contrast to tARC3, mARC3 did not co-pellet with FtsZ2 at any of the molar ratios tested confirming the previous reports that the MORN domain prevents interaction between ARC3 and FtsZ2 [39, 44]. In chloroplasts, ARC3 is believed to be activated by interaction of the inner envelope membrane protein PARC6 with the MORN domain of ARC3 [42]. The concentration- dependent effect of ARC3 on FtsZ2 combined with the dependency

on PARC6 interaction may offer an effective way of preventing aberrant Z-ring formation at the poles, similar to MinC [70].

ARC3-mediated FtsZ2 disassembly requires GTP hydrolysis

The results presented in this report suggested that ARC3 may affect the integrity of the FtsZ2 filaments disrupting the physical contacts leading to debundling and disassembly. Recent data with Fluorescence Recovery After Photobleaching (FRAP) analysis in chloroplasts indicated that ARC3 enhances FtsZ turnover [46] suggesting that ARC3 is a disassembly factor acting on pre-assembled filaments. FtsZ filaments in chloroplasts are highly dynamic [46], with individual FtsZ molecules in the filament being incorporated and then rapidly replaced. This dynamic behavior (turnover) is controlled by GTP binding and hydrolysis. Experiments employing the GTP analog GMPCPP provided an environment with virtually no disassembly or turnover of FtsZ2 molecules in and out of the assembled filaments. The lack of effect of tARC3 in GMPCPP-containing reactions demonstrated that tARC3 does not function by inhibiting FtsZ polymerization but rather causes decomposition of FtsZ filaments contingent upon GTP hydrolysis. These results also point that ARC3 requires FtsZ2 GTPase activity to exert its effect on FtsZ2, similar to prokaryotic disassembly factors such as MinC and SlmA [32, 64].

ARC3 enhances FtsZ2 GTPase activity

As the active site for GTPase activity forms only when two FtsZ monomers combine [60], FtsZ assembly is a prerequisite for GTPase activity. GTP hydrolysis, in turn, promotes dissociation of the GDP-bound FtsZ from the filament, where a new, GTP-bound molecule takes its place. Our results indicated that tARC3 increased FtsZ2 activity

and presumably caused a shift in the ratio of GTP bound to GDP bound monomers in the filament towards the GDP-bound form. This would thus promote rapid disassembly and an increase in FtsZ turnover. Although the enhancement in GTPase activity reported in this study is not large, only 1.6 to 1.9-fold increase at a 1:2 FtsZ2:tARC3 molar ratio, it has been shown that even such changes in GTPase activity affect FtsZ assembly dynamics. For example, bacterial MipZ and EzrA contribute to FtsZ assembly dynamics with similar (1.5 to 2-fold) increase in FtsZ GTPase activity [65, 66]. The moderate increase in GTPase activity indicate that ARC3 might reduce the duration of the steady-state phase or decrease the energy required for hydrolysis due to binding and conformational change (rather than directly contributing amino acid residue for hydrolysis) leading to rapid disassembly and enhanced turnover.

ARC3 enhances FtsZ2 turnover

Since the rates of Z-ring turnover in vivo and of protofilaments turnover in vitro have been shown to correlate with FtsZ GTPase activity [17, 18] we analyzed the effect of ARC3 on FtsZ2 turnover. Previous studies showed that the FtsZ1 recovery was slower in the absence in chloroplasts isolated from plants lacking ARC3 [46]. Our results showed that the half time to fluorescence recovery is decreased and recovery of FtsZ2 is increased in the presence of ARC3, suggesting that ARC3 enhances FtsZ2 turnover. These results are also in agreement with our data showing that the presence of ARC3 results in enhanced GTPase activity.

Materials and Methods

Plasmid constructs for expression and purification of recombinant proteins

Arabidopsis *Arc3* (CIW00127) and *FtsZ2-1* cDNA (U11208) clones were obtained from the Arabidopsis stock center. The TAIR accession number for ARC3 is AT1G75010 and FtsZ2 (AtFtsZ2-1) is AT2G36250. Constructs for recombinant protein expression were created by PCR amplification from a corresponding cDNA using primers with engineered restriction sites (detailed in Supplemental Table I). Primers SK-1 and SK-3 were used for full length mature form of ARC3 (mARC3, amino acid 41-741), primers SK-1 and SK-2 for a truncated form or ARC3 (tARC3, amino acid 49-598) lacking the C-terminal MORN domain, and primers fFt2_F and fFt2_R for a full-length mature form of FtsZ2-1 (FtsZ2, aa 49-478). The forward primers for ARC3 construct also contained a yeast consensus sequence to facilitate expression in yeast.

The amplified ARC3 sequences were digested with *Eco*RI and *Sna*BI and cloned into the pPICZ C vector (Invitrogen). This created a fusion construct with a C-terminal 6xHis and c-myc tags to facilitate recombinant protein purification and detection. The clones were confirmed by sequencing and transformed into the yeast, *Pichia pastoris, X-33 strain* (Invitrogen) by electroporation as described in the Easy Select *Pichia* expression kit (Invitrogen, Carlsbad, CA). Yeast transformants were selected on Zeocin (100 µg/ml) media. Positive clones were grown in basal medium with glycerol (BMGY) at 30 °C to OD_{600} of ~0.4, harvested by centrifugation and resuspended in BMMY with 1% methanol to induce expression [54]. Cells were grown at 30 °C for 48 hours, harvested by centrifugation and lysed in lysis buffer (20 mM Tris-HCl pH 8.0, 500 mM NaCl, 1 mM

phenylmethylsulfonyl fluoride, PMSF) using French press at 30,000 PSI. The lysate was centrifuged at 20,000 x g for 60 min at 4 °C to remove cell debris and the recombinant proteins in the supernatant were purified by affinity chromatography with a nickel sepharose column (His-trap, GE healthcare) followed by gel permeation chromatography (GPC) on a Superose 6 column (GE healthcare) with NGC™ liquid chromatography purification system (Bio-Rad). The purity of GPC eluates was analyzed by SDS- PAGE and Coomassie Blue staining. The protein expression was confirmed by Western blot with an anti-myc-HRP antibody (Invitrogen, 1:5000). The molecular mass of the peak fractions was estimated by comparing the relative molecular mass using the molecular mass standards (Bio-Rad). The standards used were (Fig. 1B, right panel): 1, thyroglobulin (670 kDa); 2, bovine γ-globulin (158 kDa); 3, chicken ovalbumin (44 kDa), 4: equine myoglobin (17 kDa).

For the FtsZ2 construct, the amplified cDNA sequence was digested with *Nde*I and *Xho*I, cloned into the Novagen pET28a vector (EMD Millipore, MA, USA) containing a 6xHis tag sequence. Positive clones were isolated on selection media (Ampicillin 100 µg/ml) and confirmed by sequencing. For expression, the plasmid DNA was transformed into Rosetta™ (DE3) pLysS (Invitrogen) *E. coli* cells. The cells were grown to log phase to an OD_{600} of ~0.6 at 37 °C and induced with 0.45 mM Isopropyl β-D-1-thiogalactopyranoside (IPTG; RPI, Mount Prospect, IL) overnight at 18 °C. Cells were pelleted and lysed in lysis buffer using French press at 20,000 PSI. The lysate was centrifuged at 20,000 x g for 60 min at 4 °C and the recombinant proteins in the supernatant were purified by affinity chromatography with a nickel sepharose column

(His-trap) followed by gel permeation chromatography (GPC) on a ENrich™ SEC650 (Bio-Rad) with NGC™ liquid chromatography purification system (Bio-Rad). The purity of GPC eluates was analyzed by SDS-PAGE and Coomassie Blue staining. The protein expression was confirmed by Western blot with an anti His-HRP antibody (Invitrogen, 1:5000). The molecular mass of the peak fractions was estimated as described above.

Light scattering assays

The extent of polymerization and FtsZ2 assembly in the presence and absence of tARC3 was measured by 90° light scattering. Reactions of 4 μM FtsZ2, 1 mM GTP or the slowly hydrolysable analogue GMPCPP (0.4 mM) in MES pH 6.5 buffer containing 100 mM KCl and 5 mM $MgSO_4$ were mixed and light scattering was monitored using a Hitachi F-4500 fluorescence spectrofluorometer with both the excitation and emission wavelengths set at 350 nm and a slit width of 5 nm. The data was collected continuously for 10 minutes at 25 °C and the temperature was kept constant using a circulating water bath. In disassembly experiments, tARC3 was added to FtsZ2 reactions after 5 minutes of assembly and light scattering was monitored for additional 5 minutes.

Electron microscopy of FtsZ2 filaments

FtsZ assembly reactions in the absence/presence of ARC3 were prepared and incubated as described above. Samples were adsorbed onto carbon-coated grids, negatively stained with a 2% (w/v) aqueous solution of uranyl acetate (pH 4.5) and examined in a JEOL 1200 EX (JEOL Ltd., JAPAN) transmission electron microscope operated at an accelerating voltage of 100 kV. Images were captured at calibrated

magnifications using an optically coupled slow scan CCD camera (model 15C, SIA, Duluth, GA) and Maxim DL imaging software.

Co-sedimentation assays

The extent of FtsZ co-pelleted in the absence or presence of mARC3 and tARC3 was monitored by co-sedimentation assays. FtsZ2 assembly reactions were prepared as above and the polymerization was triggered by adding 1mM GTP, GDP or 0.4 mM GMPCPP. After incubating the reactions for 10 min at room temperature, samples were sedimented for 20 min at 26 psi (~150, 000 x g) in an Airfuge® Ultracentrifuge (Beckman Coulter, Fullerton, CA) with an A-100/30 rotor, at room temperature [56]. The relative amount of FtsZ2 co-sedimented with ARC3 in the pellet versus the supernatant fractions was determined by densitometry in Coomassie Blue-stained SDS-PAGE gels, using ImageJ software [71].

FtsZ2 GTPase activity assay

The GTP hydrolysis activity of FtsZ2 polymers was determined using a malachite green based reagent, BIOMOL® GREEN (Enzo Life Sciences, Farmingdale, NY) in 384-well plates (Greiner Bio-One) as described before [72]. FtsZ2 assembly reactions (50 µl) containing 4 µM FtsZ2 in the absence or presence of tARC3 (8 µM) were prepared. The polymerization was initiated by addition of 1 mM GTP or 0.4 mM GMPCPP. The phosphate released (µM P_i) over time (0, 5, 10 and 15 min) was measured in triplicates at room temperature using Thermo Scientific Multiskan GO (Thermo Fisher Scientific) plate reader. Appropriate blanks containing the assembly buffer alone or the individual proteins without GTP/GMPCPP were subtracted and the GTPase activity was calculated as µM P_i per µM FtsZ2 per min.

CHAPTER III

STRUCTURAL CHARACTERIZATION OF ARC3

Introduction

Although ARC3 has been suggested to be a functional analog of MinC, it bears very little sequence similarity with MinC [39, 47] and no structural data is available for ARC3 to date. Prior data showed that the C-terminal Membrane Occupation and Recognition Nexus (MORN) domain of ARC3 blocks its activity and prevents its interaction with FtsZ1 and FtsZ2 [44]. It was suggested that interaction of the MORN domain with another division protein, PARC6, may activate ARC3 [39, 73]. We hypothesized that ARC3 exists in two conformational states, open and closed. The presence of MORN domain keeps full length ARC3 in closed conformation and thus prevents its interaction with FtsZ. Uncovering the mode of action of ARC3 and determining the structural basis of ARC3 effect on FtsZ assembly is of paramount importance for understanding the role of key regulators of chloroplast division. Since prior studies determined that ARC3 remodels the Z-ring through interaction with FtsZ2, but not FtsZ1 [44], the study presented here is focused on the assembly of FtsZ2 and its regulation by ARC3 We employed a combination of electron and light microscopy, single particle analysis and 3D reconstruction of ARC3 to shed light on the importance of MORN domain in ARC3-PARC6 mediated modulation of FtsZ2 assembly. The schematic of single particle analysis [74, 75] leading to 3D reconstruction is depicted in Figure 25.

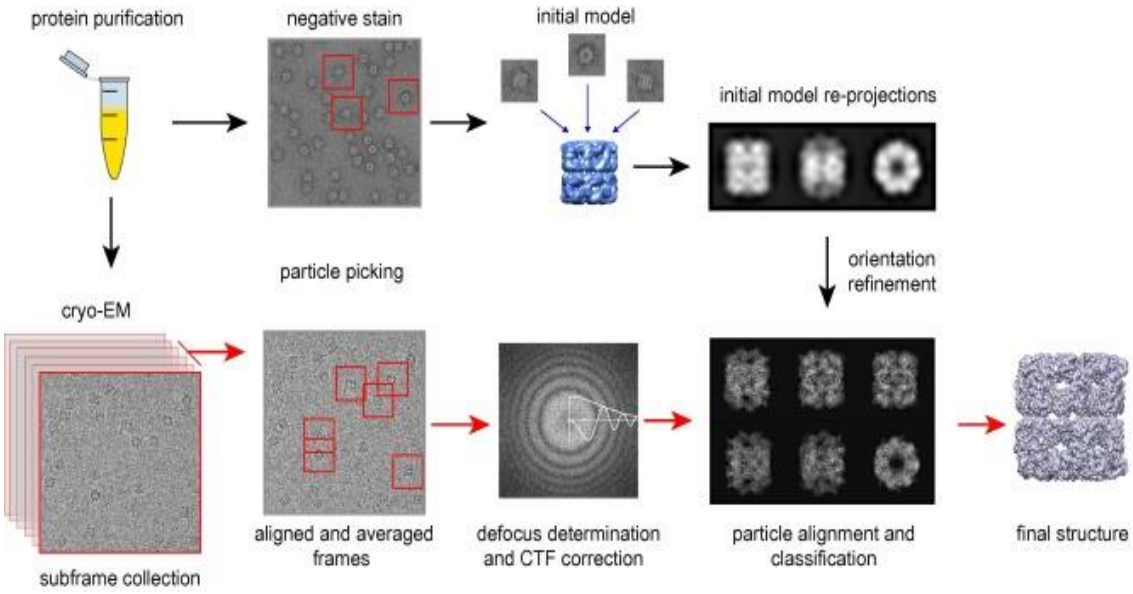

Figure 25. Schematic of single-particle reconstruction. *Protein purification.* High purity of the sample is important, as in crystallography. *Negative stain* is useful to clearly visualize the sample and check its homogeneity, especially for small particles. Particles are boxed from the micrographs, centered and aligned. Classification and averaging give improved SNR, and class averages can be used to obtain a low-resolution *initial model* by common lines or tilt methods. In *cryo-EM*, the vitrified sample is imaged by collecting movie frames that are aligned for motion correction and then averaged. *Defocus determination and CTF correction* are done on motion-corrected averaged images. After alignment, classification and cleaning of the dataset, particles are assigned orientations by projection matching to the initial model. *Orientation refinement* is performed iteratively until the structure converges [75]. Reprinted with permission from Academic Press.

Results

Single particle analysis and 3D reconstruction of ARC3 reveals an almost circular shape

Truncated form of ARC3 (tARC3) lacking the MORN domain, used in the assays described above is biochemically active. In the full length form, mARC3, binding to FtsZ1 and FtsZ2 is blocked by the C-terminal MORN domain [39, 44] in the absence of other accessory proteins. It was suggested that the MORN domain may function as a control switch for ARC3 activity and that interaction of the MORN domain with the chloroplast division protein PARC6 may activate mARC3 [73]. The mechanistic details of this activation were not known. Here, transmission electron microscopy and single particle analysis were employed to determine the three dimensional (3D) structure of mARC3.

Negatively stained TEM images showed monodisperse behavior of mARC3 (Figure 26A) without the tendency to form aggregates and permitted selection of individual particles and generation of class averages (Figure 26B, C). The FSC (Fourier shell correlation) plot (Figure 26D) showed that the refinements converged at a resolution of 3.25 nm based on FSC criterion of 0.5. The asymmetric triangle plot (Figure 26E) confirmed that a large number of independent projections provided a solid basis for sampling the 3D space. The 3D reconstruction revealed an almost circular structure. Segmentation of the 3D structure highlighted three distinct domains corresponding to a molecular mass of approx. 39.5, 24, and 17.5 kDa consistent with the published sequence-based structure [47] of ARC3 that is comprised of an FtsZ-like domain, a middle domain and the MORN domain (Figure 26F). Regardless, whether the assignment of N- and C-

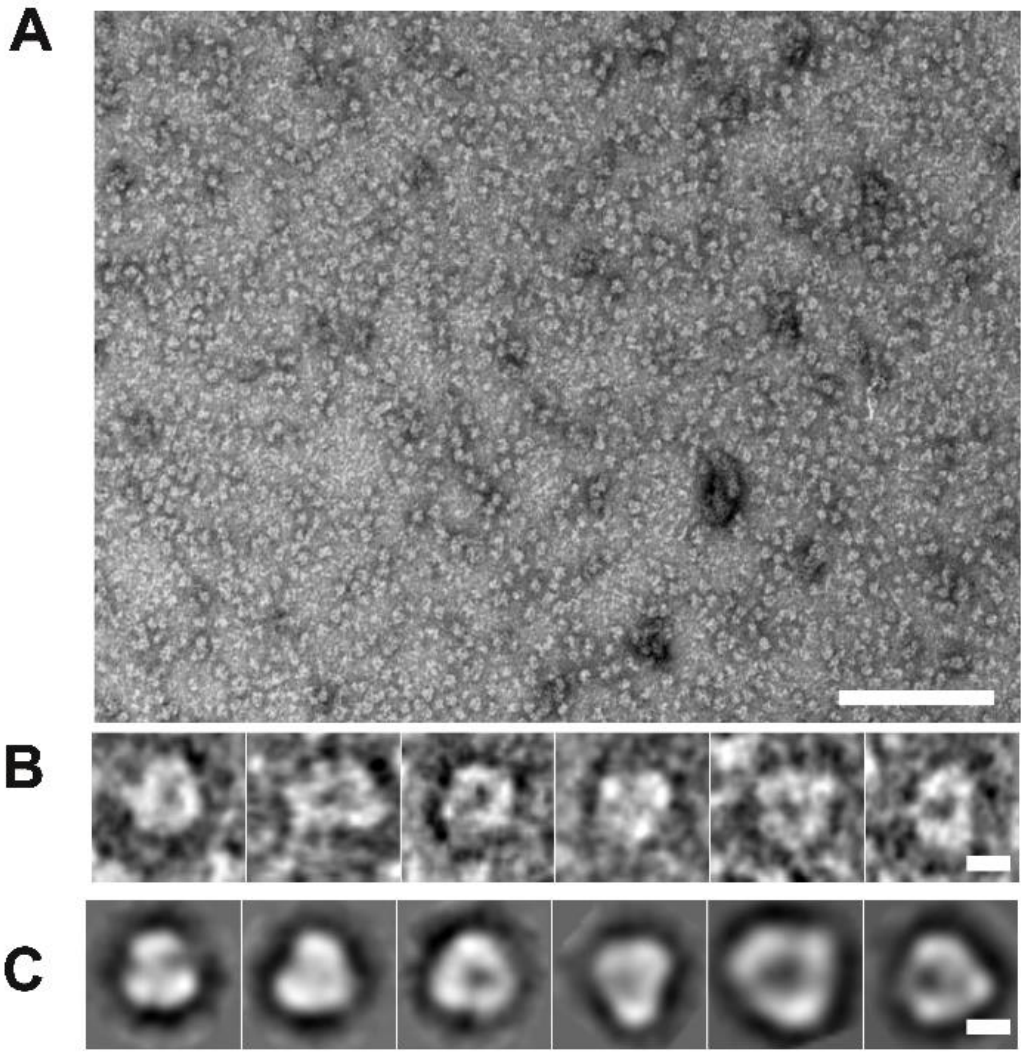

Figure 26. Single particle analysis and 3D reconstruction of mARC3. (A) Raw image of negatively stained protein particles. Scale bar corresponds to 100 nm. **(B)** Representative raw particles, **(C)** Class averages. Scale bar corresponds to 5 nm. **(D)** Fourier shell correlation after 8 iterations of refinement. FSC=0.5 corresponds to 3.25 nm (32.5 Å). **(E)** Asymmetric triangle of final reconstruction representing projection of all Euler angles. **(F)** 3D reconstruction of mARC3, front and side views. The C- and N-termini and the three distinct domains and their suggested identity are shown.

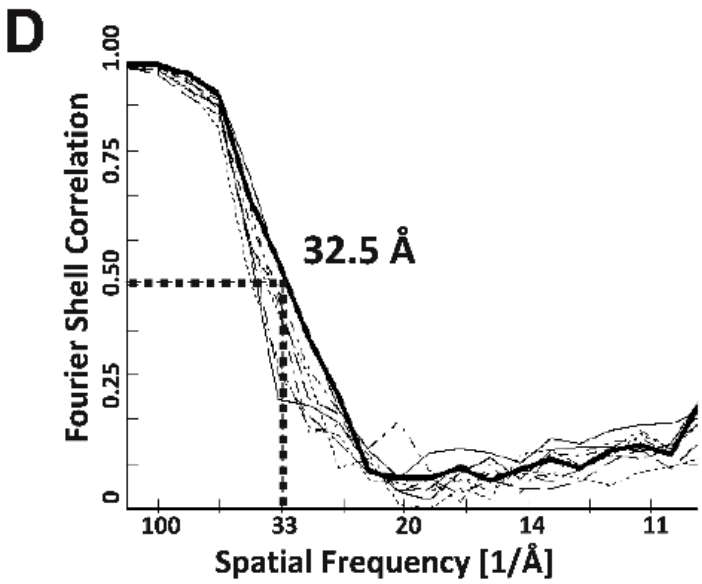

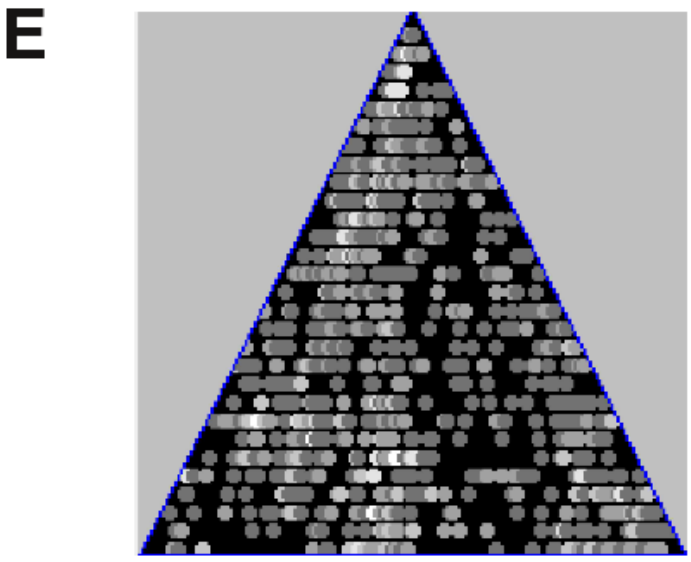

Figure 26 Continued.

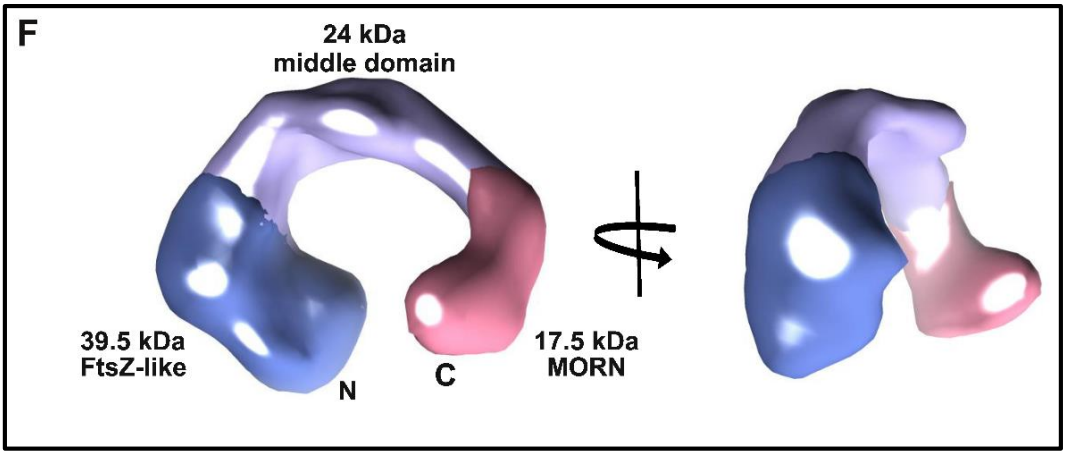

Figure 26 Continued.

terminus identity in the 3D structure were correct or not, the MORN and FtsZ-like domains were clearly in close proximity. This in turn suggests that the MORN domain may inhibit FtsZ binding via steric hindrance and that in order to enable binding of FtsZ (and several other chloroplast division proteins), mARC3 may need to undergo a conformational change to a more open shape.

Homology modeling of ARC3

The homology search for three domains of ARC3 identified templates with usable templates for FtsZ like domain and MORN domain (Figure 27A, B). The search for middle domain did not result in any usable template for model fitting. The results of the homology modeling showed a good fit of the FtsZ and MORN domains with EM density map indicating that the location of these domains in the EM density map is pointing in the right direction (Figure 27C).

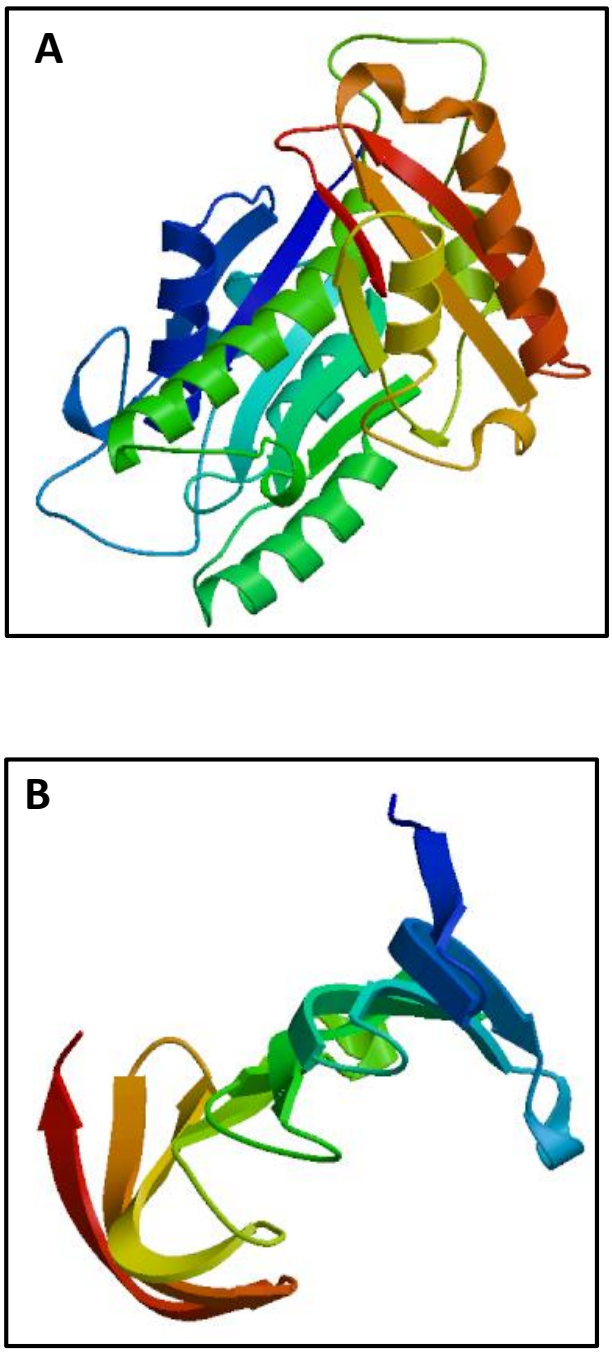

Figure 27. Homology modeling of ARC3. (A) SWISS atomic model of FtsZ-like domain of ARC3 and **(B)** MORN domain of ARC3. **(C)** Fitting of SWISS atomic models of FtsZ-like domain and MORN domain of ARC3 into EM density map of mARC3.

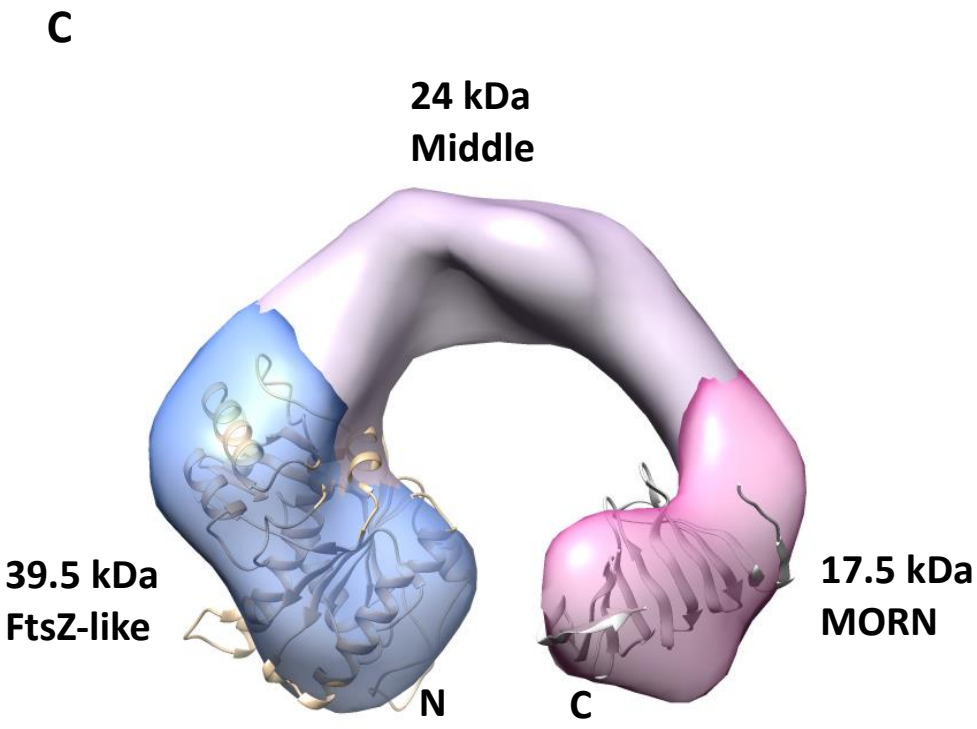

Figure 27 Continued.

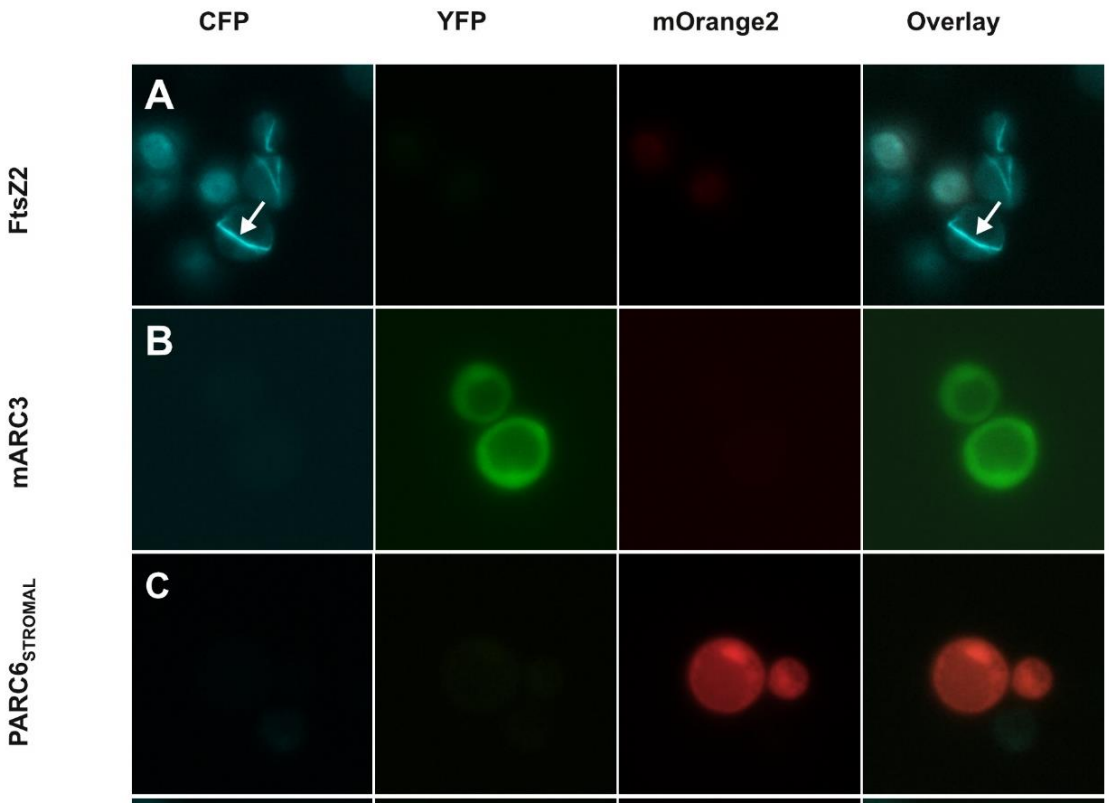

Figure 28. Expression and colocalization in *S. cerevisiae*. Expression of **(A)** FtsZ2-CFP **(B)** mARC3-YFP and **(C)** $PARC6_{STROMAL}$–mOrange2. Coexpression of **(D)** FtsZ2-mCFP and mARC3-mYFP **(E)** FtsZ2-mCFP and $PARC6_{STROMAL}$–mOrange2. (**F)** FtsZ2-mCFP, mARC3-mYFP and $PARC6_{STROMAL}$–mOrange2. Arrows point at the FtsZ2 filaments.

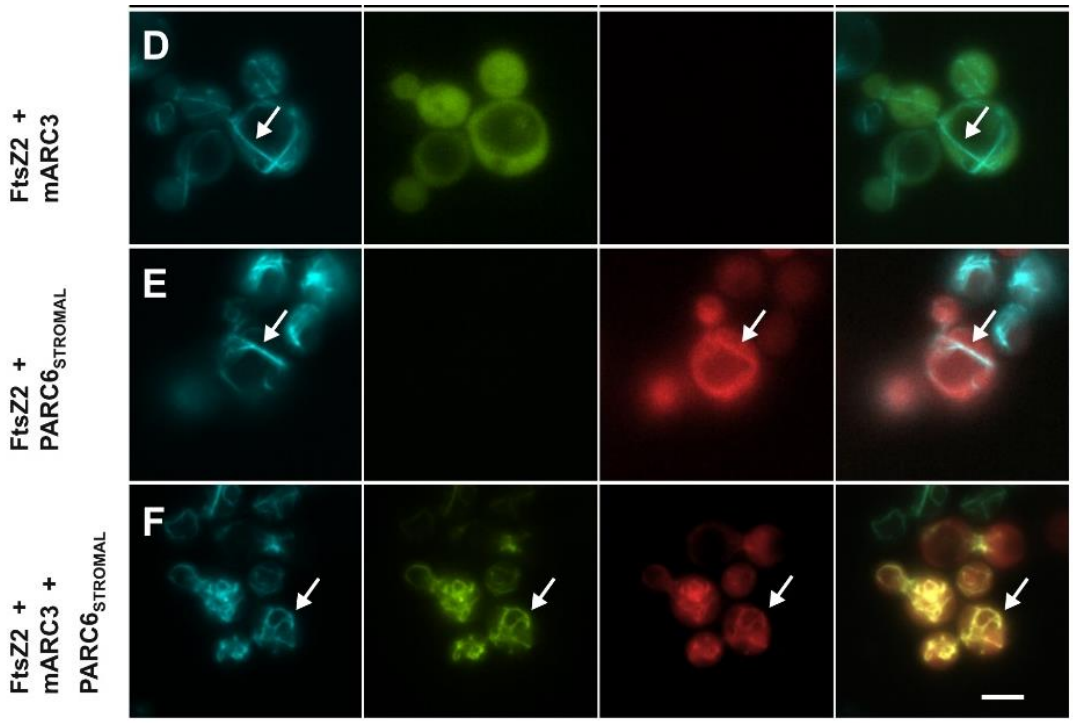

Figure 28 Continued.

Expression and colocalization of fluorescently tagged proteins in S. cerevisiae

All three constructs were expressed successfully in *S. cerevisiae*. FtsZ2-mCFP formed filaments and rings (Figure 28A) in large majority of cells. The mARC3-mYFP and $PARC6_{STROMAL}$–mOrange2 fusion constructs showed a wide range of expression levels among cells from a single colony and showed diffuse localization throughout the cytosol (Figure 28B, C). In cells coexpressing FtsZ2-mCFP with $PARC6_{STROMAL}$–mOrange2, PARC6 was colocalized with FtsZ2 filaments, in addition to diffuse $PARC6_{STROMAL}$–mOrange2 signal throughout the cytosol (Figure 28 E). mARC3-mYFP

coexpressed with FtsZ2-mCFP exhibited diffuse distribution throughout the cytoplasm of the yeast cell and did not show distinct colocalization with FtsZ2-mCFP (Figure 28D). This was the case in all cells over the entire range of mARC3-mYFP signal intensities. However, when $PARC6_{STROMAL}$–mOrange2 was also present, mARC3-mYFP colocalized with FtsZ2 and $PARC6_{STROMAL}$ in filamentous assemblies (arrows in Figure 28F), suggesting that the three proteins formed a complex.

Discussion

Functional implications of the 3D structure of ARC3

The web of interactions between the components of the division machinery is rather complex and we are only beginning to understand the interplay between the individual actors. Previous studies identified specific interactions of ARC3 regions with other chloroplast division proteins: The FtsZ-like domain of ARC3 interacts with FtsZ1 and FtsZ2, the middle domain is sufficient for interaction with AtMinD and AtMinE, and the MORN domain with PARC6 [39, 42, 44]. AtMinD is a plant homologue of bacterial MinD and is a negative regulator of FtsZ assembly [76-78], while AtMinE is a positive FtsZ assembly factor that protects FtsZ from the effect of MinD at the division site [79-81]. PARC6 (paralogue of ARC6) also called CPD1 [82] and ARC6H [83] evolved by gene duplication from PARC6 [23], a positive regulator of FtsZ assembly also located in the inner envelope membrane [23, 84]. PARC6 has an unexpected role as an FtsZ disassembly factor similar to that of MinD but contrary to that of its homolog, ARC6. In the full length ARC3, mARC3, the MORN domain acts as a negative switch that prevents interaction with FtsZ1 and FtsZ2 [44]. Similar effect of the MORN domain on protein

activity was reported for a member of Arabidopsis phosphatidylinositol phosphate kinase family, AtPIPK1 [85].

These findings suggest that MORN domain is critical to the structure and function of ARC3 and may provide a mechanism to modulate ARC3 activity *in vivo*. To gain insight into the activation mechanism we sought to determine the 3D structure of mARC3. 3D reconstruction revealed that mARC3 is almost circularly shaped with the N- and C termini slightly bent toward each other (Figure 26F). This could have functional significance as the proximity of the C- and N-terminal regions in the 3D structure may present a steric hindrance for ARC3 interaction with FtsZ2. In the current 3D model (Figure 26), the assigned identity of the termini, the bulkier N-terminal FtsZ-like domain, and the smaller C-terminal MORN domain was based on thresholding and molecular mass calculations from the 3D reconstruction. Homology modeling of ARC3 supports that the location of these domains in the EM density map indicating that the domains are pointing in the correct direction. The functional implications of the circular shape remain unaffected even if the identity of the termini were in fact reverse. What is significant is the proximity of the termini which leads to the "closed" conformation of the molecule. In chloroplasts, this closed, inactive form of ARC3 must be activated in areas away from the division site to prevent Z-ring formation at "improper" sites. This activation is most likely achieved by interaction with the stromal part of PARC6.

The experiments with fluorescently tagged FtsZ2, mARC3 and PARC6 expressed in yeast *S. cerevisiae* aimed to shed light on these interactions. Colocalization of PARC6 and FtsZ2 was in line with a previous report [73], confirming the direct interaction

between these two proteins. The lack of mARC3 colocalization with FtsZ2 (Figure 28D) was also expected since the presence of the MORN domain hinders mARC3 interaction with FtsZ2 [39, 44]. We hypothesized that binding of PARC6 to the MORN domain of mARC3 may cause a conformational change enabling mARC3-FtsZ2 interaction. The triple colocalization of FtsZ2-mCFP, mARC3-mYFP and $PARC6_{STROMAL}$–mOrange2 (Figure 28F) seems to support this hypothesis. Interestingly, though, the presence of ARC3 in the triple expressing cells did not lead to noticeable disruption or disassembly of FtsZ2 filaments. Zhang et al., [44] showed that the truncated, active form of ARC3 lacking the MORN domain disrupt FtsZ2 filaments when coexpressed at sufficient levels in yeast *S. pombe*. It is possible that mARC3-mYFP levels in the coexpression strains shown here were not sufficient to disassemble FtsZ2 filaments, or that the triple colocalization is a result of PARC6 interaction with both FtsZ2 and mARC3 rather than being indicative of mARC3 activation and direct interaction with FtsZ2. Future studies should shed light on this matter.

Materials and Methods

Single particle analysis and 3D reconstruction of mARC3

The purified full length ARC3 protein mARC3 (60 µg/ml) was adsorbed (10 s) onto carbon-coated grids and negatively stained with a 2% (w/v) aqueous solution of uranyl acetate (pH 4.5) following the method described by Valentine et al. [86]. Specimens were observed in a JEOL 1200 EX transmission electron microscope (JEOL Ltd., JAPAN) operated at an acceleration voltage of 100 kV. Electron micrographs were recorded at calibrated magnifications using a 3k slow-scan CCD camera (model 15C, SIA). Single

particle averaging and 3D modeling was carried out using routines in the EMAN software package [87]. Segmentation and identification of individual domains within the 3D structure was performed with the interactive visualization software Chimera [88, 89].

Homology modeling of ARC3 using Chimera

Homology modeling of ARC3 was performed for each of the three domains (FtsZ-like domain at the N-terminus, novel middle domain and MORN like C-terminal domain) of ARC3 on the SWISS-Model work space [90-92]. Three models were obtained for FtsZ-like domain and three models for MORN domain. Among these, the best template models were selected (based on the sequence identity, coverage etc.). Homology search for the middle domain (novel domain) did not yield any usable models due to poor matching with the available sequences in the database. The selected SWISS atomic models of FtsZ and MORN domains were fit into the existing EM density map (Figure. 23) using the "Fit in Map" function [93, 94] of the interactive visualization software, Chimera [89].

Fluorescence Microscopy and Image Analysis

Colonies of *S. cerevisiae* cells carrying the fluorescently tagged proteins of interest were picked and resuspended in small amount of water. The suspension (2 µl) was deposited on slides coated with poly-L-Lysine, covered with No. 1.5 coverslip and imaged on Olympus IX-81 fluorescence microscope (Olympus America Inc., Waltham, MA) equipped with a 60 × /1.2 water immersion objective and filter cubes for each of the fluorescent proteins (excitation and emission 426-446 nm and 460-500 nm for mCFP, 490-510 nm and 520-550 nm for mYFP, and 530-560 nm and 575-645 nm for mOrange2). Z-stacks with 0.5 µm step and pixel size corresponding to 0.108 µm were collected using

Photometrics Prime sCMOS camera controlled by the Micro-manager free software [95]. Images were viewed and contrast adjusted in ImageJ freeware [96].

CHAPTER IV

CONCLUSIONS AND FUTURE DIRECTIONS

Conclusions

Model for the ARC3 mediated modulation of FtsZ2 assembly

The results presented in this report provide a foundation for understanding structural and functional aspects of FtsZ assembly regulation by ARC3.

In the absence of ARC3, FtsZ1 and FtsZ2 co-assemble longitudinally and laterally leading to formation of protofilaments and bundles that give rise to the Z-ring as a key structure in the formation of the division machinery. The Z-ring is a dynamic structure involving continuous assembly and disassembly of FtsZ subunits. The lateral bonds between FtsZ subunits are weaker than longitudinal bonds [32]. Since ARC3-mediated inhibition of FtsZ2 assembly requires GTP hydrolysis, ARC3 may preferentially bind to GDP-FtsZ subunits and also bind where two subunits interact laterally. Binding of ARC3 could lead to conformational change and rapid dissociation and exchange of subunits causing FtsZ debundling, enhancing GTPase activity and turnover (Figure 29).

Model of interaction of ARC3 with PARC6

The MORN domain in full length form of ARC3 (mARC3) prevents interaction of mARC3 with FtsZ2 and other accessory proteins except PARC6 [39, 44, 73]. In the absence of interaction with PARC6, the MORN renders ARC3 to be in a “closed” conformation that hinders FtsZ binding. Interaction of PARC6 with ARC3 results in an

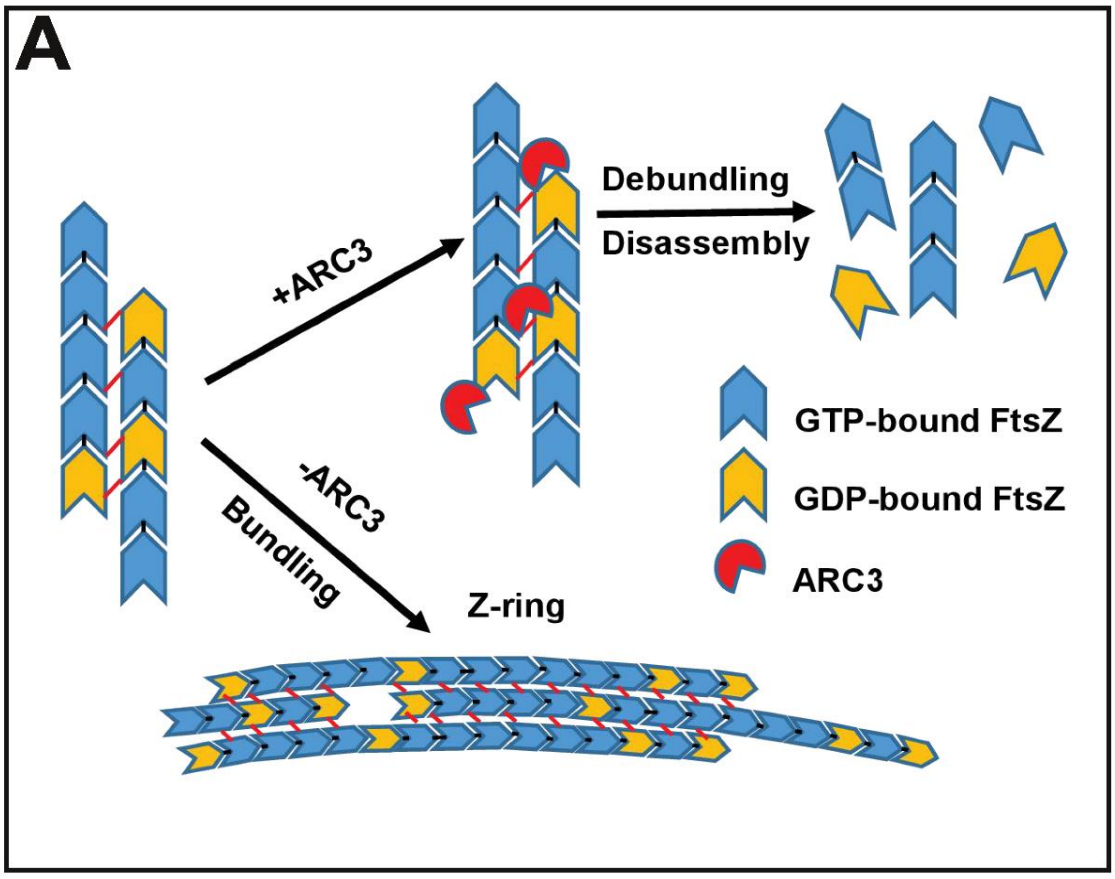

Figure 29. Model of FtsZ2 filament remodeling by ARC3. In the absence of ARC3, GTP-bound FtsZ2 molecules associate longitudinally and laterally to form bundles of protofilaments and finally the Z-ring at mid-chloroplast. In the presence of active ARC3, binding of ARC3 to FtsZ2 disrupts longitudinal and lateral interaction within the filaments and filament bundles, leading to debundling and disassembly of FtsZ filaments.

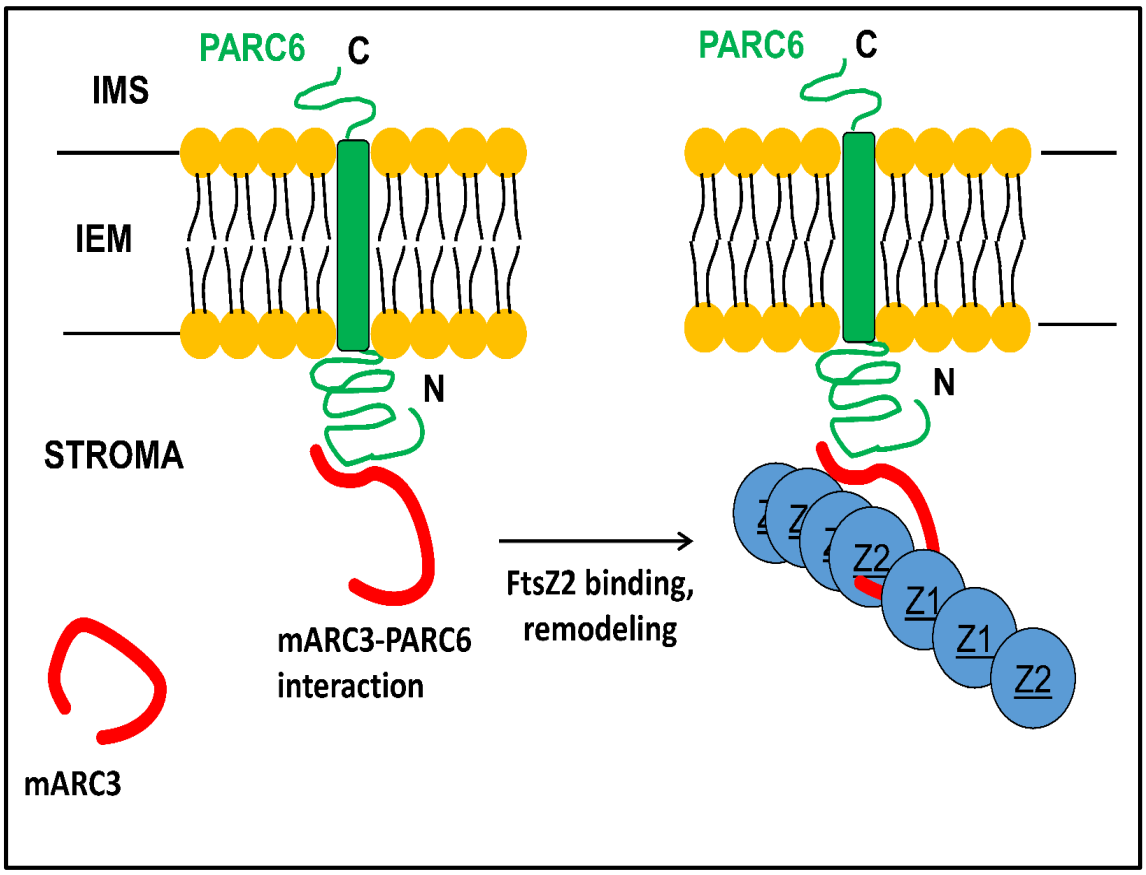

Figure 30. Model of the effect of PARC6-mARC3 interactions. In the full-length mature form of ARC3 (mARC3), the proximity of the C-terminal MORN domain to the N-terminal FtsZ-like domain prevents interaction with FtsZ2. Binding of the N-terminal region of PARC6 to the MORN domain leads to conformational change of mARC3, switching it from the "closed" to "open", active form accessible to FtsZ2 binding.

"open" conformation with activity towards FtsZ disassembly/filament remodeling (Figure 30). PARC6 has been shown to be localized predominantly to the division site but not other parts of the chloroplast, albeit the localization studies have been hampered by low expression of the fluorescently tagged PARC6 [42 and unpublished observations]. Whether PARC6 also functions away from the division site to activate ARC3 or whether other proteins or direct interaction of the MORN domain with membrane lipids mediate ARC3 activation in those locations remains one of the many unanswered questions. Previously characterized MORN motifs in other proteins function to attach to membrane phospholipids [97-99] and may be sensitive to membrane lipid composition. Interestingly, the *Arabidopsis* J-like protein CJD1 influences fatty acid composition of chloroplast lipids, and has been shown to interact with ARC6 [100].

Future Directions

Further studies should improve our understanding of ARC3 activation in chloroplast and its topological specificity within the chloroplast Min system that determines proper placement of the Z-ring. Future studies should also examine the effect of ARC3 on FtsZ1 and FtsZ2 heteropolymer filaments in chloroplasts.

REFERENCES

1. Osteryoung, K.W. and K.A. Pyke, *Division and dynamic morphology of plastids.* Annu Rev Plant Biol, 2014. **65**: p. 443-72.
2. Jarvis, P. and E. Lopez-Juez, *Biogenesis and homeostasis of chloroplasts and other plastids.* Nat Rev Mol Cell Biol, 2013. **14**(12): p. 787-802.
3. Basak, I. and S.G. Moller, *Emerging facets of plastid division regulation.* Planta, 2013. **237**(2): p. 389-98.
4. Maple, J. and S.G. Moller, *Plastid division coordination across a double-membraned structure.* FEBS Lett, 2007. **581**(11): p. 2162-7.
5. Pyke, K.A. and R.M. Leech, *Rapid image analysis screening procedure for identifying chloroplast number mutants in mesophyll cells of Arabidopsis thaliana (L.) Heynh.* Plant Physiology, 1991. **96**: p. 1193-1195.
6. Maple, J. and S.G. Møller, *Plastid Division: Evolution, Mechanism and Complexity.* Annals of Botany, 2007. **99**(4): p. 565-579.
7. Miyagishima, S.-y., *Mechanism of Plastid Division: From a Bacterium to an Organelle.* Plant Physiology, 2011. **155**(4): p. 1533-1544.
8. Miyagishima, S.Y. and Y. Kabeya, *Chloroplast division: squeezing the photosynthetic captive.* Curr Opin Microbiol, 2010. **13**(6): p. 738-746.
9. Terbush, A.D., Y. Yoshida, and K.W. Osteryoung, *FtsZ in chloroplast division: structure, function and evolution.* Curr Opin Cell Biol, 2013. **25**: p. 461–470.
10. Erickson, H.P., D.E. Anderson, and M. Osawa, *FtsZ in bacterial cytokinesis: cytoskeleton and force generator all in one.* Microbiol Mol Biol Rev, 2010. **74**(4): p. 504-28.
11. Adams, D.W. and J. Errington, *Bacterial cell division: assembly, maintenance and disassembly of the Z ring.* Nat Rev Microbiol, 2009. **7**(9): p. 642-53.
12. Lan, G., et al., *Polymerization and bundling kinetics of FtsZ filaments.* Biophys J, 2008. **95**(8): p. 4045-56.

13. Lu, C.L., M. Reedy, and H.P. Erickson, *Straight and curved conformations of FtsZ are regulated by GTP hydrolysis.* Journal of Bacteriology, 2000. **182**(1): p. 164-170.
14. Romberg, L., M. Simon, and H.P. Erickson, *Polymerization of Ftsz, a bacterial homolog of tubulin. is assembly cooperative?* J Biol Chem, 2001. **276**(15): p. 11743-53.
15. Chen, Y. and H.P. Erickson, *FtsZ filament dynamics at steady state: subunit exchange with and without nucleotide hydrolysis.* Biochemistry, 2009. **48**(28): p. 6664-73.
16. Osawa, M. and H.P. Erickson, *Inside-out Z rings--constriction with and without GTP hydrolysis.* Mol Microbiol, 2011. **81**(2): p. 571-9.
17. Chen, Y., et al., *Assembly Dynamics of Mycobacterium tuberculosis FtsZ.* J. Biol. Chem., 2007. **282**(38): p. 27736-27743.
18. Srinivasan, R., et al., *The bacterial cell division protein FtsZ assembles into cytoplasmic rings in fission yeast.* Genes Dev., 2008. **22**(13): p. 1741-1746.
19. Romberg, L. and P.A. Levin, *Assembly dynamics of the bacterial cell division protein FTSZ: poised at the edge of stability.* Annu Rev Microbiol, 2003. **57**: p. 125-54.
20. Maple, J., C. Aldridge, and S.G. Moller, *Plastid division is mediated by combinatorial assembly of plastid division proteins.* Plant J, 2005. **43**(6): p. 811-23.
21. Miyagishima, S.Y., et al., *Two types of FtsZ proteins in mitochondria and red-lineage chloroplasts: the duplication of FtsZ is implicated in endosymbiosis.* J Mol Evol, 2004. **58**(3): p. 291-303.
22. Olson, B.J., Q. Wang, and K.W. Osteryoung, *GTP-dependent heteropolymer formation and bundling of chloroplast FtsZ1 and FtsZ2.* J Biol Chem, 2010. **285**(27): p. 20634-43.

23. Vitha, S., et al., *ARC6 Is a J-domain plastid division protein and an evolutionary descendant of the cyanobacterial cell division protein Ftn2.* Plant Cell, 2003. **15**(8): p. 1918-1933.
24. Johnson, C.B., et al., *Single particle tracking analysis of the chloroplast division protein FtsZ anchoring to the inner envelope membrane.* Microsc Microanal, 2013. **19**(3): p. 507-12.
25. Mazouni, K., et al., *Molecular analysis of the key cytokinetic components of cyanobacteria: FtsZ, ZipN and MinCDE.* Mol Microbiol, 2004. **52**(4): p. 1145-1158.
26. Vitha, S., R.S. McAndrew, and K.W. Osteryoung, *FtsZ ring formation at the chloroplast division site in plants.* Journal of Cell Biology, 2001. **153**(1): p. 111-119.
27. Miyagishima, S., et al., *Plastid division is driven by a complex mechanism that involves differential transition of the bacterial and eukaryotic division rings.* Plant Cell, 2001. **13**: p. 2257-2268.
28. Gao, H., et al., *ARC5, a cytosolic dynamin-like protein from plants, is part of the chloroplast division machinery.* PNAS, 2003. **100**(7): p. 4328-4333.
29. Miyagishima, S., et al., *A plant-specific dynamin-related protein forms a ring at the chloroplast division site.* Plant Cell, 2003. **15**(3): p. 655-665.
30. Kuroiwa, H., et al., *Chloroplast division machinery as revealed by immunofluorescence and electron microscopy.* Planta, 2002. **215**(2): p. 185-190.
31. Monahan, L.G., et al., *Division site positioning in bacteria: one size does not fit all.* Front Microbiol, 2014. **5**: p. 19.
32. Dajkovic, A., et al., *MinC spatially controls bacterial cytokinesis by antagonizing the scaffolding function of FtsZ.* Curr Biol, 2008. **18**(4): p. 235-44.
33. Lutkenhaus, J., *Assembly dynamics of the bacterial MinCDE system and spatial regulation of the Z ring.* Annu Rev Biochem, 2007. **76**: p. 539-62.

34. de Boer, P.A.J., R.E. Crossley, and L.I. Rothfield, *Roles of MinC and MinD in the site-specific septation block mediated by the MinCDE system of Escherichia coli.* Journal of Bacteriology, 1992. **174**(1): p. 63-70.
35. Gregory, J.A., E.C. Becker, and K. Pogliano, *Bacillus subtilis MinC destabilizes FtsZ-rings at new cell poles and contributes to the timing of cell division.* Genes Dev, 2008. **22**(24): p. 3475-88.
36. Thomaides, H.B., et al., *Division site selection protein DivIVA of Bacillus subtilis has a second distinct function in chromosome segregation during sporulation.* Genes Dev, 2001. **15**(13): p. 1662-1673.
37. Nakanishi, H., et al., *Conservation and differences of the Min system in the chloroplast and bacterial division site placement.* Commun Integr Biol, 2009. **2**(5): p. 400-2.
38. Wang, P., et al., *The chloroplast min system functions differentially in two specific nongreen plastids in Arabidopsis thaliana.* PLoS One, 2013. **8**(7): p. e71190.
39. Maple, J., et al., *ARC3 is a stromal Z-ring accessory protein essential for plastid division.* EMBO Reporter, 2007. **8**(3): p. 293-299.
40. Glynn, J.M., et al., *Chloroplast division.* Traffic, 2007. **8**(5): p. 451-461.
41. Wilson, D.M.I. and C. Bianchi, *Imroved Immunodetection of Nuclear Antigens After Sodium Dodecyl Sulfate Treatment of Formaldehyde-fixed Cells.* Journal of Histochemistry and Cytochemistry, 1999. **47**: p. 1095-1100.
42. Glynn, J.M., et al., *PARC6, a novel chloroplast division factor, influences FtsZ assembly and is required for recruitment of PDV1 during chloroplast division in Arabidopsis.* Plant Journal, 2009. **59**(5): p. 700-711.
43. Nakanishi, H., et al., *Plant-Specific Protein MCD1 Determines the Site of Chloroplast Division in Concert with Bacteria-Derived MinD.* Current Biology, 2009. **19**(2): p. 151-156.
44. Zhang, M., et al., *Chloroplast division protein ARC3 regulates chloroplast FtsZ-ring assembly and positioning in arabidopsis through interaction with FtsZ2.* Plant Cell, 2013. **25**(5): p. 1787-802.

45. TerBush, A.D. and K.W. Osteryoung, *Distinct functions of chloroplast FtsZ1 and FtsZ2 in Z-ring structure and remodeling.* J Cell Biol, 2012. **199**(4): p. 623-37.
46. Johnson, C.B., et al., *FtsZ1/FtsZ2 Turnover in Chloroplasts and the Role of ARC3.* Microsc Microanal, 2015. **21**(2): p. 313-23.
47. Shimada, H., et al., *ARC3, a Chloroplast Division Factor, is a Chimera of Prokaryotic FtsZ and Part of Eukaryotic Phosphatidylinositol-4-phosphate 5-kinase.* Plant Cell Physiol., 2004. **45**(8): p. 960-967.
48. Mims, C.W., G.J. Celio, and E.A. Richardson, *The use of high pressure freezing and freeze substitution to study host-pathogen interactions in fungal diseases of plants.* Microsc Microanal, 2003. **9**(6): p. 522-31.
49. Crumpton-Taylor, M., et al., *Control of starch granule numbers in Arabidopsis chloroplasts.* Plant Physiol, 2012. **158**(2): p. 905-16.
50. de Pater, S., et al., *Manipulation of starch granule size distribution in potato tubers by modulation of plastid division.* Plant Biotechnology Journal, 2006. **4**(1): p. 123-134.
51. Gutierrez, O.A., M.R. Campbell, and D.V. Glover, *Starch particle volume in single- and double-mutant maize endosperm genotypes involving the soft starch (h) gene.* Crop Science, 2002. **42**(2): p. 355-359.
52. Almaraz-Delgado, A.L., et al., *Production of therapeutic proteins in the chloroplast of Chlamydomonas reinhardtii.* AMB Express, 2014. **4**: p. 57.
53. Maple, J. and S.G. Møller, *Plastid division coordination across a double-membraned structure.* FEBS Letters, 2007. **581**(11): p. 2162-2167.
54. Smith, A.G., et al., *Plant FtsZ1 and FtsZ2 expressed in a eukaryotic host: GTPase activity and self-assembly.* FEBS Letters, 2010. **584**(1): p. 166-172.
55. Wilson, M.E., G.S. Jensen, and E.S. Haswell, *Two Mechanosensitive Channel Homologs Regulate Chloroplast Division Site Placement in Arabidopsis.* The Plant Cell, 2011. **23**(8): p. 2939-2949.
56. Smith, A.G., et al., *Oligomerization of plant FtsZ1 and FtsZ2 plastid division proteins.* Arch Biochem Biophys, 2011. **513**(2): p. 94-101.

57. Mukherjee, A. and J. Lutkenhaus, *Analysis of FtsZ assembly by light scattering and determination of the role of divalent metal cations.* Journal of Bacteriology, 1999. **181**(3): p. 823-832.

58. Katembe, W.J., et al., *Immunolocalization of integrin-like proteins in Arabidopsis and Chara.* Physiologia Plantarum, 1997. **99**: p. 7-14.

59. Scheffers, D.J., et al., *GTP hydrolysis of cell division protein FtsZ: evidence that the active site is formed by the association of monomers.* Biochemistry, 2002. **41**(2): p. 521-529.

60. Scheffers, D. and A.J. Driessen, *The polymerization mechanism of the bacterial cell division protein FtsZ.* FEBS Lett, 2001. **506**(1): p. 6-10.

61. Anderson, D., F. Guerios-Filho, and H. Erickson, *Assemby Dynamics of FtsZ Rings in Bacillus subtilis and Escherichia coli and Effects of FtsZ-regulating Proteins.* Journal of Bacteriology, 2004. **186**: p. 5775-5781.

62. Dajkovic, A., A. Mukherjee, and J. Lutkenhaus, *Investigation of Regulation of FtsZ Assembly by SulA and Development of a Model for FtsZ Polymerization.* J. Bacteriol., 2008. **190**(7): p. 2513-2526.

63. Mukherjee, A., C. Cao, and J. Lutkenhaus, *Inhibition of FtsZ polymerization by SulA, an inhibitor of septation in Escherichia coli.* Proc Natl Acad Sci U S A, 1998. **95**(6): p. 2885-90.

64. Cho, H., et al., *Nucleoid occlusion factor SlmA is a DNA-activated FtsZ polymerization antagonist.* Proc Natl Acad Sci U S A, 2011. **108**(9): p. 3773-8.

65. Chung, K.M., et al., *Mechanism of regulation of prokaryotic tubulin-like GTPase FtsZ by membrane protein EzrA.* J Biol Chem, 2007. **282**(20): p. 14891-7.

66. Thanbichler, M. and L. Shapiro, *MipZ, a spatial regulator coordinating chromosome segregation with cell division in Caulobacter.* Cell, 2006. **126**(1): p. 147-62.

67. Ray, S., A. Kumar, and D. Panda, *GTP regulates the interaction between MciZ and FtsZ: a possible role of MciZ in bacterial cell division.* Biochemistry, 2013. **52**(2): p. 392-401.

68. Hu, Z., et al., *The MinC component of the division site selection system in Escherichia coli interacts with FtsZ to prevent polymerization.* Proc Natl Acad Sci U S A, 1999. **96**(26): p. 14819-24.
69. Cabre, E.J., et al., *The Nucleoid Occlusion SlmA Protein Accelerates the Disassembly of the FtsZ Protein Polymers without Affecting Their GTPase Activity.* PLoS One, 2015. **10**(5): p. e0126434.
70. Rowlett, V.W. and W. Margolin, *The bacterial Min system.* Curr Biol, 2013. **23**(13): p. R553-6.
71. Schneider, C.A., W.S. Rasband, and K.W. Eliceiri, *NIH Image to ImageJ: 25 years of image analysis.* Nat Meth, 2012. **9**(7): p. 671-675.
72. Krol, E. and D.J. Scheffers, *FtsZ polymerization assays: simple protocols and considerations.* J Vis Exp, 2013(81): p. e50844.
73. Zhang, M., et al., *Roles of Arabidopsis PARC6 in Coordination of the Chloroplast Division Complex and Negative Regulation of FtsZ Assembly.* Plant Physiol, 2016. **170**(1): p. 250-262.
74. Thuman-Commike, P.A., *Single particle macromolecular structure determination via electron microscopy.* FEBS Lett, 2001. **505**(2): p. 199-205.
75. Carroni, M. and H.R. Saibil, *Cryo electron microscopy to determine the structure of macromolecular complexes.* Methods, 2016. **95**: p. 78-85.
76. Dinkins, R., et al., *Overexpression of the Arabidopsis thaliana MinD1 gene alters chloroplast size and number in transgenic tobacco plants.* Planta, 2001. **214**: p. 180-188.
77. Kanamaru, K., et al., *Chloroplast targeting, distribution and transcriptional fluctuation of AtMinD1, a eubacteria-type factor critical for chloroplast division.* Plant and Cell Physiology, 2000. **41**(10): p. 1119-1128.
78. Colletti, K.S., et al., *A homologue of the bacterial cell division site-determining factor MinD mediates placement of the chloroplast division apparatus.* Current Biology, 2000. **10**: p. 507-516.

79. Fujiwara, M.T., et al., *The assembly of the FtsZ ring at the mid-chloroplast division site depends on a balance between the activities of AtMinE1 and ARC11/AtMinD1*. Plant Cell Physiol, 2008. **49**(3): p. 345-61.
80. Itoh, R., et al., *A Chloroplast Protein Homologous to the Eubacterial Topological Specificity Factor MinE Plays a Role in Chloroplast Division.* Plant Physiol, 2001. **127**(4): p. 1644-1655.
81. Maple, J., N.H. Chua, and S.G. Møller, *The topological specificity factor AtMinE1 is essential for correct plastid division site placement in Arabidopsis.* Plant J, 2002. **31**(3): p. 269-77.
82. Zhang, M., et al., *CDP1, a novel component of chloroplast division site positioning system in Arabidopsis.* Cell Research, 2009. **19**(7): p. 877-886.
83. Ottesen, E., R. Zhong, and G.K. Lamppa, *Identification of a chloroplast division mutant coding for ARC6H, an ARC6 homolog that plays a nonredundant role.* Plant Science, 2009. **178**(2): p. 114-122.
84. Glynn, J.M., J.E. Froehlich, and K.W. Osteryoung, *Arabidopsis ARC6 coordinates the division machineries of the inner and outer chloroplast membranes through interaction with PDV2 in the intermembrane space.* Plant Cell, 2008. **20**(9): p. 2460-70.
85. Im, Y.J., et al., *The N-terminal Membrane Occupation and Recognition Nexus Domain of Arabidopsis Phosphatidylinositol Phosphate Kinase 1 Regulates Enzyme Activity.* Journal of Biological Chemistry, 2007. **282**(8): p. 5443-5452.
86. Valentine, R.C., B.M. Shapiro, and E.R. Stadtman, *Regulation of glutamine synthetase. XII. Electron microscopy of the enzyme from Escherichia coli.* Biochemistry, 1968. **7**(6): p. 2143-2152.
87. Ludtke, S.J., P.R. Baldwin, and W. Chiu, *EMAN: semiautomated software for high-resolution single-particle reconstructions.* J Struct Biol, 1999. **128**(1): p. 82-97.

88. Pintilie, G.D., et al., *Quantitative analysis of cryo-EM density map segmentation by watershed and scale-space filtering, and fitting of structures by alignment to regions.* J Struct Biol, 2010. **170**(3): p. 427-38.
89. Pettersen, E.F., et al., *UCSF Chimera--a visualization system for exploratory research and analysis.* J Comput Chem, 2004. **25**(13): p. 1605-12.
90. Kiefer, F., et al., *The SWISS-MODEL Repository and associated resources.* Nucleic Acids Res, 2009. **37**(Database issue): p. D387-92.
91. Guex, N., M.C. Peitsch, and T. Schwede, *Automated comparative protein structure modeling with SWISS-MODEL and Swiss-PdbViewer: a historical perspective.* Electrophoresis, 2009. **30 Suppl 1**: p. S162-73.
92. Arnold, K., et al., *The SWISS-MODEL workspace: a web-based environment for protein structure homology modelling.* Bioinformatics, 2006. **22**(2): p. 195-201.
93. Allen, G.S. and D.L. Stokes, *Modeling, docking, and fitting of atomic structures to 3D maps from cryo-electron microscopy.* Methods Mol Biol, 2013. **955**: p. 229-41.
94. Gao, H. and J. Frank, *Molding atomic structures into intermediate-resolution cryo-EM density maps of ribosomal complexes using real-space refinement.* Structure, 2005. **13**(3): p. 401-6.
95. Stuurman, N., Amodaj N., and R.D. Vale, *Micro-Manager: Open Source software for light microscope imaging.* Microscopy Today, 2007. **15**(3): p. 42-43.
96. Schneider, C.A., W.S. Rasband, and K.W. Eliceiri, *NIH Image to ImageJ: 25 years of image analysis.* Nat Methods, 2012. **9**(7): p. 671-5.
97. Gubbels, M.J., et al., *A MORN-repeat protein is a dynamic component of the Toxoplasma gondii cell division apparatus.* J Cell Sci, 2006. **119**(Pt 11): p. 2236-45.
98. Ma, H., et al., *MORN motifs in plant PIPKs are involved in the regulation of subcellular localization and phospholipid binding.* Cell Res, 2006. **16**(5): p. 466-78.

99. Takeshima, H., et al., *Junctophilins: a novel family of junctional membrane complex proteins.* Mol Cell, 2000. **6**(1): p. 11-22.

100. Ajjawi, I., et al., *A J-like protein influences fatty acid composition of chloroplast lipids in Arabidopsis.* PLoS One, 2011. **6**(10): p. e25368.

APPENDIX A

PRIMERS USED IN PLASMID CONSTRUCT DESIGN

Primer name	Sequence (5' ---> 3')	Restriction site
SK-1	TTGAATTCGTTATGGCCAACTGTACATCTCGAA	EcoRI
SK-3	TATTACGTAATCTCCGGCGTCCACTTGTTT	SnaBI
SK-2	CGTACGTAAAGAATAGGACTCCATCTTTTTGAT	SnaBI
fFt2_F	CAGCTCATATGGCCGCTCAGA AATCT	*Nde*I
fFt2_R	ATCGACTCGAGTCAGACTCGG GGATAAC	*Xho*I
S-114	AGTGGTGGATCCATGGTGAGCAAGGGCGA	*Bam*HI
S-115	TGCACCCTCGAGTTACTTGTACAGCTCGTCCATGC	*Xho*I
S-116	AGTGGTTCTAGAATGGCCGCTCAGAAATCTGAATCTTC	*Xba*I
S-117	TGCACCGGATCCGACTCGGGGATAACGAGAG	*Bam*HI
SK-47	TTACTAGTCAAAATGAACTGTACATCTCGAAAG	SpeI
SK-49	ATGGATCCATCTCCGGCGTCCACTTG	*Bam*HI
SK-43	GATCTAGAATAATGGACAATGCGCCGTCTCGT	*Xba*I
SK-44	AAGGATCCACTGCTTTGAGAGAGCCACTC	*Bam*HI

APPENDIX B

Johnson, C.B., **Shaik, R.S**., Abdallah, R., Vitha, S. and Holzenburg, A.: FtsZ1/FtsZ2 Turnover in Chloroplasts and the Role of ARC3. Microsc. Microanal. 21, 313-323 (2015).

Microsc. Microanal. 21, 313–323, 2015
doi:10.1017/S1431927615000082

Microscopy AND Microanalysis

FtsZ1/FtsZ2 Turnover in Chloroplasts and the Role of ARC3

Carol B. Johnson,[1,2,†] Rahamthulla Shaik,[2] Rehab Abdallah,[2,‡] Stanislav Vitha,[1] and Andreas Holzenburg[1,2,3,*]

[1]*Microscopy & Imaging Center, Texas A&M University, College Station, TX 77843-2257, USA*
[2]*Department of Biology, Texas A&M University, College Station, TX 77843-3258, USA*
[3]*Department of Biochemistry and Biophysics, Texas A&M University, College Station, TX 77843-2128, USA*

Abstract: Chloroplast division requires filamentation temperature-sensitive Z (FtsZ), a tubulin-like GTPase of cyanobacterial endosymbiotic origin. Plants and algae possess two distinct FtsZ protein families, FtsZ1 and FtsZ2 that co-assemble into a ring (Z-ring) at the division site. Z-ring assembly and disassembly and division site positioning is controlled by both positive and negative factors via their specific interactions with FtsZ1 and FtsZ2. Here we present the *in planta* analysis of *Arabidopsis* FtsZ1 and FtsZ2 turnover in the context of a native chloroplast division machinery. Fluorescence recovery after photobleaching analysis was conducted using fluorescently tagged FtsZ at wild-type (WT)-like levels. Rapid photobleaching, low signal-to-noise ratio, and phototropic movements of chloroplasts were overcome by (i) using progressive intervals in time-lapse imaging, (ii) analyzing epidermal rather than stromal chloroplasts, and (iii) employing image stack alignment during postprocessing. In plants of WT background, fluorescence recovery half-times averaged 117 and 325 s for FtsZ1 and FtsZ2, respectively. In plants lacking ARC3, the key negative regulator of FtsZ assembly, the turnover was threefold slower. The findings are discussed in the context of previous results conducted in a heterologous system.

Key words: plastid division, FtsZ assembly, ARC3, FRAP analysis, *Arabidopsis*

Introduction

Chloroplasts in plants and algae evolved from a cyanobacterial endosymbiont (Mereschkowsky, 1905; Gray, 1989; McFadden, 1999) and divide via binary fission to maintain adequate numbers during cell division. This division process is initiated and regulated by the nuclear-encoded and plastid-targeted filamentation temperature-sensitive Z (FtsZ) proteins (Osteryoung & Pyke, 1998; Osteryoung, 2001). The FtsZ protein was first discovered in bacteria, where it is essential for cell division (Hirota et al., 1968; Lutkenhaus et al., 1980). FtsZ is a tubulin homolog GTPase that assembles into a ring (Z-ring) and acts as a scaffold for the division machinery. The Z-ring is a highly dynamic structure that undergoes subunit exchange from the continued polymerization and depolymerization of the component FtsZ subunits. In *Escherichia coli* and *Bacillus subtilis*, 50% of FtsZ subunits in the Z-ring are replaced in <10 s (Anderson et al., 2004; Srinivasan et al., 2008), whereas in *Mycobacterium*, where FtsZ GTPase activity is lower, the turnover half-times between 25 and 40 s were reported (Chen et al., 2007).

Received October 21, 2014; accepted January 8, 2015
*Corresponding author. holzen@tamu.edu

†Current address: Department of Biology, Lone Star College–North Harris, 2700 W.W. Thorne Drive, Houston, TX 77073-3499, USA.
‡Current address: Department of Biology, The American University in Cairo, P.O. Box 74, New Cairo 11835, Cairo, Egypt.

In plants, the single *FtsZ* gene from the cyanobacterial endosymbiont evolved into two gene families, *FtsZ1* and *FtsZ2*. The FtsZ2 protein is structurally similar to the ancestral prokaryotic FtsZ, whereas FtsZ1 lost the C-terminal conserved domain (Osteryoung & McAndrew, 2001; Stokes & Osteryoung, 2003; Miyagishima et al., 2004). FtsZ1 and FtsZ2 play distinct roles in chloroplast division (Osteryoung et al., 1998; Schmitz et al., 2009) and interact with different regulatory components of the division machinery. FtsZ1 interacts with the negative regulator of FtsZ assembly ARC3 (Shimada et al., 2004; Maple et al., 2007), whereas FtsZ2 interacts with both ARC3 (Zhang et al., 2013) and the stabilizing and membrane-tethering protein ARC6 (Maple et al., 2007; Glynn et al., 2008). A carefully balanced polymer stability mediated by these interactions is important for the assembly and localization of the Z-ring and normal chloroplast division (Vitha et al., 2003; Glynn et al., 2007). *In vitro*, *Arabidopsis* FtsZ1 and FtsZ2 exhibit differential GTPase activity, with FtsZ1 being more active than FtsZ2 and both forming filaments *in vitro*, either alone or when both are present in the co-assembly reaction (Olson et al., 2010; Smith et al., 2010). When expressed in yeast *Schizosaccharomyces pombe*, FtsZ1 and FtsZ2 filaments undergo dynamic turnover of subunits that is proportional to their GTPase activity, with turnover half-times ~30 and 90 s for FtsZ1 and FtsZ2, respectively (TerBush & Osteryoung, 2012). How dynamic the FtsZ filaments are *in planta* and how the subunit turnover may be affected by the negative and positive regulators of chloroplast division was not known.

To make progress toward understanding FtsZ dynamics *in planta* and of the role of ARC3 in Z-ring formation, FtsZ1 and FtsZ2 turnover rates were investigated in *Arabidopsis* plants of wild-type (WT) and *arc3* mutant background, using fluorescence recovery after photobleaching (FRAP).

Materials and Methods

Plant Material and Growth

All *Arabidopsis thaliana* plants used in the experiments were of the ecotype Columbia (Col-0), except for the *arc3-1* mutant, which were of the *Lansberg erecta* ecotype background. Seeds for the *ftsZ2 double KO (ftsZ2-1/ftsZ2-2 KO)* (Schmitz et al., 2009) were obtained from Dr. Katherine Osteryoung, Michigan State University. Germplasm identification numbers of alleles used in this work are *arc3-1* (seed stock number CS264), *ftsZ1 KO* (SALK073878), *ftsZ2-1 KD* (SALK134970), and *ftsZ2-1/ftsZ2-2 double KO* (CS65898). Plants were grown in Redi-Earth (SunGro Horticulture, Bellevue, WA, USA) in a temperature- and humidity-controlled greenhouse (22°C, relative humidity 60%).

Plasmid Constructs and Plant Transformation

Two major FtsZ proteins in *A. thaliana*, FtsZ1-1 and FtsZ2-1 (Osteryoung et al., 1998) were investigated and are referred to as FtsZ1 and FtsZ2, respectively. Another minor member of the FtsZ2 family (FtsZ2-2) is redundant for chloroplast division (Schmitz et al., 2009) and therefore was not included in this study. Sequence data can be found in the *Arabidopsis* Information Resource (TAIR; http://www.arabidopsis.org) and EMBL/GenBank data libraries under accession numbers At5g55280 (*ftsZ1-1*), At2g36250 (*ftsZ2-1*), At3g52750 (*ftsZ2-2*), At1g75010 (*arc3*), AF089738 (*ftsZ2-1* cDNA), U70495 (soluble-modified GFP, *smGFP*), and AC006921 (F2H17 BAC clone).

The *FtsZ1-GFP* construct was described previously (Vitha et al., 2001). *FtsZ2-GFP* is similar to a *cmyc*-tagged construct (McAndrew et al., 2001) except that instead of the C-terminal cmyc tag it contains a *Bam*HI-*Eco*RI fragment encoding an *smGFP* (Davis & Vierstra, 1996). The fusion construct containing the full-length *ftsZ2-1* driven by the ~1.8 kb native promoter was then transferred to pMLBART, a derivative of pART27 (Gleave, 1992), that confers resistance to the herbicide glufosinate as a selectable marker.

The mCFP and mYFP (Zacharias et al., 2002) obtained from Dr. Roger Tsien's Lab (University of California, San Diego, CA, USA) were amplified using primers 5′-GATG ACTAGTAAGGGCGAGGAGCTGTTC (forward) containing a 5′ *Spe*I site and 5′-AAATGTTTACTTGTACAGC TCGTCCATGC (reverse) introducing a 3′ STOP codon and cloned into pBluescript (Stratagene, LaJolla, CA, USA). A *Spe*I-*Pst*I fragment was then cloned into pCAMBIA1302-bar (Gao et al., 2006), from which the 35S promoter and GFP sequences were excised by *Spe*I-*Pml*I digestion. This produced vectors for C-terminal tagging with mYFP and mCFP. The FtsZ1 genomic sequence was amplified using primers 5′-TAGAATTCGCATGCGCAAAGTCAGT (forward) and 5′-TATGGATCCTGGAAGAAAAGTCTACGGGGA (reverse) to create *Eco*RI and *Bam*HI restriction sites (underlined). Similarly, *AtFtsZ2-1* c-DNA driven by a 1.8 kb native promoter region was amplified from the *FtsZ2-1-GFP* constructs described above using primers 5′-GCATGAATTCTCAG CACCGTAAATGTAGC (forward) and 5′-ATAGGATC CTGGACTCGGGGATAACGAG (reverse). The ~2.2-kb *AtFtsZ1* and the ~2.8-kb *AtFtsZ2* amplicons were inserted as an *Eco*RI-*Bam*HI fragment into the tagging vectors in front of the *mCFP* or *mYFP* and confirmed by sequencing.

Agrobacterium-mediated floral-dip transformation (Clough & Bent, 1998) and the selection of glufosinate-resistant T1 plants was performed as described previously (Vitha et al., 2001). In subsequent generations, nonsegregating progeny were selected for FRAP experiments.

Fluorescence Microscopy, FRAP, and Image Analysis

Immunofluorescence localization of FtsZ1 using specific anti-FtsZ1 antibody was performed as described (Vitha et al., 2001). Laser scanning confocal microscopy of fluorescently tagged FtsZ proteins in *Arabidopsis* leaf tissue was performed using an Olympus FV1000 confocal microscope (Olympus America Inc., Waltham, MA) equipped with a $60\times/1.2$ water immersion objective and lasers appropriate for the fluorescent proteins (405 nm for mCFP, 488 nm for GFP, and 515 nm for mYFP). Leaves were infiltrated with water to remove air pockets and improve image quality. Confocal zoom was adjusted to achieve Nyquist sampling, with a pixel size of 0.1 μm. The confocal aperture was opened to 3 Airy units. In FRAP experiments, ten prebleach images were collected at 2-s intervals. A small region of interest (ROI) of 2-μm diameter was then bleached at 100% laser intensity. The recovery of fluorescence in the photobleached section of the filament was recorded in a time-lapse sequence. In order to achieve good temporal resolution of the postbleach recovery and to minimize the overall light dose and phototoxicity by the imaging beam, the postbleach images were acquired with a variable, progressively longer time interval. The postbleach imaging sequence consisted of three segments (10×2, 20×5, up to 50×20 s). The individual imaging segments were joined (appended) in the Olympus confocal software (FV10-ASW, ver. 3) and the image stacks and the corresponding time stamps for each frame were exported for analysis. As chloroplasts exhibited significant phototropic movements when irradiated with the imaging laser, only data sets where chloroplasts remained in focus were used and aligned using ImageJ software (http://rsb.info.nih.gov/ij) and the "Rigid Body" transformation in the "stackreg" plugin (Thévenaz et al., 1998). Mean fluorescence intensity in the bleached ROI was background subtracted, corrected for photobleaching caused by imaging, and normalized to the prebleach intensity, yielding $F_{b,corr,norm}$ as described (Anderson et al., 2004). A single exponential fit of the postbleach fluorescence intensity was performed using

the Solver module in MS Excel and the recovery half-time ($t_{1/2}$), i.e., time to recover 50% of the fluorescence signal, was calculated (Anderson et al., 2004). Statistical significance between recovery half-times was assessed using the two-tailed Student's *t*-test, assuming unequal variances of the samples. Calculation of $t_{1/2}$ from the published rate constant τ of spontaneous GFP recovery (Sinnecker et al., 2005) was performed using a formula $t_{1/2} = \tau \cdot \ln 2$.

In FRAP control samples, the entire chloroplast was photobleached to check for photoswitching, i.e., spontaneous recovery of fluorescent protein signal. As an additional control, leaf tissue was vacuum infiltrated with 3% formaldehyde in phosphate-buffered saline (PBS, 0.14 M NaCl, 2.7 mM KCl, 6.5 mM Na_2HPO_4, 5 mM KH_2PO_4, 3.0 mM NaN_3; pH = 7.3) and incubated at room temperature for 30 min. It was then fixed using a cold microwave technology (Smith et al., 2008) in a Pelco Biowave (Ted Pella, Inc., Redding, CA, USA) laboratory microwave processor equipped with a ColdSpot® temperature control system, with power set to 250 W and a 6-min cycle (2 min on, 2 min off, 2 min on). The temperature cut-off was set to 37°C. Tissue was then rinsed in PBS three times, with microwave irradiation 1 min at 250 W power in each rinse and then used for FRAP analysis.

Analysis of Chloroplast Size and Number

A central segment of an almost fully expanded leaf was excised and processed (Pyke & Leech, 1991). Squash preparations of leaf cells were imaged with a Zeiss Axiophot (Zeiss, Thornwood, NJ, USA) microscope equipped with Differential Interference Contrast optics, a 40×/0.75 objective, and a CoolSNAP cf (Photometrics, Tucson, AZ, USA) digital camera. For quantitative analysis, cell area was measured using ImageJ software and the number of chloroplasts per cell was counted.

Immunoblotting

Extracts from expanding leaves from ~5-week-old plants were prepared, separated by sodium dodecyl sulfate polyacrylamide gel electrophoresis and analyzed by western blotting as described (Stokes et al., 2000). The relative amount of total protein was measured by densitometry of a Coomassie-stained gel, using ImageJ software. The amount of extract was then adjusted accordingly in subsequent gel runs to ensure equal gel loading. Extract from ~1 mg fresh tissue was loaded per lane. The anti-FtsZ1 antibody (McAndrew et al., 2001) was used at 1:10,000 dilution overnight at 4°C. For detection of FtsZ2, affinity-purified goat anti-peptide antibody, recognizing the residues 168 through 184 in *At*FtsZ2-1 (Stokes et al., 2000), was custom prepared by Alpha Diagnostics (San Antonio, TX, USA) and used at 1:50 dilution for 3 h at room temperature. Rabbit anti-goat IgG horseradish peroxidase-conjugated secondary antibody (Millipore, Billerica, MA, USA) was used at 1:10,000 dilution. Blots were developed using a SuperSignal West Pico Chemiluminescent Substrate Kit (Thermo Scientific, Portsmouth, NH, USA) and the signal was recorded on Blue X-Ray Film (Phenix Research Products, Candler, NC, USA) or on a gel Doc XR+ system (Bio-Rad Laboratories, Hercules, CA, USA). Equal loading was confirmed by Ponceau S staining of the RuBisCO band on membranes [0.1% (w/v) Ponceau S in 5% (v/v) acetic acid].

Results

In Vivo Localization and Functionality of C-Terminally Tagged FtsZ1 and FtsZ2

In order to test whether the fluorescently tagged FtsZ proteins are functional, the fusion constructs were introduced into mutant knock-out (KO) plants lacking the respective FtsZ protein. KO plants exhibit severe defects in chloroplast division and typically contain only very few large chloroplasts per leaf mesophyll cell, compared with the 60–120 chloroplasts in the WT. FtsZ1 fused to GFP, mYFP, or mCFP (generalized as FtsZ1-FP) was able to restore chloroplast division in the *ftsZ1 KO* mutant (Figs. 1a, 1c) in 60% transgenic plants (n = 100 plants) and assembled in a Z-ring at the division site (Fig. 1b) indicating that the fusion protein is fully functional in chloroplast division. Although expression of *FtsZ2* fusion constructs (FtsZ2-FP) was unable to restore chloroplast division, these fusion proteins, nevertheless, exhibited cytoskeletal behavior and assembled into filaments and Z-rings *in planta* (Figs. 2d, 2e). Taken together, these findings indicate that C-terminal fluorescent protein fusions of plant FtsZ1 and FtsZ2 exhibit the expected cytoskeletal behavior and present a useful tool to study FtsZ turnover *in vivo*.

Optimization of Data Acquisition

FRAP microscopy and analysis proved to be challenging owing to the high background fluorescence in chloroplasts and weak signals from the fluorescent proteins expressed at WT-like levels. Fluorescence proteins were easily photobleached in the extended time-lapse imaging. Chloroplasts also exhibited substantial blue-light-induced phototropic movement, often moving out of focus or out of the imaged area. These difficulties were overcome by a combination of measures. FtsZ was studied in the leaf epidermal chloroplasts that tend to provide brighter signal and lower background, and are overall optically more conducive to live imaging compared with chloroplasts in the mesophyll. After the initial rapid postbleach imaging, images were acquired using progressively longer time intervals in order to minimize the overall light dose and photobleaching of the fluorescent proteins. Opening the confocal aperture to ~3 Airy units provided a reasonable compromise between signal strength and axial resolution. Lastly, the acquired image series were postprocessed by a stack alignment algorithm to compensate for the phototropic movements of plastids and enable fluorescence intensity measurements in a fixed ROI.

FtsZ1 and FtsZ2 Turnover Rates in Chloroplasts

The present study employed a strategy well established in the bacterial cell division research, where the FtsZ-FP fusion

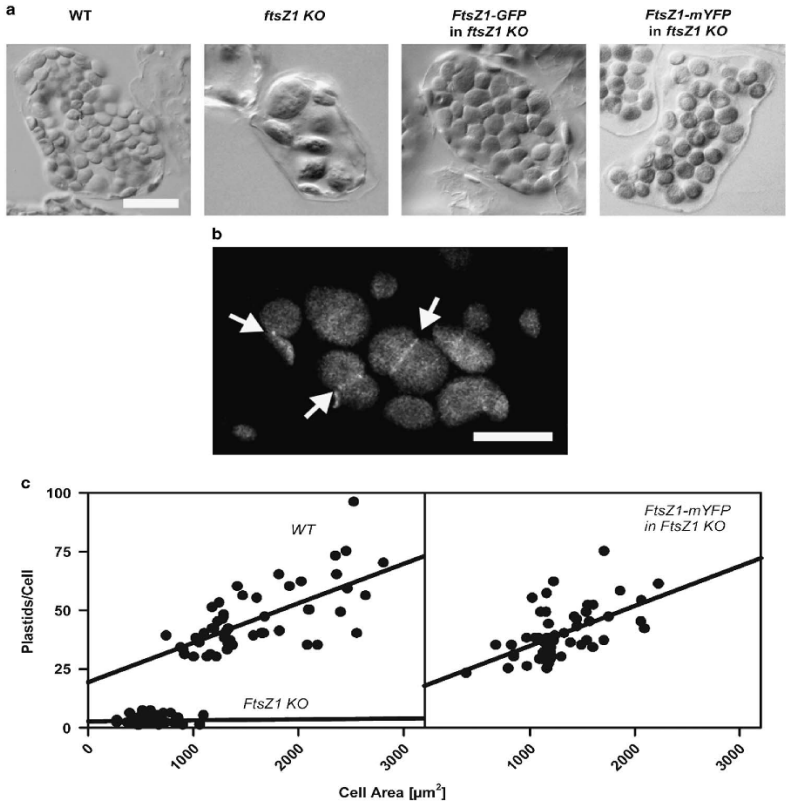

Figure 1. Complementation analysis of FtsZ1-FP fusion protein. **a:** Chloroplast phenotypes in a leaf mesophyll cell in wild-type (WT), *ftsZ1 knock-out* (KO) mutant and the *ftsZ1 KO* mutants expressing *FtsZ1-mYFP*. **b:** Fluorescence micrograph of FtsZ1-mYFP localization (arrows) in leaf mesophyll chloroplasts in a *ftsZ1 KO* plant where chloroplast division was fully restored by the fusion protein. **c:** Quantitative analysis of chloroplast numbers per cell area in leaf mesophyll cells in the WT, *ftsZ1 KO* mutant, and in the *ftsZ1 KO* mutant expressing *FtsZ1-mYFP*. Scale bar: (**a**) 20 μm and (**b**) 10 μm.

protein is co-expressed at relatively low levels and co-assembles with the intrinsic, nontagged protein (Geissler et al., 2003; Anderson et al., 2004). The analysis of subunit turnover by FRAP was carried out on plants (i) expressing the mYFP-tagged FtsZ1 or FtsZ2 in the WT genetic background, (ii) maintaining normal chloroplast division, and (iii) normal localization of FtsZ to Z-rings at mid plastid (Figs. 2b–2e). Immunoblot analysis indicated that the fusion protein was present at a level similar to the intrinsic nontagged FtsZ (0.7- and 1.1-fold the corresponding intrinsic FtsZ1 and FtsZ2; Fig. 2).

Both FtsZ1 and FtsZ2 exhibited recovery of fluorescence in the photobleached ROI indicative of subunit turnover in and out of the filament. The half-time ($t_{1/2}$) $\pm$ SD of FtsZ1-mYFP turnover was 117 ± 62 s ($n = 14$ chloroplasts), whereas FtsZ2-mYFP turnover was much slower, 325 ± 117 s ($n = 9$) (Figs. 3a, 3b). The difference between these $t_{1/2}$ values was statistically significant ($p < 0.001$). The percent of fluorescence recovered varied from 35 to almost 100% and was not different between FtsZ1 and FtsZ2. At least some of this variability may be because of differences in the size of individual chloroplasts. In smaller chloroplasts, photobleaching of the fixed-size ROI depletes the total pool of fluorescent subunits such that 100% recovery to prebleach levels is not possible. This effect is not as severe in larger chloroplasts.

FRAP presumes that photobleaching of a fluorophore is permanent and any recovery of fluorescence is because of lateral diffusion of new, unbleached molecules into the bleached ROI. However, GFP and other fluorescent proteins can also exhibit reversible photoswitching (Shaner et al., 2008) that mimics the effects of diffusion in FRAP

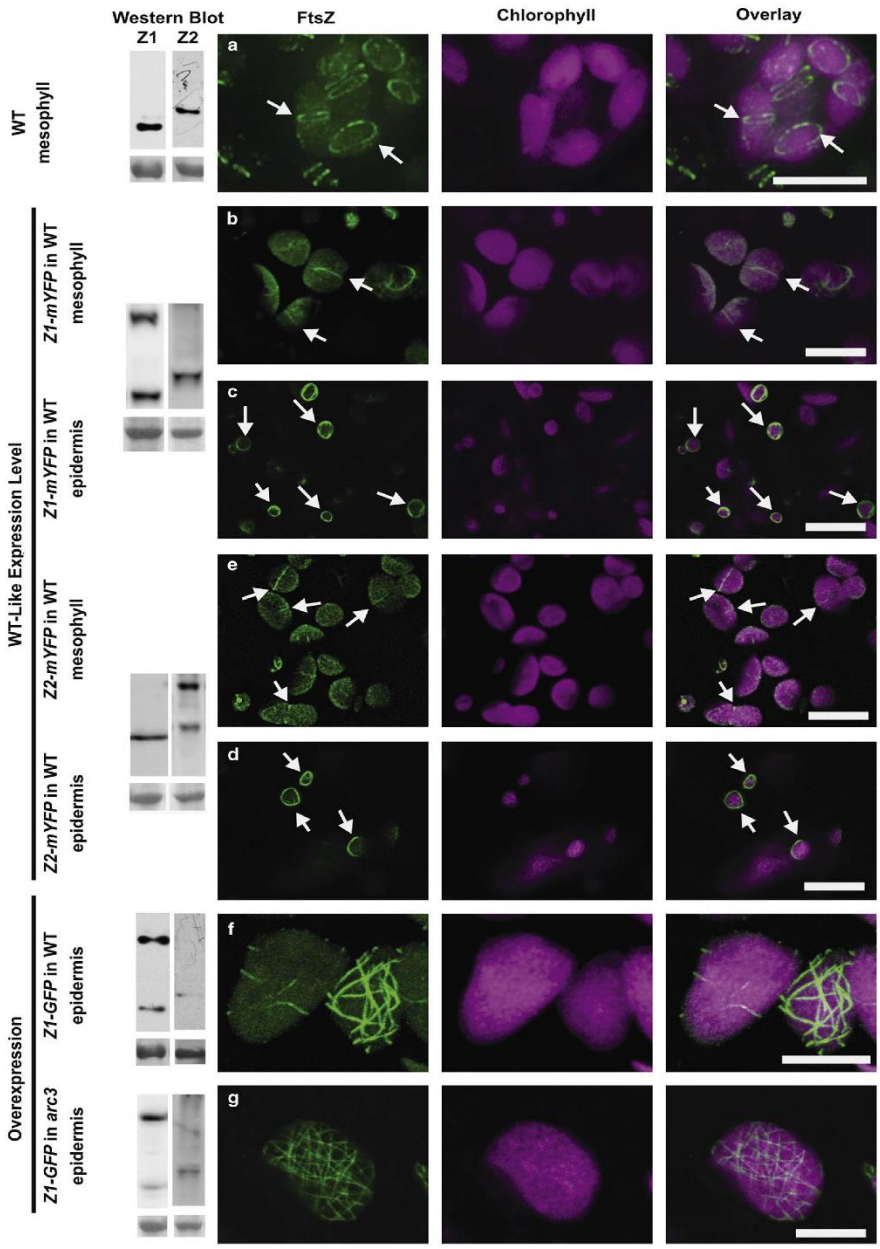

Figure 2. Fluorescence microscopy localization of FtsZ in leaf chloroplasts. First column shows western blots probed with anti-FtsZ1 (Z1) and anti-FtsZ2 (Z2) antibodies. The higher molecular mass bands represent the tagged versions of FtsZ1 and FtsZ2. A band corresponding to ~50 kDa RuBisCO after Ponceau S staining of the membrane is shown as a loading control. Arrows indicate FtsZ rings at mid-chloroplast. **a:** Wild-type (WT) plant, immunofluorescence labeling with anti-FtsZ1 antibody. **b–g:** Confocal fluorescence micrographs of mYFP- or GFP-tagged FtsZ in transgenic plants, at WT-like (**b–e**) or elevated (**f,g**) levels. **b**, **c:** FtsZ1-mYFP in WT in mesophyll (**b**) and epidermal (**c**) chloroplasts; (**d,e**) FtsZ2-mYFP in WT in mesophyll (**d**) and epidermal (**e**) chloroplasts; (**f**) FtsZ1-GFP overexpressed in WT, (**g**) FtsZ1-GFP overexpressed in the *arc3* mutant. Scale bar is 10 μm.

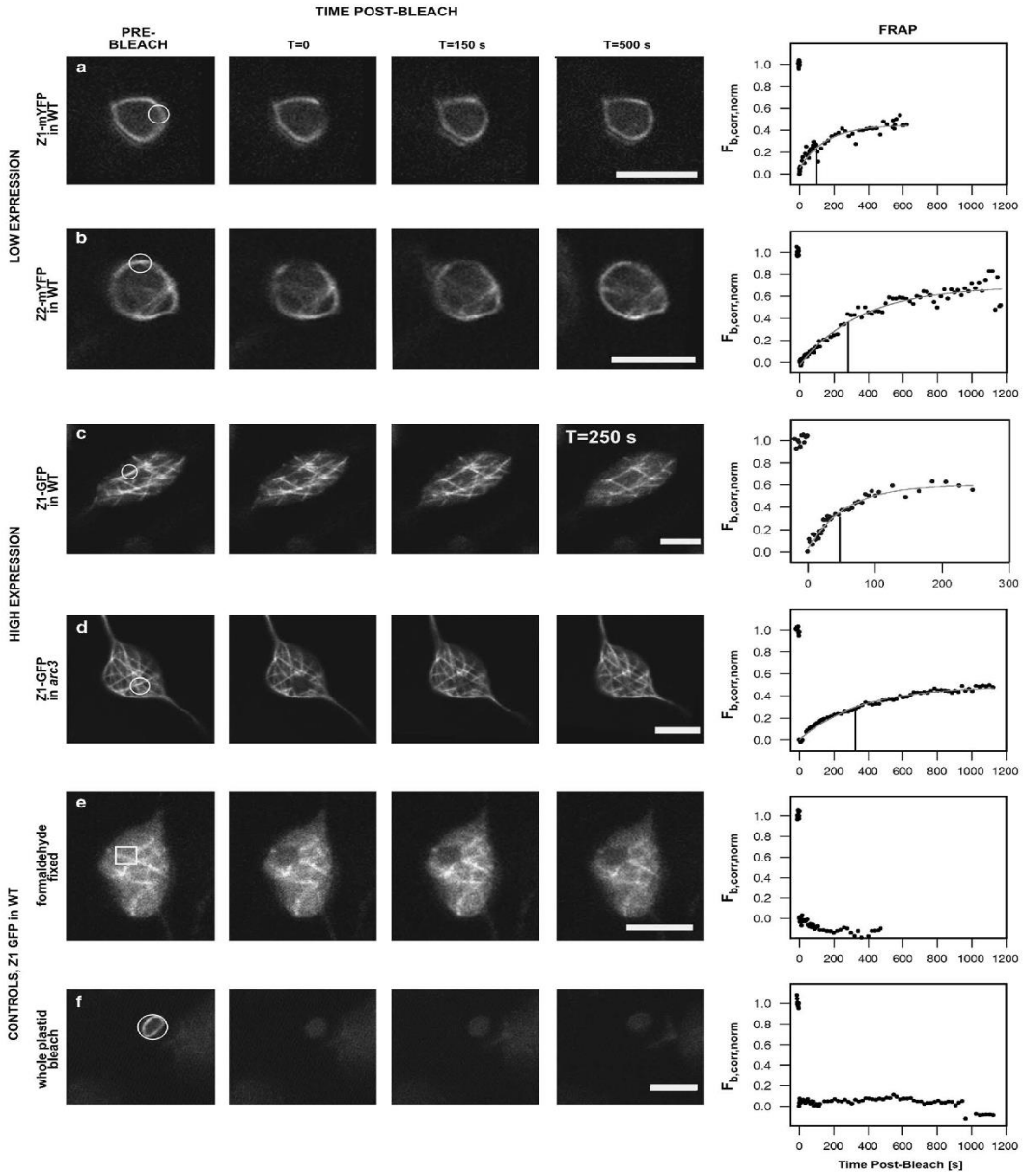

Figure 3. Fluorescence recovery after photobleaching (FRAP) analysis of FtsZ1 and FtsZ2 filament turnover in leaf epidermal chloroplasts. Prebleach and selected postbleach frames from the time-lapse sequence are shown. The circled or boxed area at $T = 0$ indicates the bleached region. The rightmost column shows representative recovery curves from FRAP experiments, the vertical axis denotes the corrected, normalized fluorescence $F_{\mathrm{b,corr,norm}}$. Vertical lines in FRAP plots indicate the $t_{1/2}$ of recovery. **a**,**b:** FRAP of FtsZ1-YFP (**a**) and FtsZ2-YFP (**b**) expressed in wild-type (WT) background at WT-like levels. **c**, **d:** FRAP of FtsZ1-GFP overexpressed in WT (**c**) or *arc3* mutant background. Please note the different time scale in the FRAP curve in (**c**). **e**, **f:** controls. FRAP of small region of interest in formaldehyde-fixed leaf tissue (**e**) and whole-plastid photobleaching in live tissue (**f**). The dip in fluorescence intensity at 1,000 s postbleach in (**f**) is because of a focus shift. Scale bar is 5 μm.

experiments. Photoswitching can cause significant errors in measurements of turnover and diffusion rates (Morisaki & McNally, 2014). Half-times of spontaneous recovery of fluorescent proteins are in the 17–40-s range (calculated from data by Sinnecker et al., 2005). This value is similar to turnover half-times of FtsZ (Anderson et al., 2004; Srinivasan et al., 2008; TerBush & Osteryoung, 2012). It was therefore critical to check for photoswitching in the current study. Two sets of controls were performed. First, FRAP with a standard size bleach area was carried out in samples that were fixed with formaldehyde in the presence of microwave radiation. Microwave-assisted fixation causes rapid cross-linking and immobilization of proteins while preserving GFP fluorescence (Ferris et al., 2009). No recovery was detected in these samples (Fig. 3e), indicating that photobleaching was permanent. A second control entailed bleaching the whole chloroplast in live tissue in order to deplete the entire fluorescent pool. No recovery of fluorescence was detected (Fig. 3f), thus confirming the absence of reversible photoswitching and validating the results of the FRAP analysis.

FtsZ Turnover is Affected by Stoichiometry

To investigate how the stoichiometry between FtsZ1, FtsZ2, and other components of the division machinery affects FtsZ dynamics, transgenic lines containing GFP- or mYFP-tagged FtsZ1 or FtsZ2 at relatively high levels, ~3.5- and 2.3-fold relative to the corresponding intrinsic FtsZ, respectively, were selected and subjected to fluorescence microscopy and FRAP analysis.

FtsZ1-GFP or -mYFP overproduction caused inhibition of chloroplast division and led to an extensive network of smooth, relatively straight filaments (Fig. 2f), consistent with the patterns reported previously in chloroplasts (Kiessling et al., 2000; Vitha et al., 2001) and in yeast (TerBush & Osteryoung, 2012). Turnover rates of FtsZ1-mYFP and FtsZ1-GFP were essentially identical, $t_{1/2}$ reached 59 ± 31 s ($n = 10$) and 57 ± 41 s ($n = 12$), respectively. The turnover was significantly faster ($p < 0.01$) than for the same protein expressed at WT-like levels as described in the previous section (Fig. 3c).

Overproduction of FtsZ2-GFP or -mYFP produced excessive FtsZ filaments and numerous mini rings, a pattern of localization previously reported for the structurally similar prokaryotic *FtsZ-GFP* expressed in yeast *S. pombe* (Srinivasan et al., 2008) and for *FtsZ2-FP* in *Arabidopsis* (TerBush & Osteryoung, 2012; Johnson et al., 2013). Turnover of fluorescently tagged FtsZ2 was significantly slower than that of FtsZ1, estimated in hundreds of seconds, but the recovery of fluorescence did not follow an exponential curve and thus the $t_{1/2}$ value could not be reliably elucidated (data not shown).

Rapid Turnover of FtsZ1 Requires ARC3

ARC3 is a key negative regulator of FtsZ assembly in chloroplasts (Maple et al., 2007). Studies in the yeast expression system showed that the presence of ARC3 is correlated with the lack of FtsZ assemblies (TerBush & Osteryoung, 2012; Zhang et al., 2013), but did not reveal the mode of ARC3 action. The functionally analogous bacterial MinC (Hu et al., 1999) does not affect GTPase activity of FtsZ and is believed to act on FtsZ polymers and promote their debundling, fragmentation, and disassembly (Dajkovic et al., 2008). To begin testing whether ARC3 functions in a similar manner, *FtsZ1-GFP* fusion construct was expressed in *Arabidopsis arc3* null mutant background and FRAP analysis performed to measure FtsZ1 turnover. Owing to weak signals and poor signal-to-noise ratio in plants expressing *FtsZ1-GFP* at WT-like levels, overexpressing transgenic lines were used. Although these plants were comparable to *FtsZ1-GFP* overexpressors described in the previous section both in fluorescence intensity and in FtsZ1-GFP localization pattern (Figs. 2f, 2g), they showed dramatically slower FtsZ1 turnover (Fig. 3d). Fluorescence recovery half-time reached 327 ± 98 s ($n = 7$), significantly longer ($p < 0.001$) than in plants of WT background described earlier (57 ± 41 s). Thus, ARC3 in WT plants appears to accelerate turnover of FtsZ1 subunits in and out of FtsZ filaments. This finding is consistent with the function of ARC3 as a destabilizing factor promoting disassembly rather than inhibiting assembly.

Discussion

Functionality of Fluorescently Tagged FtsZ1 and FtsZ2

Both FtsZ1 and FtsZ2 C-terminally tagged with FP assembled into filaments and exhibited cytoskeletal behavior and FtsZ1-FP, but not FtsZ2-FP, proved fully functional for chloroplast division *in planta*. Despite the only partial functionality of FtsZ2-FP and the structurally similar prokaryotic FtsZ-FP, these proteins are capable of assembly *in vitro* and *in vivo* and exhibit dynamic turnover *in vivo* (Stricker et al., 2002; Anderson et al., 2004; Chen & Erickson, 2005; Chen et al., 2007; Geissler et al., 2007; Srinivasan et al., 2008; TerBush & Osteryoung, 2012). The effect of the fluorescent protein tag on FtsZ functionality is a known phenomenon in both C- and N-terminal fusions with prokaryotic FtsZ (Osawa & Erickson, 2005) and also for the structurally similar plant FtsZ2 (TerBush & Osteryoung, 2012 and this study). Therefore, the present study in plants, as well as studies in prokaryotes that aim to investigate FtsZ dynamics *in vivo* within the context of a functional division machinery, use a co-expression approach. Fluorescently tagged FtsZ is expressed at relatively low levels along with the intrinsic, nontagged form of FtsZ (e.g., Anderson et al., 2004; Geissler et al., 2007). The tagged version of FtsZ serves as a tracer of the total FtsZ pool behavior. The possible negative effects of the fluorescent tag are "diluted" owing to the presence of the fully functional untagged FtsZ.

The co-expression strategy leads to an increased total amount of FtsZ in *Arabidopsis* transgenic plants. It has been previously shown that relatively small changes in FtsZ

Table 1. FtsZ Turnover and GTPase Activity in Plants and Bacteria.

Organism, protein	Turnover of FtsZ $t_{1/2}$ (s)		GTPase Activity (mol GTP mol Protein/min)	
Arabidopsis thaliana, FtsZ1 (*in planta*)	100	This report	1–3	[1, 2]
A. thaliana, FtsZ1 (in yeast)	30	[11]		
A. thaliana, FtsZ2 (*in planta*)	300	This report	0.5–1	[1, 2]
A. thaliana, FtsZ2 (in yeast)	90	[11]		
Escherichia coli, FtsZ	10	[3, 4, 10]	5–15	[1, 9]
E. coli, FtsZQ47K mutant	300	[10]	0.5	[9]
Bacillus subtilis	8	[3]	0.5 (30°C)	[6, 7]
Mycobacterium tuberculosis	25–63	[5, 10]	0.47	[8]

Turnover was measured with FtsZ tagged with fluorescent proteins. For clarity, rounded $t_{1/2}$ values are given. The reported GTPase activity is for recombinant FtsZ proteins without the fluorescent tag, measured at 37°C, pH 6.5, unless indicated otherwise. References are as follows: [1] Olson et al. (2010), [2] Smith et al. (2010), [3] Anderson et al. (2004), [4] Geissler et al. (2007), [5] Chen et al. (2007), [6] Scheffers (2008), [7] de Oliveira et al. (2010), [8] Rajagopalan et al. (2005), [9] Redick et al. (2005), [10] Srinivasan et al. (2008), [11] TerBush & Osteryoung (2012). Data for FtsZ turnover in [10] are for *E. coli* proteins expressed in yeast.

expression levels do not interfere with chloroplast division. Stokes et al. (2000) found that plants with a twofold increase of FtsZ1 had WT-like chloroplast division, whereas 3× to 6× increase in FtsZ1 resulted in intermediate levels of chloroplast division. Schmitz et al. (2009) showed that chloroplast division in plants with a 1.5× increase in total FtsZ2 levels is statistically indistinguishable from that in WT plants. In this study, visual inspection of chloroplast phenotypes in plants expressing FtsZ transgenes at WT-like levels showed chloroplast sizes and numbers indistinguishable from that of WT plants, indicating that chloroplast division proceeded normally. We therefore believe that the data presented in this report are biologically relevant and provide insight into FtsZ turnover *in planta*.

Differential Turnover of FtsZ1 and FtsZ2 in Chloroplasts

FRAP $t_{1/2}$ values for FtsZ1 tagged with either GFP or mYFP were identical, indicating that the weak tendency of standard GFP to dimerize (Zacharias et al., 2002) did not affect FtsZ dynamics. FtsZ1 turnover was found to be approximately three times faster than that of FtsZ2, both in the present report and in TerBush & Osteryoung (2012). The differential turnover rates of FtsZ1 and FtsZ2 are proportional to their GTPase activities measured *in vitro* (Olson et al., 2010; Smith et al., 2010) and consistent with findings that GTPase activity is required for rapid FtsZ turnover (Chen et al., 2007; Srinivasan et al., 2008). Nevertheless, the *in planta* $t_{1/2}$ values for both FtsZ1 and FtsZ2 reported herein were considerably larger than for most of the prokaryotic FtsZs, including *Mycobacterium tuberculosis* that has a comparable GTPase activity (Table 1). Significantly, the *in planta* turnover of both FtsZ1 and FtsZ2 was also substantially slower than was reported for the same proteins expressed in yeast in the absence of other components of the chloroplast division machinery (TerBush & Osteryoung, 2012) such as ARC6, ARC3, MinD, MinE, and PARC6 that have been shown to affect FtsZ assembly, localization, and stability (Fujiwara et al., 2008; Glynn et al., 2008; Zhang et al., 2013).

Independent transgenic lines carrying the FtsZ1-FP and FtsZ2-FP fusions exhibited a wide range of expression levels as judged by both fluorescence microscopy and immunoblotting. This allowed assessing FtsZ localization and turnover not only in plants where FtsZ-FP is expressed at WT-like levels and chloroplast division proceeds normally, but also in plants where overexpression significantly affects the stoichiometry of FtsZ1, FtsZ2, and other division proteins. FtsZ1 and FtsZ2 are believed to co-assemble to form mixed polymers (Olson et al., 2010) that are exposed to FtsZ1- and FtsZ2-interacting proteins that may either stabilize (ARC6) or destabilize (ARC3) the assemblies *in vivo*. ARC6 interacts with FtsZ2, whereas ARC3 does with both FtsZ1 and FtsZ2 (Zhang et al., 2013). Maple et al. (2005) hypothesized that a change in FtsZ1:FtsZ2 ratio within filaments may lead to altered filament properties. Here we present data in support of this hypothesis as changes in FtsZ1:FtsZ2 ratios led to changes in turnover dynamics: overexpressing FtsZ1 to acceleration and overexpressing FtsZ2 to deceleration. This would suggest that FtsZ1 mediates filament remodeling, whereas FtsZ2 is predominantly involved in filament stabilization. Zhang et al. (2013) came to a different conclusion, proposing that ARC3 functions primarily via FtsZ2 to disassemble or inhibit assembly of FtsZ filaments. Further research is needed to fully understand the specific functional roles of FtsZ1 and FtsZ2 in chloroplast division. Although the nonexponential recovery of FtsZ2-FP prevented quantitative analysis, it points at the possibility that the recruitment of new subunits into the filament may be diffusion limited. An anomalous diffusion behavior that is caused by transient binding of FtsZ has been previously demonstrated *in vivo* (Johnson et al., 2013).

ARC3 and FtsZ1 Turnover

In *E. coli*, normal cell division requires spatial regulation of division site positioning via interaction of negative and positive regulatory proteins MinC, D, and E that prevent Z-ring assembly and/or promote disassembly at positions other than the division site (de Boer, 2010; Lutkenhaus et al., 2012). MinD and MinE proteins regulate the localization and activity of MinC (de Boer et al., 1992; Raskin & de Boer, 1999; Hu & Lutkenhaus, 2003; Hu et al., 2003), which

inhibits FtsZ assembly by debundling and shortening of existing filaments (Hu et al., 1999; Dajkovic et al., 2008; Blasios et al., 2013).

Plants contain MinD and MinE, but MinC has been replaced by the plant-specific protein ARC3 (Shimada et al., 2004; Maple et al., 2007; Zhang et al., 2013). Data by Zhang et al. (2013) seem to suggest that ARC3 may act as a direct inhibitor of FtsZ assembly. On the other hand, it is possible that ARC3 functions in the same manner as the prokaryotic MinC and promotes fragmentation and shortening of existing filaments. As the FtsZ depolymerization rate is faster at the open ends of filaments than in central filament regions (Mateos-Gil et al., 2012), filament breakage is expected to increase the rate of FtsZ turnover. Elimination of MinCDE proteins in *E. coli* led to approximately two times slower turnover of FtsZ, indicating that MinC might directly interact with already formed Z-rings to inhibit or actively disassemble FtsZ polymers (Anderson et al., 2004). Similarly, the FRAP analysis presented here showed a dramatic decrease in FtsZ1 turnover in the absence of ARC3, which is consistent with the role of ARC3 as a FtsZ filament disassembly factor.

The findings contribute to our understanding of plastid division and size control, which is of interest to the food industry *vis-à-vis* starch granule optimization, and increases attention toward chloroplast engineering for antibody production.

Acknowledgments

The authors thank Dr. Katherine Osteryoung (Michigan State University) for the *ftsZ2 null* mutant seed stocks and anti-FtsZ1 antibody and Ginger Stuessy (TAMU) for taking care of the greenhouse-grown plants. The use of the Microscope and Imaging Center at Texas A&M University is acknowledged. The Olympus FV1000 confocal microscope acquisition was supported by the Division of Research at Texas A&M University.

References

Anderson, D.E., Gueiros-Filho, F.J. & Erickson, H.P. (2004). Assembly dynamics of ftsz rings in *Bacillus subtilis* and *Escherichia coli* and effects of ftsz-regulating proteins. *J Bacteriol* **186**, 5775–5781.

Blasios, V., Bisson-Filho, A.W., Castellen, P., Nogueira, M.L., Bettini, J., Portugal, R.V., Zeri, A.C. & Gueiros-Filho, F.J. (2013). Genetic and biochemical characterization of the MinC-FtsZ interaction in *Bacillus subtilis*. *PLoS One* **8**, e60690.

Chen, Y., Anderson, D.E., Rajagopalan, M. & Erickson, H.P. (2007). Assembly dynamics of *Mycobacterium tuberculosis* FtsZ. *J Biol Chem* **282**, 27736–27743.

Chen, Y.D. & Erickson, H.P. (2005). Rapid *in vitro* assembly dynamics and subunit turnover of FtsZ demonstrated by fluorescence resonance energy transfer. *J Biol Chem* **280**, 22549–22554.

Clough, S.J. & Bent, A.F. (1998). Floral dip: A simplified method for *Agrobacterium*-mediated transformation of *Arabidopsis thaliana*. *Plant J* **16**, 735–743.

Dajkovic, A., Lan, G., Sun, S.X., Wirtz, D. & Lutkenhaus, J. (2008). MinC spatially controls bacterial cytokinesis by antagonizing the scaffolding function of FtsZ. *Curr Biol* **18**, 235–244.

Davis, S.J. & Vierstra, R.D. (1996). Soluble derivatives of green fluorescent protein (GFP) for use in *Arabidopsis thaliana*. *Weeds World* **3**, 43–48.

de Boer, P.A. (2010). Advances in understanding *E. coli* cell fission. *Curr Opin Microbiol* **13**, 730–737.

de Boer, P.A.J., Crossley, R.E. & Rothfield, L.I. (1992). Roles of MinC and MinD in the site-specific septation block mediated by the MinCDE system of *Escherichia coli*. *J Bacteriol* **174**, 63–70.

de Oliveira, I.F.F., de Sousa Borges, A., Kooij, V., Bartosiak-Jentys, J., Luirink, J. & Scheffers, D.-J. (2010). Characterization of *ftsZ* mutations that render *Bacillus subtilis* resistant to MinC. *PLoS One* **5**, e12048.

Ferris, A.M., Giberson, R.T., Sanders, M.A. & Day, J.R. (2009). Advanced laboratory techniques for sample processing and immunolabeling using microwave radiation. *J Neurosci Meth* **182**, 157–164.

Fujiwara, M.T., Hashimoto, H., Kazama, Y., Abe, T., Yoshida, S., Sato, N. & Itoh, R.D. (2008). The assembly of the FtsZ ring at the mid-chloroplast division site depends on a balance between the activities of AtMinE1 and ARC11/AtMinD1. *Plant Cell Physiol* **49**, 345–361.

Gao, H., Sage, T.L. & Osteryoung, K.W. (2006). FZL, an FZO-like protein in plants, is a determinant of thylakoid and chloroplast morphology. *Proc Natl Acad Sci USA* **103**, 6759–6764.

Geissler, B., Elraheb, D. & Margolin, W. (2003). A gain-of-function mutation in *ftsA* bypasses the requirement for the essential cell division gene *zipA* in *Escherichia coli*. *Proc Natl Acad Sci USA* **100**, 4197–4202.

Geissler, B., Shiomi, D. & Margolin, W. (2007). The ftsA* gain-of-function allele of *Escherichia coli* and its effects on the stability and dynamics of the Z ring. *Microbiology* **153**, 814–825.

Gleave, P. (1992). A versatile binary vector system with T-DNA organisational structure conducive to efficient integration of cloned DNA into the plant genome. *Plant Mol Biol* **20**, 1203–1207.

Glynn, J.M., Froehlich, J.E. & Osteryoung, K.W. (2008). *Arabidopsis* ARC6 coordinates the division machineries of the inner and outer chloroplast membranes through interaction with PDV2 in the intermembrane space. *Plant Cell* **20**, 2460–2470.

Glynn, J.M., Miyagishima, S., Yoder, D.W., Osteryoung, K.W. & Vitha, S. (2007). Chloroplast division. *Traffic* **8**, 451–461.

Gray, M.W. (1989). The evolutionary origins of organelles. *Trends Genet* **5**, 294–299.

Hirota, Y., Ryter, A. & Jacob, F. (1968). Thermosensitive mutants of *E. coli* affected in the processes of DNA synthesis and cellular division. *Cold Spring Harb Symp Quant Biol* **33**, 677–693.

Hu, Z. & Lutkenhaus, J. (2003). A conserved sequence at the C-terminus of MinD is required for binding to the membrane and targeting MinC to the septum. *Mol Microbiol* **47**, 345–355.

Hu, Z., Mukherjee, A., Pichoff, S. & Lutkenhaus, J. (1999). The MinC component of the division site selection system in *Escherichia coli* interacts with FtsZ to prevent polymerization. *Proc Natl Acad Sci USA* **96**, 14819–14824.

Hu, Z., Saez, C. & Lutkenhaus, J. (2003). Recruitment of MinC, an inhibitor of Z-ring formation, to the membrane in *Escherichia coli*: Role of MinD and MinE. *J Bacteriol* **185**, 196–203.

JOHNSON, C.B., TANG, L.K., SMITH, A.G., RAVICHANDRAN, A., LUO, Z., VITHA, S. & HOLZENBURG, A. (2013). Single particle tracking analysis of the chloroplast division protein FtsZ anchoring to the inner envelope membrane. *Microsc Microanal* **19**, 507–512.

KIESSLING, J., KRUSE, S., RENSING, S.A., HARTER, K., DECKER, E.L. & RESKI, R. (2000). Visualization of a cytoskeleton-like FtsZ network in chloroplasts. *J Cell Biol* **151**, 945–950.

LUTKENHAUS, J., PICHOFF, S. & DU, S. (2012). Bacterial cytokinesis: From Z ring to divisome. *Cytoskeleton* **69**, 778–790.

LUTKENHAUS, J., WOLF-WATZ, H. & DONACHIE, W.D. (1980). Organization of genes in the *ftsZ-envA* region of the *Escherichia coli* genes map and identification of a new *fts* locus *(ftsZ)*. *J Bacteriol* **142**, 615–620.

MAPLE, J., ALDRIDGE, C. & MØLLER, S.G. (2005). Plastid division is mediated by combinatorial assembly of plastid division proteins. *Plant J* **43**, 811–823.

MAPLE, J., VOJTA, L., SOLL, J. & MØLLER, S.G. (2007). ARC3 is a stromal Z-ring accessory protein essential for plastid division. *EMBO Rep* **8**, 293–299.

MATEOS-GIL, P., PAEZ, A., HORGER, I., RIVAS, G., VICENTE, M., TARAZONA, P. & VELEZ, M. (2012). Depolymerization dynamics of individual filaments of bacterial cytoskeletal protein FtsZ. *Proc Natl Acad Sci USA* **109**, 8133–8138.

MCANDREW, R.S., FROEHLICH, J.E., VITHA, S., STOKES, K.D. & OSTERYOUNG, K.W. (2001). Colocalization of plastid division proteins in the chloroplast stromal compartment establishes a new functional relationship between FtsZ1 and FtsZ2 in higher plants. *Plant Physiol* **127**, 1656–1666.

MCFADDEN, G.I. (1999). Endosymbiosis and evolution of the plant cell. *Curr Opin Plant Biol* **2**, 513–519.

MERESCHKOWSKY, C. (1905). Über natur un ursprung der chromatophoren im pflanzenreiche. *Biol Centralbl* **25**, 593–604. (English translation in MARTIN, W. & KOWALLIK, K.V. (1999). Annotated English translation of Mereschkowsky's 1905 paper "Über Natur und Ursprung der Chromatophoren im Pflanzenreiche". *Eur J Phycol* **24**, 287–296.

MIYAGISHIMA, S.Y., NOZAKI, H., NISHIDA, K., NISHIDA, K., MATSUZAKI, M. & KUROIWA, T. (2004). Two types of FtsZ proteins in mitochondria and red-lineage chloroplasts: The duplication of FtsZ is implicated in endosymbiosis. *J Mol Evol* **58**, 291–303.

MORISAKI, T. & MCNALLY, J.G. (2014). Photoswitching-free FRAP analysis with a genetically encoded fluorescent tag. *PLoS One* **9**, e107730.

OLSON, B.J., WANG, Q. & OSTERYOUNG, K.W. (2010). GTP-dependent heteropolymer formation and bundling of chloroplast FtsZ1 and FtsZ2. *J Biol Chem* **285**, 20634–20643.

OSAWA, M. & ERICKSON, H.P. (2005). Probing the domain structure of FtsZ by random truncation and insertion of GFP. *Microbiology* **151**, 4033–4043.

OSTERYOUNG, K.W. (2001). Organelle fission in eukaryotes. *Curr Opin Microbiol* **4**, 639–646.

OSTERYOUNG, K.W. & MCANDREW, R.S. (2001). The plastid division machine. *Annu Rev Plant Physiol Plant Mol Biol* **52**, 315–333.

OSTERYOUNG, K.W. & PYKE, K.A. (1998). Plastid division: Evidence for a prokaryotically derived mechanism. *Curr Opin Plant Biol* **1**, 475–479.

OSTERYOUNG, K.W., STOKES, K.D., RUTHERFORD, S.M., PERCIVAL, A.L. & LEE, W.Y. (1998). Chloroplast division in higher plants requires members of two functionally divergent gene families with homology to bacterial *ftsZ*. *Plant Cell* **10**, 1991–2004.

PYKE, K.A. & LEECH, R.M. (1991). Rapid image analysis screening procedure for identifying chloroplast number mutants in mesophyll cells of *Arabidopsis thaliana* (L.) Heynh. *Plant Physiol* **96**, 1193–1195.

RAJAGOPALAN, M., ATKINSON, M.A.L., LOFTON, H., CHAUHAN, A. & MADIRAJU, M.V. (2005). Mutations in the GTP-binding and synergy loop domains of *Mycobacterium tuberculosis* ftsZ compromise its function in vitro and in vivo. *Biochem Biophys Res Commun* **331**, 1171–1177.

RASKIN, D.M. & DE BOER, P.A.J. (1999). MinDE-dependent pole-to-pole oscillation of division inhibitor MinC in *Escherichia coli*. *J Bacteriol* **181**, 6419–6424.

REDICK, S.D., STRICKER, J., BRISCOE, G. & ERICKSON, H.P. (2005). Mutants of FtsZ targeting the protofilament interface: Effects on cell division and GTPase activity. *J Bacteriol* **187**, 2727–2736.

SCHIEFFERS, D.J. (2008). The effect of MinC on FtsZ polymerization is pH dependent and can be counteracted by ZapA. *FEBS Lett* **582**, 2601–2608.

SCHMITZ, A.J., GLYNN, J.M., OLSON, B.J.S.C., STOKES, K.D. & OSTERYOUNG, K.W. (2009). *Arabidopsis* FtsZ2-1 and FtsZ2-2 are functionally redundant, but FtsZ-based plastid division is not essential for chloroplast partitioning or plant growth and development. *Mol Plant* **2**, 1211–1222.

SHANER, N.C., LIN, M.Z., MCKEOWN, M.R., STEINBACH, P.A., HAZELWOOD, K.L., DAVIDSON, M.W. & TSIEN, R.Y. (2008). Improving the photostability of bright monomeric orange and red fluorescent proteins. *Nat Methods* **5**, 545–551.

SHIMADA, H., KOIZUMI, M., KUROKI, K., MOCHIZUKI, M., FUJIMOTO, H., OHTA, H., MASUDA, T. & TAKAMIYA, K.-I. (2004). ARC3, a chloroplast division factor, is a chimera of prokaryotic FtsZ and part of eukaryotic phosphatidylinositol-4-phosphate 5-kinase. *Plant Cell Physiol* **45**, 960–967.

SINNECKER, D., VOIGT, P., HELLWIG, N. & SCHAEFER, M. (2005). Reversible photobleaching of enhanced green fluorescent proteins. *Biochemistry* **44**, 7085–7094.

SMITH, A.G., JOHNSON, C.B., ELLIS, A.E., VITHA, S. & HOLZENBURG, A. (2008). Protein screening using cold microwave technology. *Anal Biochem* **375**, 313–317.

SMITH, A.G., JOHNSON, C.B., VITHA, S. & HOLZENBURG, A. (2010). Plant FtsZ1 and FtsZ2 expressed in a eukaryotic host: GTPase activity and self-assembly. *FEBS Lett* **584**, 166–172.

SRINIVASAN, R., MISHRA, M., WU, L., YIN, Z. & BALASUBRAMANIAN, M.K. (2008). The bacterial cell division protein FtsZ assembles into cytoplasmic rings in fission yeast. *Genes Dev* **22**, 1741–1746.

STOKES, K.D., MCANDREW, R.S., FIGUEROA, R., VITHA, S. & OSTERYOUNG, K.W. (2000). Chloroplast division and morphology are differentially affected by overexpression of *FtsZ1* and *FtsZ2* genes in *Arabidopsis*. *Plant Physiol* **124**, 1668–1677.

STOKES, K.D. & OSTERYOUNG, K.W. (2003). Early divergence of the *FtsZ1* and *FtsZ2* plastid division gene families in photosynthetic eukaryotes. *Gene* **320**, 97–108.

STRICKER, J., MADDOX, P., SALMON, E.D. & ERICKSON, H.P. (2002). Rapid assembly dynamics of the *Escherichia coli* FtsZ-ring demonstrated by fluorescence recovery after photobleaching. *Proc Natl Acad Sci USA* **99**, 3171–3175.

TERBUSH, A.D. & OSTERYOUNG, K.W. (2012). Distinct functions of chloroplast FtsZ1 and FtsZ2 in Z-ring structure and remodeling. *J Cell Biol* **199**, 623–637.

THÉVENAZ, P., RUTTIMANN, U.E. & UNSER, M. (1998). A pyramid approach to subpixel registration based on intensity. *IEEE Trans Image Process* **7**, 27–41.

Vitha, S., Froehlich, J.E., Koksharova, O., Pyke, K.A., van Erp, H. & Osteryoung, K.W. (2003). ARC6 is a J-domain plastid division protein and an evolutionary descendant of the cyanobacterial cell division protein Ftn2. *Plant Cell* **15**, 1918–1933.

Vitha, S., McAndrew, R.S. & Osteryoung, K.W. (2001). FtsZ ring formation at the chloroplast division site in plants. *J Cell Biol* **153**, 111–119.

Zacharias, D.A., Violin, J.D., Newton, A.C. & Tsien, R.Y. (2002). Partitioning of lipid-modified monomeric GFPs into membrane microdomains of live cells. *Science* **296**, 913–916.

Zhang, M., Schmitz, A.J., Kadirjan-Kalbach, D.K., Terbush, A.D. & Osteryoung, K.W. (2013). Chloroplast division protein ARC3 regulates chloroplast FtsZ-ring assembly and positioning in *Arabidopsis* through interaction with FtsZ2. *Plant Cell* **25**, 1787–1802.

APPENDIX C

Johnson, C.B., Long, Z., Luo, Z., **Shaik, R.S**., Sung, M.W., Vitha, S. and Holzenburg, A.: In situ structure of FtsZ mini-rings in *Arabidopsis* chloroplasts. Adv. Struct. Chem. Imag. 1:12, 1-12. (2015).

Reprinted with permission from Springer.

Johnson *et al. Adv Struct Chem Imag (2015) 1:12*
DOI 10.1186/s40679-015-0013-7

Advanced Structural and Chemical Imaging
a SpringerOpen Journal

RESEARCH Open Access

In situ structure of FtsZ mini-rings in *Arabidopsis* chloroplasts

Carol B. Johnson[1], Zheng Long[2], Zhiping Luo[3], Rahamthulla S. Shaik[1], Min Woo Sung[1], Stanislav Vitha[4] and Andreas Holzenburg[1,4,5*]

Abstract

Chloroplasts are essential plant organelles that divide by binary fission through a coordinated ring-shaped division machinery located both on the outside and inside of the chloroplast. The first step in chloroplast division is the assembly of an internal division ring (Z-ring) that is composed of the key filamentous chloroplast division proteins FtsZ1 and FtsZ2. How the individual FtsZ filaments assemble into higher-order structures to form the dividing Z-ring is not well understood and the most detailed insights have so far been gleaned from prokaryotic FtsZ. Here, we present in situ data of chloroplast FtsZ making use of a smaller ring-like FtsZ assembly termed mini-rings that form under well-defined conditions. Structured illumination microscopy (SIM) permitted their mean diameter to be determined as 208 nm and also showed that 68 % of these rings are terminally attached to linear FtsZ filaments. A correlative microscopy-compatible specimen preparation based on freeze substitution after high-pressure freezing is presented addressing the challenges such as autofluorescence and specific fluorescence attenuation. Transmission electron microscopy (TEM) and scanning TEM (STEM) imaging of thin sections exhibited ring-like densities that matched in size with the SIM data, and TEM tomography revealed insights into the molecular architecture of mini-rings demonstrating the following key features: (1) overall, a roughly bipartite split into a more ordered/curved and less ordered/curved half is readily discernible; (2) the density distribution in individual strands matches with the X-ray data, suggesting they constitute FtsZ protofilaments; (3) in the less ordered half of the ring, the protofilaments are able to assemble into higher-order structures such as double helices and supercoiled structures. Taken together, the data suggest that the state of existence of mini-rings could be described as metastable and their possible involvement in filament storage and Z-ring assembly is discussed.

Keywords: Chloroplast division, Correlative imaging, FtsZ mini-rings, Fluorescence microscopy, Transmission electron microscopy, Electron tomography, Structured illumination microscopy, High-pressure freezing, Freeze substitution

Background

Chloroplasts are essential plant organelles that arose from cyanobacterial ancestors by the process of endosymbiosis. Chloroplast division is required to maintain both the size and number of chloroplasts, which in turn affect photosynthetic performance of the plant via the control of surface-to-volume ratio with larger ratios facilitating the exchange of metabolites between the chloroplast and the cytosol. The size of starch-storing plastids (amyloplasts) affects the properties of starch granules. Controlling the latter in crops is of interest to industries concerned with the applications of starch [1, 2], and to this end it is critical to understand by what mechanism plastid/chloroplast size is controlled. Basically, both bacteria and chloroplasts divide by the process of binary fission. Following on from that, the division process is initiated by assembly of the cytoskeletal protein FtsZ into filaments that form a ring structure, the Z-ring, at the division site [3, 4]. Plants and algae encode two conserved FtsZ families, FtsZ1 and FtsZ2 [5–7], which are functionally different and are both required for plastid division and plastid size control. Changes in FtsZ expression levels or assembly lead to dramatic phenotypes such

*Correspondence: holzen@tamu.edu
[4] Microscopy and Imaging Center, Texas A&M University, Interdisciplinary Life Sciences Building, 2257 TAMU, College Station, TX 77843-2257, USA
Full list of author information is available at the end of the article

as single giant chloroplasts covering entire mesophyll cells [8–10]. Z-ring formation/assembly depends on the balance between FtsZ and accessory chloroplast division proteins, which either stabilize (ARC6 [11, 12], MinE [3, 13, 14]) or destabilize (ARC3 [15], PARC6 [16]) FtsZ assemblies.

The properties and the assembly mechanism of plant FtsZ1 and FtsZ2 have been explored in vitro. FtsZ1 and FtsZ2 have differential guanosine triphosphatase (GTPase) activity [17, 18] and are capable of linear co-assembly to form heteropolymers [17]. FtsZ1 and FtsZ2 exhibit dynamic turnover in vivo [19] that is promoted by the ARC3 protein [20]. How the individual FtsZ filaments assemble into higher-order structures to form the chloroplast dividing Z-ring is not well understood. Some insight has been gained from studies with FtsZ from prokaryotes. Cryo-TEM tomography revealed that the Z-ring is composed of short, partially overlapping protofilaments [21]. In contrast, in vitro reconstitution with only FtsZ and FtsA showed a continuous protofilament encircling the constricted liposomes several times [22]. The constriction force is thought to result from either bending of FtsZ protofilaments upon guanosine triphosphate (GTP) hydrolysis [23, 24] or, as was proposed recently, may involve protofilament sliding that is independent of GTP hydrolysis [22]. GTP hydrolysis and dynamic turnover are nevertheless essential for spatial regulation of Z-rings by accessory proteins that also mediate remodeling of FtsZ filaments into highly curved bundles and vortices [25, 26].

In contrast to bacterial FtsZ, the in vitro assembled plant FtsZ1 and FtsZ2 proteins did not show highly curved filaments [17, 27], hinting that in chloroplast the curvature and force for constriction could be generated by other components of the division machinery, such as the dynamin-related protein ARC5 residing on the outside of the chloroplast envelope [28, 29]. The arrangement of FtsZ protofilaments in the Z-ring in chloroplasts and how they bend and proceed in chloroplast division remains unknown. Highly curved, small ring-like FtsZ assemblies, termed mini-rings, have been reported in plant chloroplasts and studied by optical microscopy [3, 15, 30, 31]. It is hypothesized that the structural signature principles identified in these highly curved small assemblies may also play a role in the actual Z-ring. In this study, a detailed analysis of FtsZ mini-ring structure was conducted using SIM and electron tomography in *Arabidopsis thaliana* chloroplasts.

Methods

Plant material

Arabidopsis thaliana was chosen for this study as it is an established model organism. The *A. thaliana* ecotype Columbia (Col-0) and the mutants used in this study were obtained from the Arabidopsis Biological Resource Center (ABRC; http://www.arabidopsis.org): *arc6* (AT5G42480, CS286) and *arc12* (At1G69390, CS16472). Negative control plants were untransformed *ftsZ2-1/2-2* double knockout plants [10]. The *At*FtsZ2–mYFP construct has been described previously [20]. Plants were grown in Redi-Earth (SunGro Horticulture, Bellevue, WA, USA) substrate in a rooftop greenhouse at a temperature of 72 °C and a relative humidity of 62 %. *Agrobacterium*-mediated transformation of *Arabidopsis* wild-type Col-0 plants and selection of the herbicide-resistant seedlings were performed as described [4, 32].

Immunofluorescence labeling and optical microscopy

Leaf and shoot meristematic tissue was fixed, embedded in Steedman's wax, immunolabeled with anti-FtsZ2 antibody and documented by wide-field fluorescence microscopy as described previously [4]. Live imaging was performed using an Olympus FV1000 confocal microscope (Olympus Scientific Solutions America, Waltham, MA, USA) equipped with a 60×/1.2 water immersion objective and a 515-nm laser for excitation. Prior to imaging, a drop of perfluorodecalin [33] was placed on the leaf tissue to remove air pockets from intercellular spaces and ensure good optical quality. YFP fluorescence was detected through a 535- to 575-nm bandpass filter, while the chlorophyll autofluorescence was collected in the 670- to 700-nm range. Sections from resin-embedded tissue after HPF–FS were mounted in immersion oil and imaged using a 100×/1.4 oil immersion objective.

For structured illumination microscopy, leaf tissue was formaldehyde fixed under microwave irradiation, a process that preserves both the structural detail and the fluorescent protein signal [20, 34]. The tissue was vacuum infiltrated with 3 % formaldehyde in phosphate-buffered saline (PBS, 0.14 M NaCl, 2.7 mM KCl, 6.5 mM Na_2HPO_4, 5 mM KH_2PO_4, 3.0 mM NaN_3; pH = 7.3) and incubated at room temperature for 30 min. It was then fixed in a Pelco Biowave (Ted Pella, Inc., Redding, CA, USA) laboratory microwave processor equipped with a ColdSpot® temperature control system, with power set to 250 W and a 6-min cycle (2 min on, 2 min off, 2 min on). The temperature cutoff was set to 37 °C. The tissue was then rinsed in PBS three times, with microwave irradiation 1 min at 250 W power in each rinse and then gradually infiltrated with 30, 50, 80 % v/v Glycerol in PBS mixture, with microwave irradiation of 1 min at 250 W power in each step. The tissue was then left in fresh 80 % v/v glycerol/PBS at 4 °C overnight and then either sent for imaging on the OMX microscope to GE Healthcare (formerly Applied Precision, Inc. Issaquah, WA, USA) or imaged on a Zeiss Elyra-S system. OMX imaging was

performed using a 100×/1.4 oil immersion objective, excitation 488 nm, emission centered at 525 nm, and voxel size 40 × 40 × 120 nm. Elyra-S imaging was performed with a 63×/1.4 oil immersion objective and voxel size 40 × 40 × 110 nm. Mini-ring diameter was measured using ImageJ software (http://imagej.nih.gov/ij/) for mini-rings that were parallel to the XY plane. A line intensity profile across the mini-ring was plotted and the peak-to-peak distance, which corresponds to mini-ring diameter, was determined from these plots.

Immunoblotting

Extracts from expanding leaves from approximately 5-week old plants were prepared, separated by SDS-PAGE and analyzed by immunoblotting as described [35]. Extract from approximately 1-mg fresh tissue was loaded per lane. Immunodetection with affinity-purified goat anti-peptide antibody, recognizing the residues 168 through 184 in AtFtsZ2-1 [35] was performed as described in Johnson et al. [20]. Equal loading was confirmed by Ponceau S staining of the RuBisCO band on membranes (0.1 % (w/v) Ponceau S in 5 % (v/v) acetic acid).

High-pressure freezing (HPF)–freeze substitution (FS)

Transgenic plants 3–4 weeks old were prescreened using a laser scanning confocal microscope for the presence of FtsZ mini-rings prior to HPF. A small piece of leaf tissue from either a plant expressing a *FtsZ2*–mYFP or from a control plant lacking FtsZ2 proteins was extracted from the base of young (20–30 mm) leaves using either a 2-mm-diameter biopsy punch or a scalpel and loaded into a Type B 0.3-mm deep specimen carrier (Technotrade, Manchester, NH, USA) filled with the cryoprotectant, 1-hexadecene (Sigma-Aldrich, Saint Louis, MO, USA). The filled specimen carrier was covered with the flat side of another specimen carrier. Subsequently, the specimen carrier sandwich was immediately loaded into a specimen carrier holder, inserted into the Wohlwend Compact 01 HPF machine (Technotrade, Manchester, NH, USA) and cryoimmobilized at −190 °C and 204.5 MPa of pressure. Afterward, the specimen holder was rapidly removed from the HFP machine and plunged into a liquid nitrogen (LN_2)-filled chamber. The specimen carriers containing the frozen hydrated samples were transferred under LN_2 to the pre-chilled cryovials using pre-cooled tweezers and stored in LN_2 until further processing. The FS solution used on the HFP samples was 4 % (w/v) uranyl acetate (UA) dissolved in glass-distilled acetone (EMS, Hatfield, PA, USA) that was opened immediately prior to use. Steps in the conventional as well as the quick freeze substitution (QFS) procedure are outlined in Table 1. The QFS method is a modification of the protocol that was first described by McDonald and Webb [36].

Table 1 Conventional FS and modified QFS procedures

Conventional FS	Modified QFS
FS (1 % UA/acetone)	FS (1 % UA/acetone)
−90 °C (76 h)	−169 to 23 °C over the course of 5 h
−45 °C (30 h)	
Infiltration schedule (−25 °C)	Infiltration schedule (25 °C)
Lowicryl-HM20/acetone	LR White/acetone
10 % (6 h)	10 % (13 h)
25 % (16 h)	20 % (3 h)
50 % (7.5 h)	30 % (2 h)
75 % (14.5 h)	40 % (19 h)
100 % (6.5, 19, 7 h)	50 % (2 h)
	60 % (2 h)
	70 % (3 h)
	80 % (1 h)
	90 % (1 h)
	100 % (15, 2, 2 h)
UV polymerization	Polymerization
−45 °C (48 h)	60 °C (24 h)
20 °C (48 h)	

UA uranyl acetate, *FS* freeze substitution

Microtomy and immunogold labeling

Semi-thin (300 nm) sections were cut on a Reichert-Jung Ultracut E microtome equipped with a diamond knife and mounted onto silane-coated microscope slides for light microscopy. Thin sections (80–100 nm) were cut in the same manner and picked up on uncoated nickel grids. Thin sections were blocked with 4 % (v/v) cold water fish gelatin (Sigma) in PBS in the Biowave microwave processor with power set to 250 W and a 2–2–2 cycle (2 min on, 2 min off, 2 min on). The temperature cutoff was set to 37 °C. The grids were reacted with monoclonal mouse anti-GFP antibody (Millipore, Temecula, CA, USA) diluted 1:500 in the PBS blocker, using the 2–2–2 cycle. Grids were washed 2 × 1 min with PBS and 2 × 1 min with Tris-buffered saline (TBS; 0.15 M NaCl, 20 mM Tris–HCl pH 7.4), then blocked with 4 % (v/v) cold water fish gelatin in TBS at 250 W using the 2–2–2 cycle. Grids were incubated in a 1:30 dilution of donkey anti-mouse IgG conjugated to 12-nm colloidal gold (Jackson ImmunoResearch, West Grove, PA, USA) at 250 W with a 2–2–2 cycle. Grids were washed in TBS 3 × 1 min followed by 3 × 1 min with deionized water, then reacted with 1 % (v/v) glutaraldehyde for 5 min on the bench before being washed for 3 × 1 min with deionized water and dried on a slide warmer.

Transmission electron microscopy and tomography

Grids were viewed in an FEI (Hillsboro, OR, USA) Tecnai™ G2 F20 operated at an acceleration voltage of 200 kV and equipped with a dedicated Fischione (Export, PA, USA) high-angle annular dark-field (HAADF) STEM detector, a GATAN (Pleasanton, CA, USA) Tridiem energy filter and a 2 k × 2 k GATAN Ultrascan 1000 CCD camera. Micrographs were recorded at calibrated magnifications, leading to a sampling of 1.1 nm/pixel in STEM and 0.39 nm/pixel in energy-filtered TEM mode. Tilt series were acquired from −75° to +73° in 1° increments using the FEI Xplore3D™ software. Datasets were reviewed using FEI Inspect 3D.

Reconstruction, segmentation and 3D rendering

All processing was performed in EM3D [37, 38]. Micrographs from −50° to 50° tilt could effectively be used yielding a total of 101 projections. Where gold fiducials were not present, alignment was done using statistically consistent features in the background as fiducial markers. Aligned projections were reconstructed into a 3D volume with 72 slices. The object edge on each slice was defined by dots, and the spline option provided a smooth edge for the connected dots. With filaments extending over 8–20 slices and with stacked regions, sudden changes in features were defined as edges between filaments. Segmented protofilaments were then colored and rendered with 40 % saturation of isosurface value so as not to smooth out surface modulations. Curvature measurements were performed in ImageJ with the three-point circular ROI plugin. The curvature was calculated as the inverse of the circle radius ($1/r$).

Images for publication were adjusted for contrast using Gimp 2.8. freeware (http://www.gimp.org) and multipanel figures assembled using Scribus ver. 1.4.2. freeware (http://www.scribus.net).

Results and discussion

FtsZ rings and mini-rings

In wild-type mature plants, consistent with previous reports [4, 9, 39], immunofluorescence labeling with an anti-FtsZ2 antibody showed FtsZ rings (Z-rings) encircling the mid-chloroplast in leaf mesophyll cells (Fig. 1a). Meristematic cells that harbor smaller plastids or proplastids contained much smaller Z-rings (Fig. 1b) that also presumably encircled the plastid, but the shape of these small plastids could not be determined from the micrographs. Another type of FtsZ assembly, small Z-rings, was often encountered in leaf mesophyll chloroplasts under conditions described below. These circular FtsZ assemblies are not restricted to the mid-plastid, their size is not dictated by the diameter of the plastid and they measure reproducibly and significantly less than 1 μm in diameter. Some are so small that they are only resolved as puncta in a standard light microscope., i.e., their diameter is ≤250 nm. These small circular FtsZ assemblies have been termed FtsZ mini-rings or mini-rings for short. The conditions under which they are formed are varied and complex. Mini-rings have for instance been observed in *Arabidopsis* wild-type background, moderately expressing FtsZ2–mYFP (Fig. 1c), wild-type background plants overexpressing FtsZ2–mYFP (Fig. 1d) or in mutants lacking the Z-ring-stabilizing factors ARC6 [31] or MinE [30] (Fig. 1e, f). Figure 1e, f is particularly relevant as native, untagged FtsZ was detected by a fluorescently labeled antibody. This means that min-ring formation need not be considered an artifact of fluorescent protein tagging.

Characterization of mini-rings by superresolution light microscopy

SIM capable of analyzing samples at a resolution beyond the Abbe limit [40] was chosen for a more detailed analysis of mini-rings in FtsZ2–mYFP overexpressing plants. The resolution of SIM images was estimated by measuring full width at half maximum (FWHM) ± SD of linear FtsZ filaments. Data from the OMX microscope provided a resolution of 118 ± 11 nm (n = 28) laterally and 354 ± 26 nm (n = 27) axially. Ringing artifacts were noted, probably due to aggressive image reconstruction. Resolution in the Zeiss Elyra-S images was 138 ± 13 nm (n = 29) laterally and 547 ± 70 nm (n = 25) axially with less pronounced processing artifacts. The latter images also contained chlorophyll fluorescence channel suitable for measurement of chloroplast size and volume. Nearly, all of the small punctate structures were resolved as mini-rings (Fig. 2a) with a mean diameter of 208 ± 68 nm (n = 248) (Fig. 2b). The mean chloroplast volume was determined as 660 ± 450 μm^3 (n = 20) containing between 10 and 16 rings in most cases with an occasional surge up to 40–80. The increased resolution afforded by SIM images allowed to resolve the mini-rings below the diffraction limit and to investigate the spatial relationship between circular and linear FtsZ assemblies. It was noted that while some (32.2 %; n = 214) mini-rings appeared to be isolated from other FtsZ assemblies, most (67.8 %; n = 214) appeared to be terminally attached to FtsZ filaments. Examples of mini-ring attachments to filaments are shown in Fig. 2c. The attachment of mini-rings to linear FtsZ filaments was previously observed by (1) immunofluorescence labeling in the *arc6* mutant (S. Vitha, unpublished), (2) in vivo time-lapse microscopy in the *Arabidopsis minE* mutant [30] and (3) in yeast *S. pombe* expressing bacterial FtsZ–GFP [41]. It has been proposed that the mini-rings are formed by spooling the end of single or multiple filaments [30, 41].

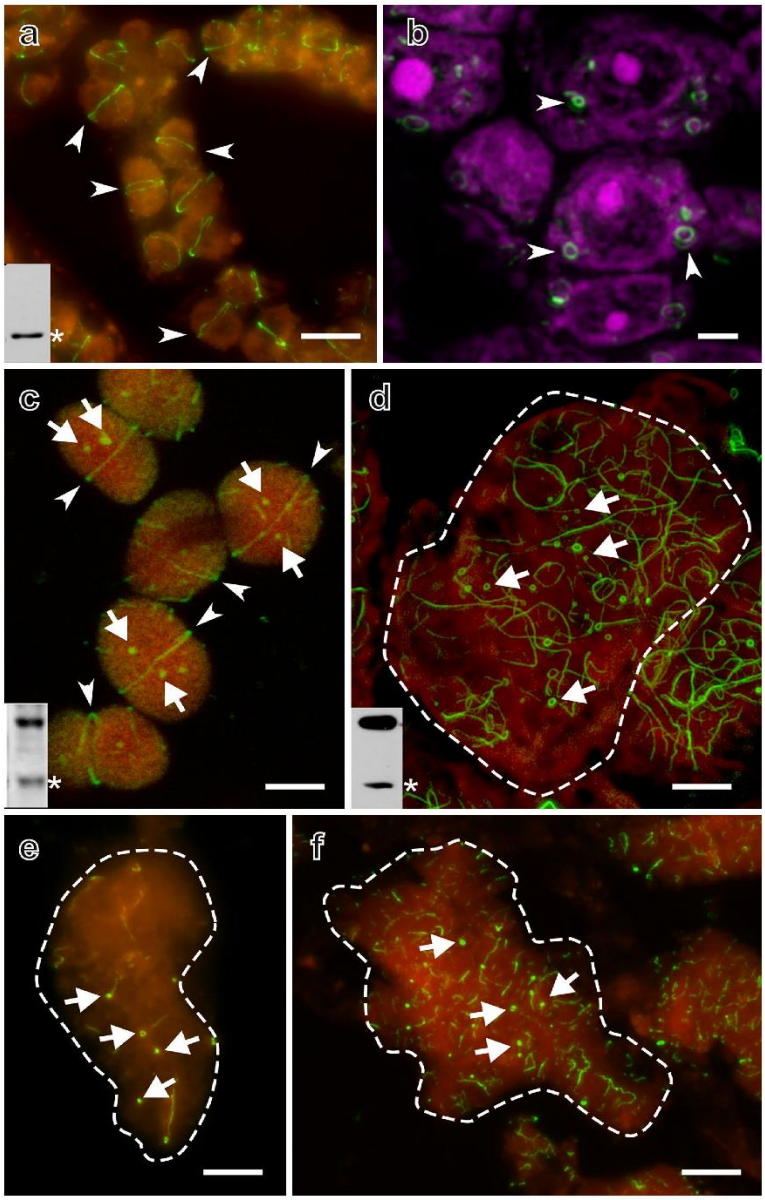

Fig. 1 Fluorescence microscopy of FtsZ2 assemblies in situ. **a**, **b** Wide-field immunofluorescence micrograph of FtsZ2 in Z-rings (*arrowheads*) in wild-type leaf chloroplasts (**a**) and smaller-size Z-rings in cells of the apical meristem (**b**). Individual proplastids cannot be discerned in meristematic cells. **c**, **d** Confocal micrographs of filamentous and circular (*arrows*) FtsZ assemblies in leaf mesophyll chloroplasts in a plant expressing FtsZ2–mYFP at moderate (**c**) and high (**d**) levels. The *arrowheads* in **c** denote Z-rings at mid-chloroplast. *Inserts* in **a**, **c**, **d** depict immunoblots showing relative levels of the intrinsic, untagged FtsZ2 (marked by an *asterisk*) vs. FtsZ2-fusion protein. **e**, **f** Immunofluorescence localization of FtsZ2 in leaf mesophyll chloroplasts of mutants lacking MinE and ARC6 proteins, respectively. FtsZ mini-rings are indicated by *arrows*. The *dashed lines* in **d**–**f** denote chloroplast shapes. *Scale bars* correspond to 5 μm in **a**, **c** **f** and 2 μm in **b**

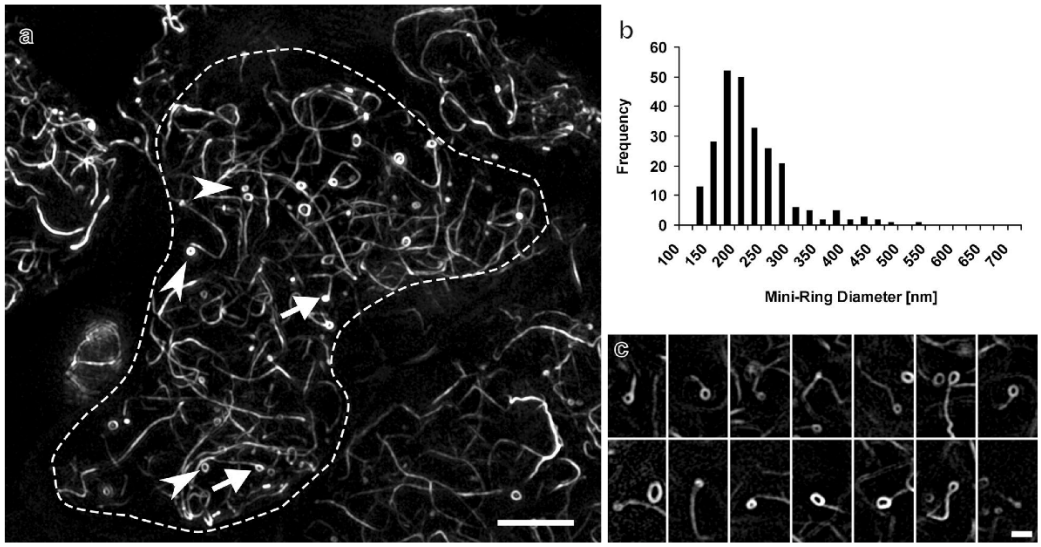

Fig. 2 SIM imaging of FtsZ2–mYFP mini-rings and filamentous assemblies in leaf mesophyll chloroplasts. **a** Maximum intensity projection showing both filaments and mini-rings in an enlarged leaf chloroplast. The *dashed line* delineates the shape of the chloroplast. Some mini-rings appear attached to the end of linear FtsZ filaments (*arrows*), while others are unattached (*arrowheads*). **b** Distribution of mini-ring diameters. **c** Optical sections showing FtsZ mini-rings contiguous with linear FtsZ filaments. *Scale bars* correspond to 5 μm in **a** and 1 μm in **c**

HPF–FS for correlative imaging of plant chloroplasts

To investigate the mini-ring assemblies at macromolecular dimensions in situ, leaf samples had to be prepared for electron microscopy. The ability to study-specific molecular targets and their 3D organization by fluorescence microscopy and to subsequently explore the same object in detail by electron microscopy sidesteps the limitations of either technique. The challenge of plant tissue and especially the localization of fluorescent proteins inside chloroplast is quenching of the fluorescent protein signal and high tissue autofluorescence that can be induced during sample preparation. The requirements for sample preparation were (1) structural preservation, (2) maintaining specific fluorescence to aid correlative light and electron microscopy, and (3) minimizing the autofluorescence of the plant chloroplast. Initially, methods employing isolation of intact chloroplasts, and extraction and fractionation on density gradients [42] were explored to obtain chloroplast division machineries. These attempts needed to be eventually abandoned as they met with little to no success. Following on from this, microwave-assisted aldehyde fixation of leaf tissue followed by dehydration and resin embedding were pursued. While live leaf tissue before embedding (Fig. 3a) was characterized by an excellent signal-to-noise ratio showing several mini-rings per chloroplast, semi-thin section of embedded tissue exhibited a loss of YFP fluorescence in combination with a substantial increase in autofluorescence background (Fig. 3b) preventing the detection of FtsZ2–mYFP assemblies. Ultimately, high-pressure freezing in conjunction with freeze substitution (HPF–FS) and embedding in acrylic resins led to a successful preservation of the specific fluorescence signal as well as an attenuation of autofluorescence. The QFS procedure developed by McDonald and Webb [36] was adapted to introduce time and cost savings. In keeping with the main objectives, i.e., maintaining signal and minimizing fluorescence background, it was necessary to modify the infiltration procedure. This entailed changing the resin from Epon/acetone to LR White/acetone and extending the infiltration to a more gradual protocol (see "Methods"). FtsZ–mYFP fluorescence within chloroplasts was preserved and easily detected in semi-thin sections (300 nm), and a low autofluorescence background was maintained revealing both mini-rings and short linear FtsZ assemblies (Fig. 3c). The lack of chloroplast-localized FtsZ signals in sections from control tissue lacking FtsZ2 (Fig. 3d) confirmed that the signals observed in Fig. 3c were due to FtsZ2–mYFP.

The HPF approach offers to preserve organelles and other cellular components by instantaneous stabilization [43] in a manner superior to chemical fixatives [44].

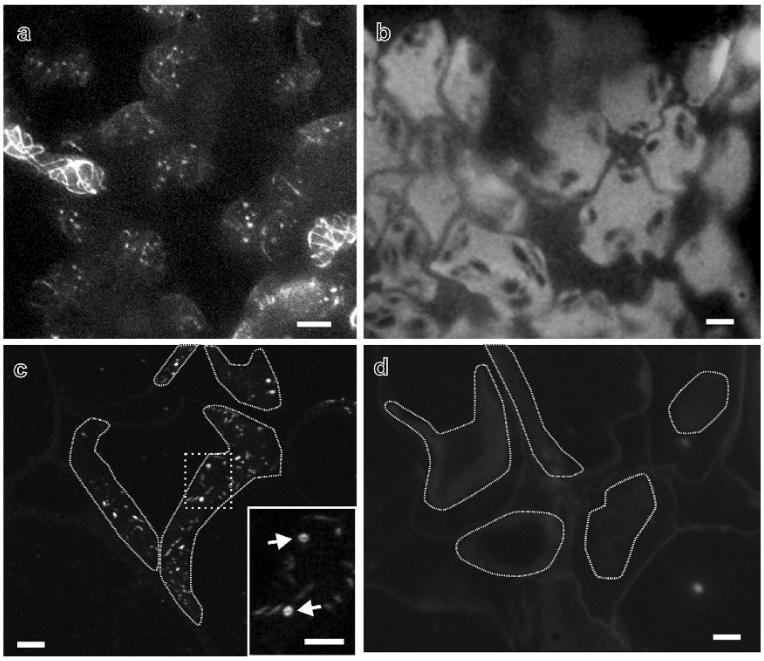

Fig. 3 Preservation of YFP fluorescence after resin embedding. **a** Wide-field fluorescence microscopy of live leaf tissue showing multiple FtsZ2–mYFP mini-rings per chloroplast. **b** Semi-thin section from aldehyde-fixed tissue embedded in LR White. Chloroplasts are recognized by their high fluorescence background. **c**–**d** Semi-thin sections from leaf tissue subjected to HPF–FS and embedding in LR White. Chloroplasts are delineated by *dotted lines*. **c** Punctate and short linear FtsZ2–mYFP assemblies in resin sections. The area corresponding to the *highlighted square* is shown at higher magnification in the *insert* where some of the assemblies are resolved as mini-rings (*arrows*). **d** Mutant plant lacking FtsZ2 proteins (negative control). *Scale bars* represent 5 µm in **a**–**d** and 2 µm in the *insert* in **c**

Both acrylic resins used, Lowicryl HM20 and LR White, proved capable of maintaining the fluorescent protein signal. This is in agreement with previous reports where methacrylates, LR White or Lowicryl have been employed in conjunction with plant and animal tissue and yeast cells [45–48].

In situ electron microscopy/tomography of chloroplast mini-ring assemblies

Prior studies with prokaryotic FtsZ, which is closely related to the plant FtsZ2 protein [5–7], showed the presence of small circular assemblies under certain in vitro assembly conditions. Some were very small, measuring approximately 25 nm in diameter and were termed mini-rings [49, 50]. Under conditions of molecular crowding, larger circular assemblies (~200 nm) termed mini-rings or toroids were reported [51, 52]. The relevance of these in vitro assemblies to the assembly of FtsZ in vivo is being debated.

In the current study, both STEM and TEM imaging of thin sections from resin-embedded tissue revealed small circular structures (Fig. 4a, b, respectively) with a mean diameter of 183 ± 50 nm (n = 21), which is in excellent agreement with the mini-ring diameter distribution determined by SIM imaging (Fig. 2). In negative control samples from FtsZ2-null mutant *Arabidopsis*, no circular assemblies could be observed. While mini-rings presented themselves as 'solid' rings by conventional light microscopy as well as SIM imaging, much more complex features were discernible by TEM and STEM. The rings appeared to be made up of multiple strands and bundles of various diameters and different degrees of order (Fig. 4). In particular, it was noted that roughly half of each ring was 'tight', while the other half appeared somewhat frayed. In the STEM dark-field image (Fig. 4a), because of the higher contrast when compared with the TEM bright-field image (Fig. 4b), even individual strands in a parallel packing arrangement between 10 and 12

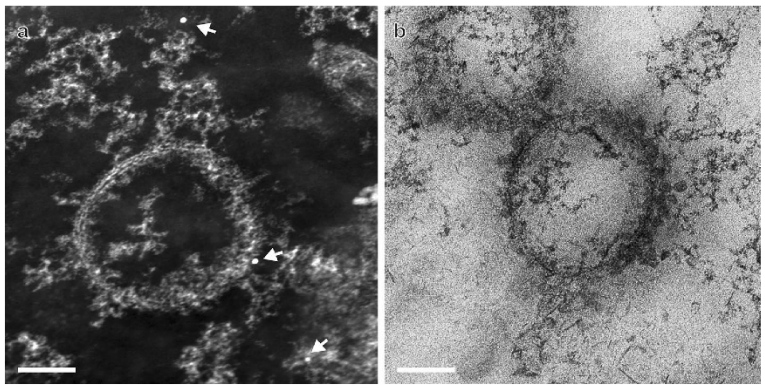

Fig. 4 STEM and TEM of mini-ring assemblies in thin sections. Single images from a tomographic tilt series are shown. **a** STEM dark-field image with 12 nm gold fiducial markers indicated by *arrows*. **b** TEM bright field image depicting a different mini ring. *Scale bars* correspond to 100 nm

o'clock are readily discernible. To further decipher the intrinsic architecture of these mini-rings and improve the signal-to-noise ratio, tomography in conjunction with 3D reconstruction was employed. With only 10–16 mini-rings per chloroplast (see above) and one thin section of approximately 100 nm (the thickness of a chloroplast is between 5 and 10 μm corresponding to 50–100 thin sections) needing to harbor a mini-ring that is located sufficiently central in a grid window not affected by grid bars upon tilting the specimen and aligned parallel with the plane of the thin section, tomography-compatible mini-rings were rarely encountered. While the criteria for extended slab geometry in tomographic reconstructions suggests in this case an isotropic 3D resolution of only around 4–5 nm, given the tilt angle range, thickness and number of projections [53], the resolution of a single section in projection is less constrained by these parameters and thus may reveal detail not readily available in the 3D rendering. This is demonstrated in the section of a tomogram shown in Fig. 5. Surveying the overall structural revealed a region with clearly separated strands as highlighted by the boxed area (Fig. 5a). Further magnifications of the area of interest (Fig. 5b, c) show clearly discernible linearly arranged densities measuring 12.6 nm over three repeats making one repeat 4.2 nm along the axis and approximately 3 nm perpendicular to it (strand thickness). Comparing the observed density distribution with the overall structural characteristics of an FtsZ protofilament (Fig. 5e, f) suggests that the observed strands correspond to protofilaments. While single sections may show more details for small regions of interest like those highlighted area in Fig. 5, other regions in the mini-ring appear very disordered, such as the entire right-hand side of the mini-ring. Here, clearly discernible features may only stand out by taking the entire 3D information into consideration. This was achieved by tracking individual protofilaments through 3D space and subjecting the tomograms to segmentation, the results of which are shown in Fig. 6. A previous tomography study revealed segments of FtsZ protofilaments during bacterial cell division and showed that the Z-ring was composed of multiple parallel, relatively short and overlapping protofilaments [21]. The present data reveal that the FtsZ mini-ring has a more complex, multilayered structure composed of many protofilaments: 49 have been counted for the mini-ring shown (Fig. 6a).

On comparing the left-hand side (LHS) with the right-hand side (RHS) of the ring, different degrees of orders are observed echoing the trend already observed before segmentation and rendering (Figs. 4, 5). The RHS shows a higher degree of unraveling and entanglement, while the LHS is characterized by one curvilinear bundle consisting of parallel protofilaments surrounded by loosely interwoven filaments. Another distinct difference between the LHS and RHS relates to overall filament curvature. While the RHS of the ring showed only a slight degree of curvature, the LHS' curvature was on average threefold higher (Fig. 6b). This suggests a correlation between protofilament bundling and curvature. Upon closer inspection of the 3D reconstruction, it appears that the protofilaments can participate in higher-order structures at three levels. (1) The primary level is characterized by the aforementioned protofilaments. Distinct grooves delineate the long axis of the protofilaments at around 4-nm

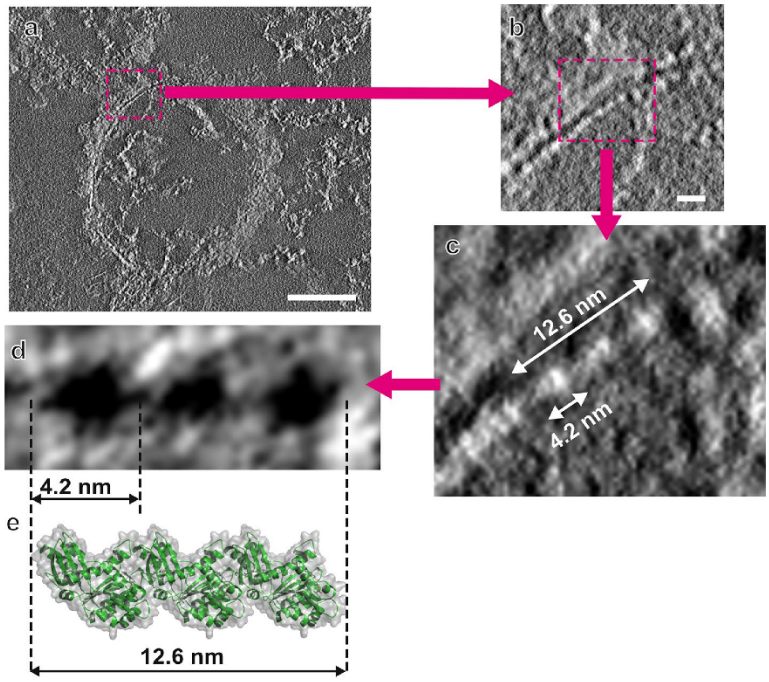

Fig. 5 Molecular details in an FtsZ mini-ring strand. **a** Central section from a 3D tomographic reconstruction of an in situ mini-ring revealing individual filamentous strands. **b**, **c** Zooming into the areas *highlighted* shows periodic densities as part of an individual strand. **d** Contrast inverted final enlargement of three periodic densities extending over 12.6 nm with a 4.2-nm repeat. Length scale, periodicity and shape are in excellent agreement with the X-ray structure of an FtsZ protofilament in **e**. Fitted atomic structures of individual FtsZ subunits are shown in *green*. *Scale bars* correspond to 100 nm in **a** and 10 nm in **b**

intervals and these filaments measure approximately 3 nm across (Fig. 6c). (2) Secondary-level structures are represented by two protofilaments together twisting around a central axis, thus creating quasi-double helical structures. These structures have a pitch of between 10 and 15 nm and a width of 7.6 nm (Fig. 6d). These data are in good agreement with the 13.25-nm pitch observed with double-stranded FtsZ protofilaments from *Mycobacterium tuberculosis* [21]. (3) A tertiary level of hierarchical structures is observed when double helical structures intertwine into superhelical assemblies, the example of which is depicted in Fig. 6e. As a general trend for this particular mini-ring, the higher-order structures dominate the RHS of the ring while the more orderly structured LHS appears to be more populated by protofilaments. Such a dichotomy points at a dynamics not reported previously. In essence, the structure looks as if it presents a balance between two states: a state of disassembly and one of assembly. The latter could lead from an interwoven and entangled arrangement to orderly layered structures. We speculate that if the tightly arranged filament bundles are disturbed, individual filaments may be able to assume different higher-order structures such as the ones described above.

While the mini-rings could be considered metastable as per the earlier reasoning, they may also serve in this capacity as an energetically favorable way of protofilament storage. This would be particularly important in times of high abundance of FtsZ such as that observed in young, metabolically active cells. By virtue of their curvature, they could also bestow the assembly with inherent energy leading to pre-energized, 'ready-to-assemble' protofilaments for a more responsive supply of Z-ring building blocks. The relatively high percentage of mini-rings found attached to linear filaments corroborate such an idea.

In a broader context, the presented data provide first insights into the molecular architecture of plant FtsZ assemblies in situ featuring bundling of filaments, a

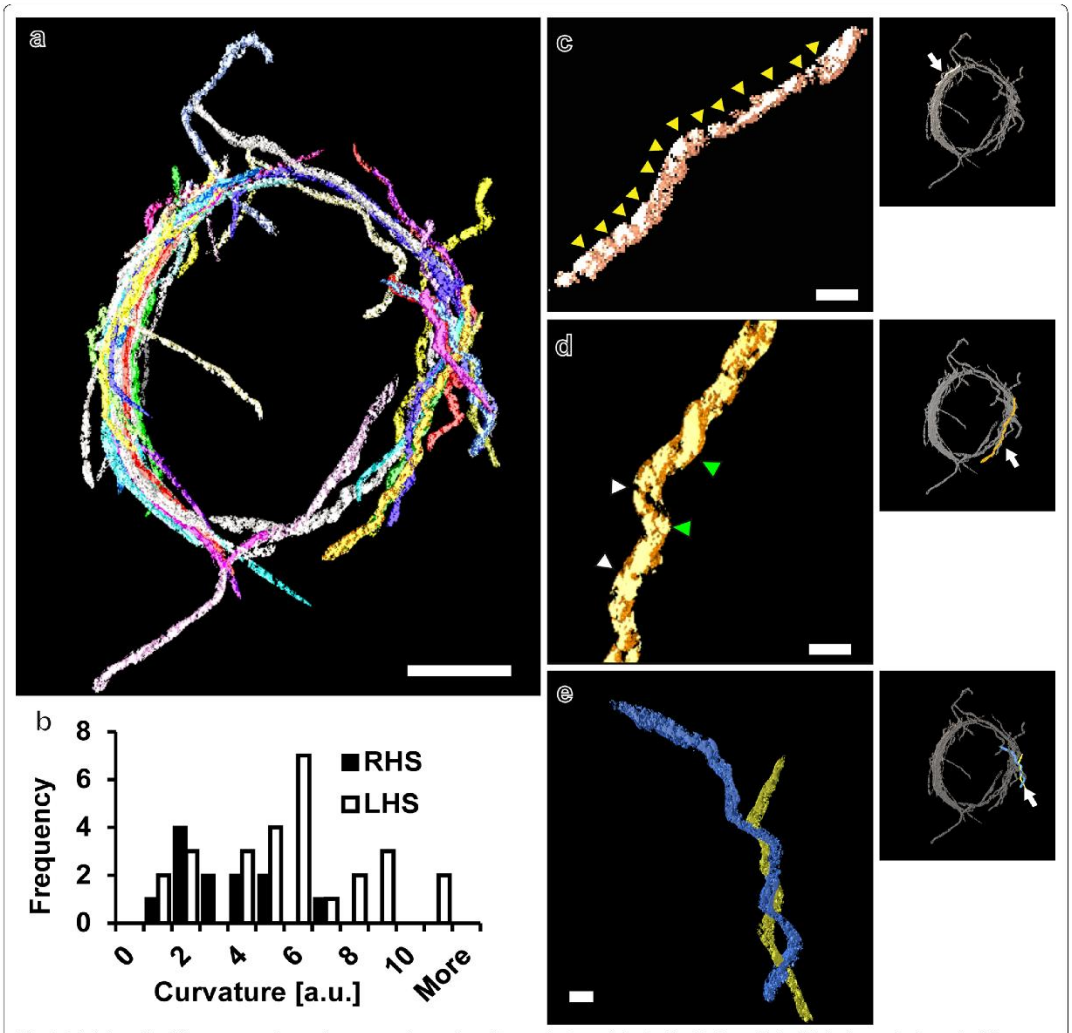

Fig. 6 Mini-ring after 3D reconstruction and segmentation. **a** Overall organization of the FtsZ mini-ring with individual strands shown in *different colors*. **b** Distribution of protofilament curvature measured in the left and right hand side of the mini ring (*LHS* and *RHS*, respectively). **c** A protofilament with 4- to 6-nm longitudinal repeats highlighted by *yellow arrowheads*. **d** Twisted filaments (double helix) with a pitch between 10 and 15 nm. *White* and *green arrowheads* are separated by 360° each, i.e., one turn along the central axis. **e** Intertwined superhelices. In **c**–**e**, the accompanying *panels* highlight the position of the featured objects (marked by an *arrow*) in the mini-ring. *Scale bars* correspond to 100 nm in **a**, 5 nm in **c** and 10 nm in **d**, **e**

multilayered structure, differential protofilament curvature as well as higher-order structures such as superhelices. While the curvature of plant FtsZ protofilaments was not observed in vitro [17, 27], clearly the mini-rings show that FtsZ is able to form curved assemblies without depending on cytosolic components such as ARC5 [28, 29]. Perhaps, the propensity of FtsZ to curve is predicated on the features summarized above. On the other hand, these features could also echo the dynamic remodeling that FtsZ assemblies are constantly undergoing [19, 20].

Conclusions

1. Chloroplast division is highly complex and of societal importance as the mechanisms underlying this process also control the starch granule size.
2. FtsZ is a key protein of chloroplast division and this report presents the first electron tomographic 3D structure of plant FtsZ assembly in situ. The assembly form presented here are the FtsZ mini-rings which occur under defined physiological conditions.
3. Comparative SIM and EM imaging yielded matching mini-ring diameters. Combining light microscopy screening with a detailed EM analysis via tomography laid the foundations for the development of correlative microscopy-compliant protocols involving HPF and FS.
4. Assessment of resolution for the tomographic data set according to the Crowther theorem [53] only suggests 4 to 5-nm resolution in the 3D reconstruction; however, the resolution is much better in projection as demonstrated by a comparison with X-ray data. The latter led to the identification of protofilaments in the tomogram. These protofilaments can also assemble into higher-order structures such as double helices and superhelical arrangements.
5. The data provide a glimpse into the dynamic life of FtsZ assemblies. Electron microscopy and tomography readily revealed a very dynamic picture of the mini-rings highlighted by a bipartite structure splitting the ring into an ordered and less ordered half. This implies that the rings may undergo dynamic remodeling by providing FtsZ building blocks for Z-ring assembly or a form of storage of protofilaments.

Authors' contributions

CBJ carried out the cloning, plant transformation and sample preparation for TEM, participated in the design of experiments and drafted the manuscript. ZLo performed the reconstruction and segmentation of the EM tomograms. ZLu performed the STEM and EFTEM imaging. RS carried out the immunoassays and MWS the fitting of/comparison with X-ray data. SV performed the confocal microscopy and carried out sample preparation for SIM. AH conceived the study and participated in EM data analysis. AH and SV participated in the design of experiments and carried out the SIM data analysis. AH and SV co-wrote the manuscript. All authors read and approved the final manuscript.

Author details

[1] Department of Biology, Texas A&M University, College Station, TX 77843-3258, USA. [2] Department of Chemistry and Biochemistry, University of California San Diego, La Jolla, CA 92093, USA. [3] Department of Chemistry and Physics, Fayetteville State University, Fayetteville, NC 28301, USA. [4] Microscopy and Imaging Center, Texas A&M University, Interdisciplinary Life Sciences Building, 2257 TAMU, College Station, TX 77843-2257, USA. [5] Department of Biochemistry and Biophysics, Texas A&M University, College Station, TX 77843-3258, USA.

Acknowledgements

The authors thank the Office of the Vice President for Research at Texas A&M University for the continued support of the Microscopy and Imaging Center. SIM was performed by GE Healthcare Life Sciences (formerly Applied Precision; Issaquah, WA, USA) and Zeiss Microimaging (Thornwood, NJ, USA). The *ftsZ2-1/2-2* double knockout plants were obtained from Dr. Katherine Osteryoung (Michigan State University).

Compliance with ethical guidelines

Competing interests

The authors declare that they have no competing interests.

Received: 28 July 2015 Accepted: 28 August 2015
Published online: 17 September 2015

References

1. Lindeboom, N., Chang, P.R., Tyler, R.T.: Analytical, biochemical and physicochemical aspects of starch granule size, with emphasis on small granule starches: a review. Starch Starke **56**(3–4), 89–99 (2004)
2. de Pater, S., Caspers, M., Kottenhagen, M., Meima, H., ter Stege, R., de Vetten, N.: Manipulation of starch granule size distribution in potato tubers by modulation of plastid division. Plant. Biotech. J. **4**(1), 123–134 (2006)
3. Maple, J., Aldridge, C., Møller, S.G.: Plastid division is mediated by combinatorial assembly of plastid division proteins. Plant J. **43**(6), 811–823 (2005)
4. Vitha, S., McAndrew, R.S., Osteryoung, K.W.: FtsZ ring formation at the chloroplast division site in plants. J. Cell Biol. **153**(1), 111–119 (2001)
5. Miyagishima, S.Y., Nozaki, H., Nishida, K., Nishida, K., Matsuzaki, M., Kuroiwa, T.: Two types of FtsZ proteins in mitochondria and red-lineage chloroplasts: the duplication of FtsZ is implicated in endosymbiosis. J. Mol. Evol. **58**(3), 291–303 (2004)
6. Stokes, K.D., Osteryoung, K.W.: Early divergence of the *FtsZ1* and *FtsZ2* plastid division gene families in photosynthetic eukaryotes. Gene **320**, 97–108 (2003)
7. Terbush, A.D., Yoshida, Y., Osteryoung, K.W.: FtsZ in chloroplast division: structure, function and evolution. Curr. Opin. Cell Biol. (2013). doi:10.1016/j.ceb.2013.04.006
8. Osteryoung, K.W., Stokes, K.D., Rutherford, S.M., Percival, A.L., Lee, W.Y.: Chloroplast division in higher plants requires members of two functionally divergent gene families with homology to bacterial *ftsZ*. Plant Cell **10**(12), 1991–2004 (1998)
9. Yoder, D.W., Kadirjan-Kalbach, D., Olson, B.J.S.C., Miyagishima, S.Y., DeBlasio, S.L., Hangarter, R.P., Osteryoung, K.W.: Effects of mutations in *Arabidopsis* FtsZ1 on plastid division, FtsZ ring formation and positioning, and FtsZ filament morphology in vivo. Plant Cell Physiol. **48**(6), 775–791 (2007)
10. Schmitz, A.J., Glynn, J.M., Olson, B.J.S.C., Stokes, K.D., Osteryoung, K.W.: *Arabidopsis* FtsZ2-1 and FtsZ2-2 are functionally redundant, but FtsZ-based plastid division is not essential for chloroplast partitioning or plant growth and development. Mol. Plant **2**(6), 1211–1222 (2009). doi:10.1093/mp/ssp077
11. Glynn, J.M., Froehlich, J.E., Osteryoung, K.W.: *Arabidopsis* ARC6 coordinates the division machineries of the inner and outer chloroplast membranes through interaction with PDV2 in the intermembrane space. Plant Cell **20**(9), 2460–2470 (2008)
12. Vitha, S., Froehlich, J.E., Koksharova, O., Pyke, K.A., van Erp, H., Osteryoung, K.W.: ARC6 is a J-domain plastid division protein and an evolutionary descendant of the cyanobacterial cell division protein Ftn2. Plant Cell **15**(8), 1918–1933 (2003)
13. Maple, J., Chua, N.H., Møller, S.G.: The topological specificity factor AtMinE1 is essential for correct plastid division site placement in *Arabidopsis*. Plant J. **31**(3), 269–277 (2002)
14. Fujiwara, M.T., Hashimoto, H., Kazama, Y., Abe, T., Yoshida, S., Sato, N., Itoh, R.D.: The assembly of the FtsZ ring at the mid chloroplast division site depends on a balance between the activities of AtMinE1 and ARC11/AtMinD1. Plant Cell Physiol. **49**(3), 345–361 (2008)
15. Zhang, M., Schmitz, A.J., Kadirjan-Kalbach, D.K., Terbush, A.D., Osteryoung, K.W.: Chloroplast division protein ARC3 regulates chloroplast FtsZ-ring assembly and positioning in *Arabidopsis* through interaction with FtsZ2. Plant Cell **25**(5), 1787–1802 (2013). doi:10.1105/tpc.113.111047

16. Glynn, J.M., Yang, Y., Vitha, S., Schmitz, A.J., Hemmes, M., Miyagishima, S.Y., Osteryoung, K.W.: PARC6, a novel chloroplast division factor, influences FtsZ assembly and is required for recruitment of PDV1 during chloroplast division in *Arabidopsis*. Plant J. **59**(5), 700–711 (2009)
17. Olson, B.J., Wang, Q., Osteryoung, K.W.: GTP-dependent heteropolymer formation and bundling of chloroplast FtsZ1 and FtsZ2. J. Biol. Chem. **285**(27), 20634–20643 (2010). doi:10.1074/jbc.M110.122614
18. Smith, A.G., Johnson, C.B., Vitha, S., Holzenburg, A.: Plant FtsZ1 and FtsZ2 expressed in a eukaryotic host: GTPase activity and self-assembly. FEBS Lett. **584**(1), 166–172 (2010)
19. TerBush, A.D., Osteryoung, K.W.: Distinct functions of chloroplast FtsZ1 and FtsZ2 in Z-ring structure and remodeling. J. Cell Biol. **199**(4), 623–637 (2012). doi:10.1083/jcb.201205114
20. Johnson, C.B., Shaik, R., Abdallah, R., Vitha, S., Holzenburg, A.: FtsZ1/FtsZ2 turnover in chloroplasts and the role of ARC3. Microsc. Microanal. 1–11 (2015). doi:10.1017/S1431927615000082
21. Li, Z., Trimble, M.J., Brun, Y.V., Jensen, G.J.: The structure of FtsZ filaments in vivo suggests a force-generating role in cell division. EMBO J. **26**(22), 4694–4708 (2007)
22. Szwedziak, P., Wang, Q., Bharat, T.A.M., Tsim, M., Löwe, J.: Architecture of the ring formed by the tubulin homologue FtsZ in bacterial cell division. Elife **3**, e04601 (2014). doi:10.7554/eLife.04601
23. Li, Y., Hsin, J., Zhao, L., Cheng, Y., Shang, W., Huang, K.C., Wang, H.W., Ye, S.: FtsZ protofilaments use a hinge-opening mechanism for constrictive force generation. Science **341**(6144), 392–395 (2013). doi:10.1126/science.1239248
24. Osawa, M., Erickson, H.P.: Liposome division by a simple bacterial division machinery. Proc. Natl. Acad. Sci. USA. **110**(77), 11000–11004 (2013). doi:10.1073/pnas.1222254110
25. Loose, M., Mitchison, T.J.: The bacterial cell division proteins FtsA and FtsZ self-organize into dynamic cytoskeletal patterns. Nat. Cell Biol. **16**, 38–46 (2014). doi:10.1038/ncb2885
26. Arumugam, S., Petrasek, Z., Schwille, P.: MinCDE exploits the dynamic nature of FtsZ filaments for its spatial regulation. Proc. Natl. Acad. Sci. USA. **111**(13), E1192–E1200 (2014). doi:10.1073/pnas.1317764111
27. Smith, A.G., Johnson, C.B., Vitha, S., Holzenburg, A.: Oligomerization of plant FtsZ1 and FtsZ2 plastid division proteins. Arch. Biochem. Biophys. **513**(2), 94–101 (2011). doi:10.1016/j.abb.2011.07.001
28. Gao, H., Kadirjan-Kalbach, D., Froehlich, J.E., Osteryoung, K.W.: ARC5, a cytosolic dynamin-like protein from plants, is part of the chloroplast division machinery. Proc. Natl. Acad. Sci. USA. **100**(7), 4328–4333 (2003)
29. Miyagishima, S.Y., Froehlich, J.E., Osteryoung, K.W.: PDV1 and PDV2 mediate recruitment of the dynamin-related protein ARC5 to the plastid division site. Plant Cell **18**(10), 2517–2530 (2006)
30. Fujiwara, M.T., Sekine, K., Yamamoto, Y.Y., Abe, T., Sato, N., Itoh, R.D.: Live imaging of chloroplast FtsZ1 filaments, rings, spirals, and motile dot structures in the AtMinE1 mutant and overexpressor of *Arabidopsis thaliana*. Plant Cell Physiol. **50**(6), 1116–1126 (2009). doi:10.1093/pcp/pcp063
31. Johnson, C.B., Tang, L.K., Smith, A.G., Ravichandran, A., Luo, Z., Vitha, S., Holzenburg, A.: Single particle tracking analysis of the chloroplast division protein FtsZ anchoring to the inner envelope membrane. Microsc. Microanal. **19**(3), 507–512 (2013). doi:10.1017/S143192761300038X
32. Clough, S.J., Bent, A.F.: Floral dip: a simplified method for *Agrobacterium*-mediated transformation of *Arabidopsis thaliana*. Plant J. **16**, 735–743 (1998)
33. Littlejohn, G.R., Gouveia, J.D., Edner, C., Smirnoff, N., Love, J.: Perfluorodecalin enhances in vivo confocal microscopy resolution of *Arabidopsis thaliana* mesophyll. N. Phytol. **186**(4), 1018–1025 (2010)
34. Ferris, A.M., Giberson, R.T., Sanders, M.A., Day, J.R.: Advanced laboratory techniques for sample processing and immunolabeling using microwave radiation. J. Neurosci. Meth. **182**(2), 157–164 (2009)
35. Stokes, K.D., McAndrew, R.S., Figueroa, R., Vitha, S., Osteryoung, K.W.: Chloroplast division and morphology are differentially affected by overexpression of *FtsZ1* and *FtsZ2* genes in *Arabidopsis*. Plant Physiol. **124**(4), 1668–1677 (2000)
36. McDonald, K.L., Webb, R.I.: Freeze substitution in 3 hours or less. J. Microsc. **243**(3), 227–233 (2011). doi:10.1111/j.1365-2818.2011.03526.x
37. Ress, D.B., Harlow, M.L., Marshall, R.M., McMahan, U.J.: Methods for generating high-resolution structural models from electron microscope tomography data. Structure **12**(10), 1763–1774 (2004). doi:10.1016/j.str.2004.07.022
38. McMahan, U.J., Marshall, R., Szule, J., Jung, J.H.: Software for electron tomography. http://em3d.stanford.edu/ (2011). 2011
39. Glynn, J.M., Miyagishima, S., Yoder, D.W., Osteryoung, K.W., Vitha, S.: Chloroplast division. Traffic **8**(5), 451–461 (2007)
40. Gustafsson, M.G.L., Shao, L., Carlton, P.M., Wang, C.J.R., Golubovskaya, I.N., Cande, W. Z.D., Agard, A., Sedat, J.W.: Three-dimensional resolution doubling in widefield fluorescence microscopy by structured illumination. Biophys. J. (2008). doi:10.1529/biophysj.107.120345
41. Srinivasan, R., Mishra, M., Wu, L., Yin, Z., Balasubramanian, M.K.: The bacterial cell division protein FtsZ assembles into cytoplasmic rings in fission yeast. Genes Dev. **22**(13), 1741–1746 (2008). doi:10.1101/gad.1660908
42. Yoshida, Y., Kuroiwa, H., Misumi, O., Nishida, K., Yagisawa, F., Fujiwara, T., Nanamiya, H., Kawamura, F., Kuroiwa, T.: Isolated chloroplast division machinery can actively constrict after stretching. Science **313**(5792), 1435–1438 (2006). doi:10.1126/science.1129689
43. Gilkey, J.C., Staehelin, L.A.: Advances in ultra rapid freezing for the preservation of cellular ultrastructure. J. Electron Microsc. Techn. **3**(2), 177–210 (1986). doi:10.1002/jemt.1060030206
44. Kellenberger, E.: The response of biological macromolecules and supramolecular structures to the physics of specimen cryopreparation. In: Steinbrecht, R., Zierold, K. (eds.) Cryotechniques in Biological Electron Microscopy, pp. 35–63. Springer, Berlin (1987)
45. Kukulski, W., Schorb, M., Welsch, S., Picco, A., Kaksonen, M., Briggs, J.A.G.: Correlated fluorescence and 3D electron microscopy with high sensitivity and spatial precision. J. Cell Biol. **192**(1), 111–119 (2011). doi:10.1083/jcb.201009037
46. Watanabe, S., Punge, A., Hollopeter, G., Willig, K.I., Hobson, R.J., Davis, M.W., Hell, S.W., Jorgensen, E.M.: Protein localization in electron micrographs using fluorescence nanoscopy. Nat. Methods **8**(1), 80–84 (2011). doi:10.1038/nmeth.1537
47. Bell, K., Mitchell, S., Paultre, D., Posch, M., Oparka, K.: Correlative imaging of fluorescent proteins in resin-embedded plant material. Plant Physiol. **161**(4), 1595–1603 (2013). doi:10.1104/pp.112.212365
48. Xiong, H., Zhou, Z., Zhu, M., Lv, X., Li, A., Li, S., Li, L., Yang, T., Wang, S., Yang, Z., Xu, T., Luo, Q., Gong, H., Zeng, S.: Chemical reactivation of quenched fluorescent protein molecules enables resin-embedded fluorescence microimaging. Nat. Commun. **5** (2014). doi:10.1038/ncomms4992
49. Erickson, H.P., Taylor, D.W., Taylor, K.A., Bramhill, D.: Bacterial cell division protein FtsZ assembles into protofilament sheets and minirings, structural homologs of tubulin polymers. Proc. Natl. Acad. Sci. USA. **93**(1), 519–523 (1996)
50. Lu, C.L., Reedy, M., Erickson, H.P.: Straight and curved conformations of FtsZ are regulated by GTP hydrolysis. J. Bacteriol. **182**(1), 164–170 (2000)
51. Popp, D., Iwasa, M., Narita, A., Erickson, H.P., Maeda, Y.: FtsZ condensates: an in vitro electron microscopy study. Biopolymers **91**(5), 340–350 (2009)
52. Mingorance, J., Rivas, G., Velez, M., Gomez-Puertas, P., Vicente, M.: Strong FtsZ is with the force: mechanisms to constrict bacteria. Trends Microbiol. **18**(8), 348–356 (2010). doi:10.1016/j.tim.2010.06.001
53. Crowther, R.A., DeRosier, D.J., Klug, A.: The reconstruction of a three-dimensional structure from projections and its application to electron microscopy. Proc. Roy. Soc. Lond. A. **317**(1530), 319–340 (1970). doi:10.1098/rspa.1970.0119

APPENDIX D

VITA

Name: Rahamthulla S. Shaik

Email: rshaik@bio.tamu.edu

Address: The Microscopy and Imaging Center, ILSB, Texas A&M University, College Station, Texas 77843-2257

Education: B.S., Biology, ANGR Agricultural University, India, 1997
M.S., Biology, ICAR, Mumbai, India, 1999
M.S., Biotechnology, West Virginia State University, USA, 2006

Awards: Travel Award, Dept. of Biology, Texas A&M University, 2016

Publications:

1. Johnson, C.B., Long, Z., Luo, Z., **Shaik, R.S**., Sung, M.W., Vitha, S. and Holzenburg, A.: In situ structure of FtsZ mini-rings in *Arabidopsis* chloroplasts. Adv. Struct. Chem. Imag. 1:12, 1-12. (2015).

2. Johnson, C.B., **Shaik, R.S**., Abdallah, R., Vitha, S. and Holzenburg, A.: FtsZ1/FtsZ2 Turnover in Chloroplasts and the Role of ARC3. Microsc. Microanal. 21, 313-323 (2015).

3. Haspel JA, Chettimada S, **Shaik RS**, Chu JH, Raby BA, Cernadas M, Carey V, Process V, Hunninghake GM, Ifedigbo E, *et al*. Circadian rhythm reprogramming during lung inflammation. *Nat Commun* 2014; 5:4753.

4. Parikh VN, Jin RC, Rabello S, Gulbahce N, White K, Hale A, Cottrill KA, **Shaik RS**, Waxman AB, Zhang YY, Maron BA, Hartner JC, Fujiwara Y, Orkin SH, Haley KJ, Barabási AL, Loscalzo J, Chan SY. MicroRNA-21 integrates pathogenic signaling to control pulmonary hypertension: results of a network bioinformatics approach. Circulation.2012 Mar 27; 125(12):1520-32.

5. Haspel JA **Shaik RS**, Ifedigbo E, Nakahira K, Dolinay T, Englert JA, Choi AM. Characterization of macroautophagic flux in vivo using a leupeptin-based assay. Autophagy. 2011 Jun; 7(6):629-42.

6. Zhao G, **Shaik RS**, Zhao H, Beagle J, Kuo S, Hales CA. Low molecular weight heparin inhibits injury-induced femoral artery remodeling in mouse via up regulating CD44 expression. Journal of Vascular Surgery. 2011 May; 53(5):1359-67.

7. Kolliputi N, **Shaik RS**, Waxman AB. The inflammasome mediates hyperoxia-induced alveolar cell permeability. Journal of Immunology. 2010 May 15; 184(10):5819-26.

8. Thibault HB, Kurtz B, Raher MJ, **Shaik RS**, Waxman A, Derumeaux G, Halpern EF, Bloch KD, Scherrer-Crosbie M. Non-invasive assessment of murine pulmonary arterial pressure: validation and application to models of pulmonary hypertension. Cardiovascular Imaging. 2010 Mar; 3(2):157-63.

Presentations:

1. **Shaik RS,** Sung MW, Vitha S, Holzenburg A. Structural and Functional characterization of the Chloroplast Division Protein ARC3. American Society for Plant Biology, July 9-13 2016, Austin, Texas, USA.
2. **Shaik RS,** Sung MW, Vitha S, Holzenburg A. Structural characterization of the chloroplast division protein ARC3. Department of Biology Annual Conference Oct 10-12, 2014, Texas A&M University, College Station, TX, USA.
3. **Shaik RS**, Fernandez IE, An CH, Waxman AB. Isolation and characterization of endothelial progenitor cells from patients with Pulmonary Arterial Hypertension. American Journal of Respiratory and Critical Care Medicine. 2012; 185: A3410.
4. Haspel J, **Shaik RS**, Chu JH, Raby B, Choi AM. Identification of mouse lung transcripts exhibiting circadian variation in expression. American Journal of Respiratory and Critical Care Medicine. 2012; 185: A4916.
5. Parikh VN, Jin RC, Rabello S, Gulbahce N, Hale AE, **Shaik RS**, Waxman AB, Hartner JC, Fujiwara Y, Orkin SH, Barabasi AL, Loscalzo J, Chan SY. A systems-biology approach reveals that microRNA-21 integrates diverse pathogenic signaling to control Pulmonary Hypertension. Circulation. 2011; 124:A13395.
6. Hardin C, Krishnan R, Tambe D, **Shaik RS**, Manomohan G, Fredberg J, Waxman AB. Endothelial cell mechanics are altered in pulmonary arterial hypertension. European Respiratory Journal 2011; 38: Suppl.55.

7. **Shaik RS,** Waxman AB. Dysregulation of cell cycle proteins is associated with IL-6 induced pulmonary vascular remodeling and Pulmonary Arterial Hypertension. American Journal of Respiratory and Critical Care Medicine. May 2011; 183: A4976.

8. Haspel J, **Shaik RS**, Ifedigbo E, Choi AM. Diurnal variation in macroautophagic activity in vivo. American Journal of Respiratory and Critical Care Medicine. May 2011; 183: A2112.

9. Kolliputi N, **Shaik RS**, Waxman AB. Extracellular ATP triggers hyperoxia-induced lung inflammation. American Journal of Respiratory and Critical Care Medicine. May 2011; 183: A2105.

10. .**Shaik RS**, Kolliputi N, Waxman AB. Activation of inflammasome in Pulmonary Arterial Hypertension. American Journal of Respiratory and Critical Care Medicine. 2010; 181: A4865.

11. Kolliputi N, **Shaik RS**, Waxman AB. MicroRNA expression profiling in hyperoxic acute lung Injury: A Role of MiR-155? American Journal of Respiratory and Critical Care Medicine. May 2010; 181: A2032.

12. Kolliputi N, **Shaik RS**, Waxman AB. Suppressor of cytokine signaling-1 Inhibits hyperoxic induced inflammasome activation. FASEB Journal. 2010; 24:796.1.

13. Thibault H, Kurtz B, Raher M, **Shaik RS,** Waxman AB, Halpern E, Bloch KD, Scherrer-Crosbie M. Non- invasive assessment of murine pulmonary arterial pressure: validation and application to models of pulmonary hypertension. Archives of cardiovascular diseases, January 2010; Vol 2, No.1, p.81.

14. Kolliputi N, **Shaik RS**, and Waxman AB. Inflammasome: A pivotal role in hyperoxia-induced acute lung injury? FASEB Journal. 2009; 23:1025.1.

15. Kolliputi N, **Shaik RS**, and Waxman AB. Adenovirus-mediated transfer of the SOCS-1 gene to mouse lung protects against hyperoxic injury. American Journal of Respiratory and Critical Care Medicine. 2009; 179:A5692.

16. Zhao G, John B, Syrkina O, Kolliputi N, Zhao H, **Shaik RS**, Hales C. Aorta to main pulmonary shunt induces significantly more intraacinar arteriole remodeling in the left lung than right lung. 2009. American Journal of Respiratory and Critical Care Medicine. 2009; 179:A3398.

17. **Shaik RS,** Rice KM, Desai DH, Blough ER, Harris RT. Resveratrol affects stretch-induced reorientation of A7r5 cells in culture.

Medicine & Science in Sports & Exercise. November 2006; 38(11):S36.